Functional and structural characterization of gating mechanisms in K2P channels

Dissertation

for the attainment of the academic degree of

Doctor rerum naturalium

at

the Christian-Albrechts University Kiel

Faculty of Mathematics and Natural Sciences

Presented by

Elena Riel

Kiel, 2021

1. Evaluator: Prof. Dr. Thomas Baukrowitz
2. Evaluator: Prof. Dr. Eric Beitz

Date of the disputation: 12.08.2021

“Vor der Wirkung

glaubt man an andere Ursachen

als nach der Wirkung.”

“Before the effect

one believes in different causes

than after the effect.”

Friedrich Nietzsche [1954, Die fröhliche Wissenschaft]

Table of Content

Abbreviations

2-APB	2-aminoethoxydiphenyl borate
Å	Angstrom
A / Ala	Alanine
AA	Arachidonic acid
ATP	Adenine triphosphate
BiFC	Biomolecular fluorescence complementation
BKCa	Calcium sensitive big potassium channel
BL-1249	(5,6,7,8-Tetrahydro-naphthalen-1-yl)-[2-(1H-tetrazol-5-yl)-phenyl]-amine
BSA	Bovine serum albumin
C / Cys	Cysteine
Ca^{2+}	Calcium
CHO	Chinese hamstar ovary
Co-IP	Co-immunoprecipitation
(c)RNA	(complementary) Ribonucleic acid
Cs^{+}	Caesium
C-terminal	in direction of the protein sequence caroboxyl group
cyro-EM	Cryogenic electron microscopy
D / Asp	Aspartic acid
DAG	1,2-Diacylglycerol
Decyl-MTS	Decyl Methanethiosulfonate
DiC8	1,2-Dioctanoyl-sn-glycerol
DNA	Deoxyribonucleic acid
dNTP	Deoxy nucleotide triphosphate
DRG	dorasl root ganglia
Drofenine	Drofenine hydrochloride
E / Glu	Glutamic acid / glutamine
E.coli	*Escherichia coli*
EC1 / EC2	Extracelular helices 1 / 2 (cap structure)
EC_{50}	Concentration that exalts the initial current by 50 %
eGFP	Enhanced green flurescent protein

Ephys	Electrophysiological
F / Phe	Phenylalanine
FRET	Fluorescence resonance energy transfer
G / Gly	Glycine
GqPCR	Gq-protein coupled receptor
H / His	Histidine
HEK293	Human embryonic kidney cells 293
HEPES	4-(2-Hydroxyethyl) piperazine-1-ethanesulfonic acid
hERG	human Ether-à-go-go-Related Gene (Kv 11.1 channel)
HRE	halothane response element
I / Ile	Isoleucine
IC_{50}	Concentration that inhibits the initial current by 50 %
IP3	Inositol(1,4,5)trisphosphate
K / Lys	Lysine
K^+	Potassium
K2P	Two-pore domain potassium channel
K_{ATP}	ATP sensitive potassium channel
KcsA	Potassium channel of S*treptomyces lividans*
K_{ir}	Inward rectifier potassium channels
K_v	Voltage-gated potassium channels
K_vAP	Voltage-gated potassium channels of *Aeropyrum Pernic*
L / Leu	Leucine
LC-CoA (18:1)	Oleoyl-Coenzym A
M / Met	Methionine
MD	molecular dynamics
Mg^{2+}	Magnesium
MthK	Calcium-gated potassium channel of *Methanothermobacter thermautotrophicus*
MTSET	(2-(trimethylammonium)ethyl)Methanethiosulfonate bromide
MTS-TBAO	8-(Tributylammonium)octyl Methanethiosulfonate Bromide
N / Asn	Asparagine
Na^+	Sodium
NCA	negatively charged activator
NFx	Fluoxetine (Prozac)

ONO	ONO-RS-082
P / Pro	Proline
P1 / P2	Pore loop 1 / Pore loop 2
PAH	Pulmonary arterial hypertention
PDB	Proteine data base
pHe	extracellular pH
pHi	intracellular pH
PIP_2	Phosphatidylinositol(4,5)bisphosphate
PKA	Protein kinase A
pKa	negative base-10 logarithm of the acid dissociation constant (Ka)
PKC	Protein Kinase C
PKC	Proteinkinase C
Po	open probability
Q / Gln	Glutamine
QA	quaternary ammonium ions
R / Arg	Arginine
Rb^+	Rubidium
rpm	Revolutions per minute
RT	Room temperature
S / Ser	Serine
S 1-4	Ion binding sites at the selectivity filter 1-4
SEM	standard error of the mean
SF	selectivity filter
SiMPull	Single molecule pull down
SUMO	small ubiquitin-related modifier proteine
T / Thr	Threonine
TALK	TWIK-Related Alkaline pH-Activated K^+ Channel
TASK	TWIK-Related Acid-Sensitive K^+ Channel
TbutA	Tetrabutylammonium chloride
TEA	tetraetylammonium
TG	Trigeminal ganglion
THIK	Tandem-pore domain halothane inhibited potassium channel
TM	Transmembrane domaine
TPA	Tetrapentylammonium chloride

TRAAK	TWIK-related arachidonic acid stimulated potassium channel
TREK	TWIK-related potassium channel
TRESK	TWIK-related spinal cord potassium channel
TWIK	Tandem of P domains in weak inward rectifier potassium channel
V / Val	Valine
W / Trp	Tryptophan
WT	Wild type
Y / Tyr	Tyrosine

Abstract

The regulation of electrical stimuli is a key element of cellular communication within all living organisms. Centre of this regulation are the membrane spanning ion channels, that allow ion currents essential for neuronal activity and electrical signal propagation through an organism. The mechanisms that underlie the opening or closing of their selective pores (gating) is very diverse and differs among the distinct ion channel families. This work investigates the gating control of potassium channels of the tandem of two-pore-domain (K2P) channel family with a special focus on the relation of structural properties and the regulation of channel activity by pharmacological and physiological stimuli.

By screening all functional expressing mammalian K2P channels (12 in total), this work reveals that most K2P channels are regulated by negatively charged lipids, such as PIP_2 and Oleoyl-CoA. The response to those lipids, however, varied strongly within the K2P channel family. However, with few exceptions, similar effects were observed for members of the individual subgroups, with TREK, TALK and THIK channels being activated and TWIK, TASK and TRESK channels being inhibited by either one or both tested lipids. Outstanding were the results for THIK-1 as the polyanionic lipids were the first potent physiological activators identified for this subfamily. Furthermore, Oleoyl-CoA led to a very strong activation (>100-fold) of TALK-2 channels, removing an intracellular constriction identified within this work. In addition, this study provides evidence, that PIP_2 stabilizes the closed conformation of an intracellular gate found in TASK-1 and TASK-3 channels.

To study the relation of these gating processes with the structural properties of the investigated K2P channels, compounds such as open channel blocker (i.e. TPA, A1899, AVE0118) as well as negatively charged activators (i.e. BL-1249, ML67-33, DCPIB) or registered drugs such as ONO-RS-082, 2-APB or Norfluoxetine were screened within this work. Additionally, mutagenetic analyses of gating critical residues as well as cysteine modifying MTS-reagents were deployed to study the involvement of the C-terminal domain in channel gating and to investigate the intracellular pore accessibility of K2P channels. Even though hypothesised in previous studies, here it is shown for the first time, that TREK-1 and TRAAK channels are activated by the engagement of the C-terminal domain with the lipid bilayer. Further, it is shown that TALK-2 and TRESK channels comprise a state dependent pore accessibility, suggesting that these channels possess a lower cytoplasmatic gate, similar to the recently discovered intracellular gates in TASK-1 and TASK-2 channels.

Finally, this work presents a novel classification of K2P channels upon their gating regulation. It includes K2P channels possessing a lower intracellular gate and an upper voltage-gate at the selectivity filter (i.e. TASK-1, TASK-2, TASK-3, TALK-2, TRESK) and K2P channels that are strictly gated at the selectivity filter (i.e. TREK-1, TREK-2, TRAAK and TWIK-1).

Zusammenfassung

Die Regulation elektrischer Signale bildet das Schlüsselelement zellulärer Kommunikation in allen lebenden Organismen. Zentrum dieser Regulation sind in die Membran eingebettete Ionenkanäle. Diese erlauben die Regulation von Ionenströmen über die Membran und sind essentiell für die neuronale Aktivität und die Weiterleitung elektrischer Signale durch den Organismus. Die Mechanismen, welche dem Öffnen oder Schließen der ionenselectiven Pore ('gating') zugrunde liegen sind divers und unterscheiden sich stark innerhalb der verschiedenen Ionenkanalfamilien. Diese Arbeit erforscht die 'gating' Kontrolle der K2P Kanalfamilie und legt einen besonderen Fokus auf den Zusammenhang zwischen der Proteinstruktur und der Regulation der Kanalaktivität durch pharmakologische und physiologische Stimuli.

In dieser Arbeit wurde die Wirksamkeit der negative geladenen Lipide PIP_2 und Oleoyl-CoA für alle funktionell exprimierenden K2P Kanäle (insgesamt 12) getestet. Die Wirkung war dabei sehr unterschiedlich innerhalb der K2P Kanalfamilien, jedoch konnten ähnliche Effekte für die Mitglieder der einzelnen Subfamilien beobachtet werden. Dabei wurden TREK, TALK und THIK Kanäle durch die polyanionischen Lipide aktiviert, wohingegen TWIK, TASK und TRESK Kanäle inhibiert wurden. Besonders interessant war dabei, die PIP_2 und Oleoyl-CoA Aktivierung des im Gehirn exprimierten THIK-1 Kanals, da diese Aktivierung einen bisher unbekannten Regulationsmechanismus innerhalb dieser Kanalsubfamilie darstellt. Weiter konnte gezeigt werde, dass TALK-2 Kanäle ebenfalls sehr wirksam durch Oleoyl-CoA aktiviert werden (> 100-fach) und dabei ein in dieser Arbeit identifizierts, intrazelluläres ‚Gate' geöffnet wird. Umgekehrt konnte gezeigt werde, dass PIP_2, die geschlossene Konformation eines intrazellulären ‚Gates' in TASK-1 und TASK-3 Kanälen stabilisiert.

Um weiter die Verbindung von 'gating' Prozessen mit den strukturellen Eigenschaften der K2P Kanäle zu erforschen, wurden verschiedene chemische Stoffe, wie Kanalblocker (z.B. TPA, A1899, AVE0118) sowie die Klasse der negative geladenen Aktivatoren (z.B. BL1249, ML67-33, DCPIB) oder registrierte Medikamente wie ONO-RS-082, 2-APB oder Norfluoxetine in dieser Arbeit getestet. Zusätzlich wurden mutagenetische Analysen 'gating'-relevanter Aminosäuren durchgeführt. Außerdem wurden Cystein modifizierende MTS-Reagenzien eingesetzt, um die Beteiligung der C-terminalen Domaine an der Schaltung des Kanals, sowie die Zugänglichkeit der intrazellulären Kanalpore zu erforschen.

Im Zuge dessen konnte hier zum ersten Mal experimentell gezeigt werden, dass TREK-1 und TRAAK Kanäle durch das verankern der C-terminalen Domaine an die Lipiddoppelschicht

geöffnet werden. Außerdem konnte gezeigt werden, dass die Poren der TALK-2 und TRESK Kanäle in Abhängigkeit ihrer Kanalaktivität zugänglich sind, was auf die Anwesenheit eines intrazellulären ‘Gates’ hindeutet. Ähnliche ‘Gates‘ wurden für TASK-1 und TASK-2 Kanäle kürzlich beschrieben. Anhand der hier gemachten Beobachtungen und bereits bestehenden Veröffentlichungen wurde eine neue Klassifizierung der K2P Kanäle erstellt, bei welcher die Mitglieder der K2P Familie in zwei Kategorien geteilt wurden. Die erste Gruppe wird ausschließlich am Selektivitätsfilter geschaltet, während die zweite Gruppe ein oberes ‚Selektivitätsfiltergate‘ und ein unteres intrazelluläres ‚Gate‘, besitzt.

Zusammenfassend hebt diese Arbeit die polymodale Regulation der K2P Kanäle hervor und präsentiert außerdem eine neue Klassifizierung der K2P Kanäle anhand ihrer strukturellen Schaltmechanismen.

1. Introduction

The communication by electrical activity of cells among each other is a basic property of living organisms. The membrane spanning ion channels represent the key element of this sophisticated cross-talk by the tight regulation of ion fluxes across the membrane. The resulting ion currents are essential for neuronal activity and allow the propagation of electrical signals through the hole organism (Hille 2001). In plants, they are essential for cell growth and control the cellular response to external stimuli, such as light, humidity or temperature (Hedrich 2012). In humans, their functionality is i.e. coupled to the proper coordination of muscles and neuronal activities, but also modulate a large number of key processes and signal transductions in all kinds of cells (Hille 2001). Thus, they enable us to move, think and feel.

Among the very diverse spectrum of ion channels, the potassium (K^+) selective channels are the largest group of ion channels and are found in all kinds of eukaryotic, eubacterial and archaeal organisms (Miller 2000). Thereby, K^+ channels share the common property of selectivity for K^+ over the smaller Na^+ ions. However, the regulation mechanisms that underly the opening or closing of their selective pores (gating) is very diverse and differs among the members of this ion channel family (Doyle et al. 1998). Upon their transmembrane topology, there are two broad classes of K^+ channels, the six-transmembrane-helix voltage gated (Kv) channels and the two-transmembrane-helix inward-rectifier (Kir). However, several variations within this architecture contribute to a large diversity within this family. For example, the Ca^{2+}-activated K^+ channels share a large similarity with the Kv subtype, but possess an additional transmembrane segment near the amino (N) terminus of the primary sequence. Furthermore, the two-pore potassium (K2P) channels consist of two tandem pairs of K^+ channel sequences, that are mainly formed by two Kir-type sequences (Lesage, Guillemare, et al. 1996; Miller 2000). The letter, are in the centre of the present work, with a focus on the regulation of their gating mechanisms by pharmacological and physiological stimuli.

1.1 Members of the K2P channel family

Two pore domain potassium (K2P) channels are a widespread channel superfamily found in animals and plants. In mammals, they play an important role in cellular excitability, signalling

pathways and the transduction of external stimuli (Enyedi and Czirják 2010; González et al. 2012, 2015; Renigunta, Schlichthörl, and Daut 2015).

In 1996, TWIK-1 (tandem of pore domains in a weak inward rectifying K^+ channel) was the first two-pore domain potassium channel to be discovered within the human genome (Lesage, Guillemare, et al. 1996). Since then 14 further genes were identified to encode for this class of ion channels (Ashmole, Goodwin, and Stanfield 2001; Chavez et al. 1999; Decher et al. 2001; Duprat et al. 1997; Fink et al. 1996; Girard et al. 2001; Kim, Bang, and Kim 2000; Kim and Gnatenco 2001; Lesage, Terrenoire, et al. 2000; Lesage, Maingret, and Lazdunski 2000; Rajan et al. 2000, 2001; Reyes et al. 1998; Salinas et al. 1999; Sano et al. 2003). As their family name suggests, characteristically, all 15 members share a similar molecular topology (that will be discussed in more detail in section 1.2) of four transmembrane domains (TM1 to TM4) and 2 pore loops (P1 and P2) in tandem (Figure 1). On the basis of their sequential similarities and functional properties homomeric K2P channels were further divided into 6 subfamilies, namely TWIK, TREK, TASK, TALK, THIK and TRESK (Figure 1 A) (Gada and Plant 2019; Honoré 2007).

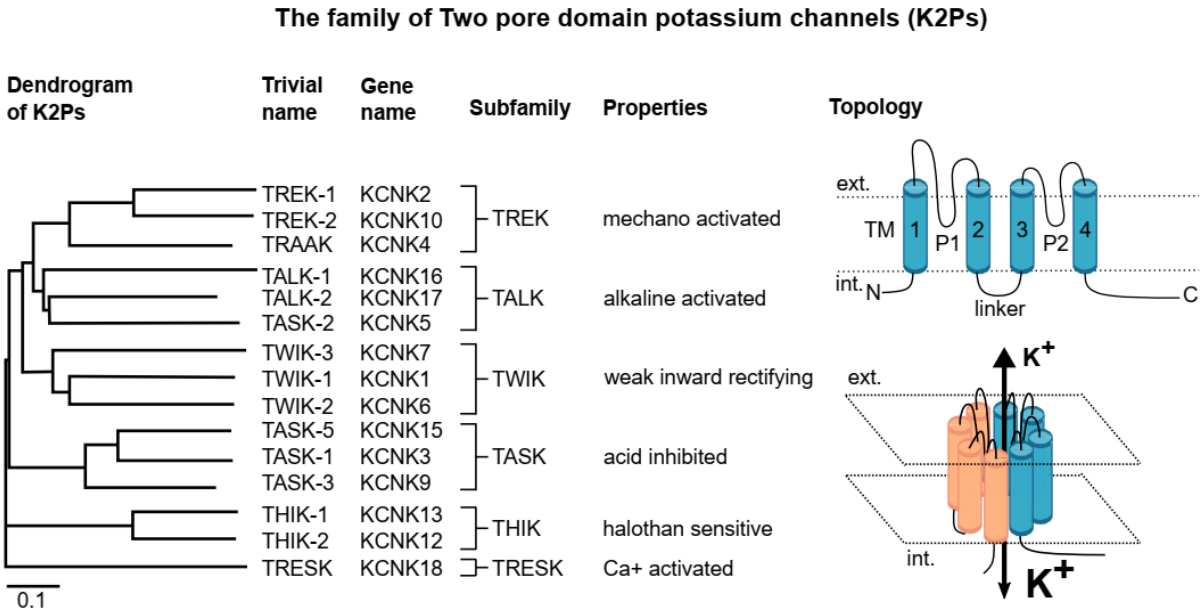

Figure 1 – The Two pore domain potassium channel family. Phylogenetic tree of the two pore domain potassium (K2P) channel family in humans (based on ClustalW alignments of the IUPHAR accession numbers for each clone (Enyedi and Czirják 2010)) and a following description of their trivial name, gene name and their division into subfamilies by shared properties. On the right, the topology model of the K2P channels depicts the relatively short N-terminal domain (N) that is connected from the cytosol to the first (TM1) of the four membrane spanning domains (TM1 to TM4). TM1 and TM2, as well as TM3 and TM4 are connected by a pore loop (P1 and P2, respectively) that form the tetrameric selectivity filter of the ion channel upon dimerization (lower figure). TM2 and TM3 are connected by an

intracellular linker. The C-terminal domain looms deep into the cytosol. The cap structure is built by the ascending and descending P1 areas arising into the cytosol.

Additionally, several heterodimers in- and outside of their subgroups were identified by biomolecular methods in *in vitro* experiments, but were also found in mammalian tissue, shown in the following table:

Table 1 – Heteromeric K2P channels

Monomers	Method used for identification	Reference
TREK-1 / TREK-2	Single molecule pull down (SiMPull), photobleaching analysis of GFP tagged channels, electrophysiology with concatemers.	(Levitz et al. 2016)
TREK-1 / TRAAK	SiMPull, photobleaching analysis of GFP tagged channels, Co-immunoprecipitation CO-IP, electrophysiology (ephys) with concatemers, Co-expression with dominant negative TRAAK.	(Blin et al. 2016; Levitz et al. 2016)
TASK-1 / TALK-2	Single molecular imaging (pancreatic QGP-1 cell line), BiFC, (HEK293 cells), FRET, ephys (co-expression of dominant-negative TALK-2 and TASK-1 and concatemers.	(Suzuki et al. 2017)
TWIK-1 / TREK-1	Co-IP, BiFC, membrane yeast two-hybrid, proximity ligation assay, ephys (co-expression in astrocytes).	(Hwang et al. 2014)
TWIK-1 / TREK-2	Co-IP.	(Hwang et al. 2014)
TWIK-1 / TRAAK	Co-IP.	(Hwang et al. 2014)
TWIK-1 / TASK-1 (-3)	FRET, (cerebellar granule neurons, CHO cells) ephys (co expression).	(Gada and Plant 2019)
THIK-1 / THIK-2	FRET, proximity ligation assay, ephys (Co-expression, Single channel recordings concatemers), (MDCK cells, *Xenopus laevis* oocytes.	(Blin et al. 2014)
TASK-1 / TASK-3	Co-IP, ephys (concatemers, co-expression dominant negative TASK-1),	(Berg et al. 2004; Czirják and Enyedi 2002)

	(HEK293 cells, rat brain slices – hypoglossal motoneurons)	
TRESK / TREK-2	Ephys (concatemers, co-expression, single channel recorings), HEK293 cells, *Xenopus laevis* oocytes, trigeminal ganglion (TG) neurons	(Lengyel et al. 2020)
TRESK / TREK-1	SiMPull, ephys (concatemers, co-expression, dominant negative TRESK) Xenopus laevis Oocytes, TG neurons	(Royal et al. 2019)

SiMPull: Single molecule pull down, Co-IP: Co-immunoprecipitation, Ephys: Electrophysiological, TG: trigeminal ganglion, FRET: Fluorescence resonance energy transfer BiFC: bimolecular fluorescence complementation, GFP: green fluorescent protein.

1.2 Structure and gating mechanisms of K2P channels

K2P channels consist of two homo- or heteromeric subunits. Each of them provides a relatively short cytosolic N-terminal domain (N-term) that is connected to the first of the four membrane spanning domains (TM1 to TM4). TM1 and TM2, as well as TM3 and TM4 are each connected by a pore loop (P1 and P2, respectively) that form the tetrameric selectivity filter of the ion channel upon dimerization (Lesage, Reyes, et al. 1996; Lopes, Zilberberg, and Goldstein 2001). In contrast to tetrameric potassium channels, like K_v or K_{ir} channels, those pore loops are not identical, thus forming an asymmetric selectivity filter (see section 1.2.1). Characteristically, the P1 loop is larger than the second P2 loop, as depicted in the topology model in figure 1. This about 55 amino acid long extension into the extracellular room forms another characteristic structure found in K2P channels, the cap structure. This structure is built by the two helices E1 and E2 (of each monomer) from the anterior ascending and descending area in P1 that arise into the extracellular matrix (Figure 2). Most of the K2P channels possess a conserved cysteine at the apex of

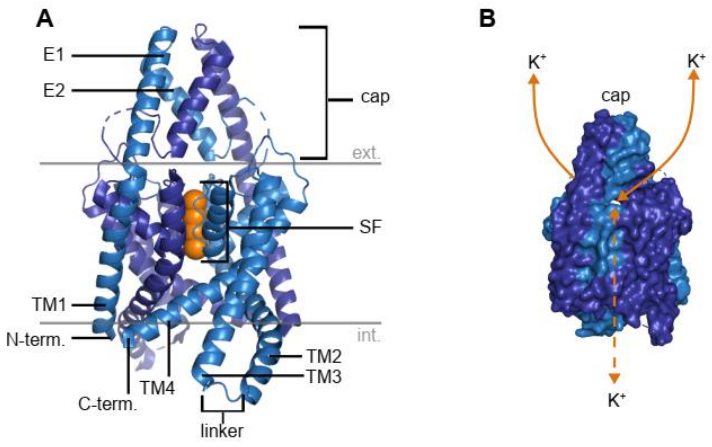

Figure 2 – Structure of K2P channels on the example of TREK-2 K2P channels (PDB Entry: 4BW5). A) Cartoon view, depicting cap helices E1 and E2, Transmembrane domains TM1-TM4, N- and C-terminal domains and the selectivity filter (SF). **B)** surface view, showing the two-sided extracellular entrance of the potassium pathway.

their cap structure that forms a covalent bond between each subunit, thereby holding the monomers in place. However, members of the TASK, THIK and TRESK subfamily do not inherit this bonding cysteine but share a hydrophobic core region, that is constituted of highly conserved residues at the two monomers within the K2P channel family (Brohawn, del Mármol, and MacKinnon 2012; Miller and Long 2012). Furthermore, it was shown that the two helices are interacting in a coiled-coil conformation, where the E1 and E2 of each subunits are crossed, so that E1 interacts with E2 of the other monomer, also referred as domain swapping (Goldstein et al. 2016). Even though, the cap structure that extends about 35 Å above the membrane represents a very characteristic feature among the K2P channel family, little is known about its function. However, early on the discovery of this channel class, it was observed that K2P channels show resistance to extracellularly applied blockers, such as tetraetylammonium (TEA) that were used to block Kv channels right above the extracellular mouth of the SF. This suggest a protective function from extracellular molecules blocking the ion pathway. Due to the cap, this pathway is split into two funnels that join right before the SF. Thereby, several residues that cover the wall of each pathway are negatively charged as well as two residues at the C-terminal end of E2. Those residues are positioned right above the SF, causing an increase of the local potassium concentration right over the selective pore (Brohawn et al. 2012; Miller and Long 2012). The following TM2 and TM3 are connected by an intracellular linker and the long C-terminal domain adjacent to TM4 looms deep into the cytosol. Figure 2 resumes the discussed structures on the example of the TREK-2 crystal structure (PDB Enrty: 4BW5), however, it is noteworthy that the C-terminal domain was truncated for crystallisation. In the following sections, gating mechanisms arising from the different structures found in K2P channels are discussed in more detail.

1.2.1 Ion selectivity and filter gating of K2P channels

The bacterial channels KcsA, MthK and KvAP as well as the mammalian Kv, Kir or K2P channels all conduct selectively potassium ions from one side to the other side of the membrane. Crystallographic studies suggest a highly conserved mechanism for ion selectivity and gating mechanisms for all K^+ channels (Doyle et al. 1998). Thereby, potassium channel activity is thought to be regulated at two conserved gates. A lower intracellular ‘helix bundle crossing’ gate that regulates the accessibility of potassium ions to a second selectivity filter gate (C-type gating) that resides within the membrane, close to the extracellular side. Some Kv channels

possess a third gating mechanism, referred as N-type inactivation, were an accessory peptide as part of the N-terminal domain of the ion channel is employed to auto-inhibit the ion current by clogging the inner pore cavity (Hoshi, Zagotta, and Aldrich 1990; Yellen 2002). However, to understand ion selectivity, the extreme favourable interaction of K^+ ions (and other positively charged ions) with water has to be considered. In the vicinity of K^+ ions water molecules reorient with their negatively charged end facing towards the positively charged ion.

Instead of a narrow pore through the full thickness of the plasma membrane, the general architecture of K^+ channels is characterized by a large pore that is accessible from the intracellular side and allows the access of water and hydrated K^+ ions into the permeation pathway. Furthermore, K^+ channels possess four pore helices, which all represent dipoles due to the dipole alignment of their hydrogen bonds. Due to the orientation of the negative pole pointing to the core of the intracellular cavity, ions within the cavity are electrostatically stabilized near the narrow SF (Doyle et al. 1998; Roux and MacKinnon 1999; Zhou et al. 2001). The SF of ion channels comprises a series of polar oxygen atoms that mimic the hydrogen cage of an ion surrounded by water. Thereby, the size of this assembly is highly critical to the selectivity of the channel. In potassium channels it adopts exactly the structure that is built by the water molecules surrounding a K^+ ion. Thus, each K^+ ion within the selectivity filter is coordinated (as in water) by two groups of four oxygen atoms that origin from the backbone carbonyl oxygen atoms of the 4 pore loops of the assembled protein subunits (P1 and P2 in each dimer of K2P channels). In accordance, in sodium selective channels the filter adopts the more compact structure that is found surround Na^+ ions. Once within the selectivity filter, K^+ ions line behind each other with a space of about 7 Å at the canonical positions S1 – S4. The mutual electrostatic repulsion between each K^+ ion leads to a destabilisation of the ions within the selective pore, thus preventing an overly tight binding that would slow ion permeation (Doyle et al. 1998; Morais-Cabral, Zhou, and MacKinnon 2001; Zhou et al. 2001). The pore helices as well as the residues of the SF are conserved among the tetrameric K^+ channels with canonical signature residues TXGYGDX (X refers as space holder for any amino acid). The dehydrated K^+ ions are thereby (as already said) coordinated by the carbonyl oxygen atoms of the residues as well as the side chain of the threonine. The second glycine of the pore motifs are oriented in a ring, where the carbonyl oxygens are pointing towards the extracellular solution. This highly electronegative ring attracts K^+ ions and therefore assists in dehydration (or hydration) of K+ ions at the extracellular entry of the SF (Zhou et al. 2001). Thereby, all pore domains of the tetramers are identical and very sensitive to mutational changes (Doyle et al. 1998). By contrast,

the dimeric K2P channels comprise 2 pore domains per subunit, that possibly differ in their SF sequence.

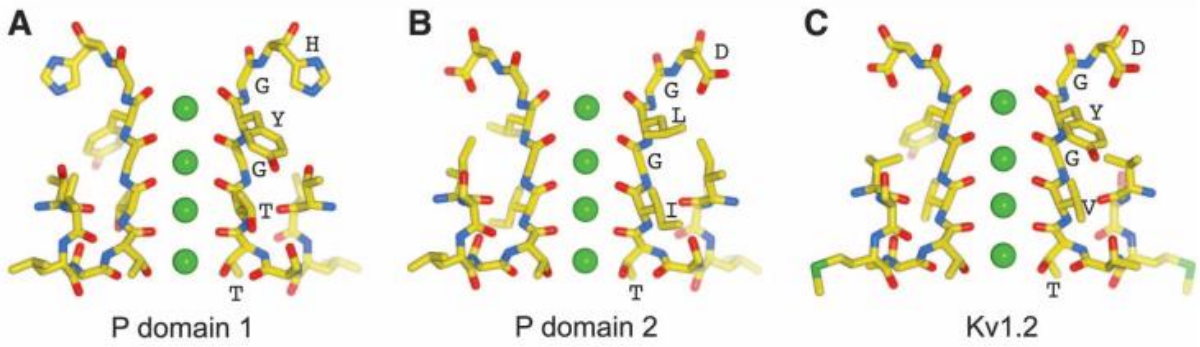

Figure 3 – Selectivity Filter in TWIK-1 K2P channels and Kv1.2 channels (Miller and Long 2012). '**A – C)** Conformation of amino acids comprising the selectivity filter from P domain 1 (A) and P domain 2 (B) compared with the selectivity filter of Kv1.2 (C) (PDB ID 2R9R). Two subunits are shown from the side, with the extracellular solution located above. The filter sequence is labeled in single-letter amino acid code (D, Asp; G, Gly; H, His; I, Ile; L, Leu; T, Thr; V, Val; Y, Tyr). Amino acids are drawn as colored sticks (yellow, carbon; blue, nitrogen; red, oxygen; and green, sulfur), and K+ ions are depicted as green spheres […]' (Figure 3, A, B, C) **(Miller and Long 2012).**

The SF motif in K2P channels therefore shows greater variation and possesses only two conserved residues (TXGXXX). The threonine, however is conserved in P1 and P2 suggesting a crucial role for K2P channel gating. At the second position in P1 and P2 is usually an isoleucine or valine found. Only the TWIK-1 channel possesses a threonine at this site, which might play a role for Na^+ conductance of TWIK-1 channels under low K^+ concentrations (Ma, Zhang, and Chen 2011). The following residues are GYG and GFG in P1 and P2, respectively. Only TWIK channel differ again, possessing a leucine instead of the phenylalanine in P2. The non-conductive K2P channel TWIK-3 (KCNK7) even replaces the second G of the P2 motif by a glutamate, which might be the origin of its non-functionality (Salinas et al. 1999). However, the final position in P2 is conserved again (aspartic acid, D) among all K2P channels. The interaction of this D with the Y in P1 of the neighbouring subunit was shown to be crucial for ion selectivity and conductance (Chapman, Krovetz, and VanDongen 2001). In P1, the last position differs among the K2P channel family. While TREK/TRAAK and TALK channels possess an asparagine at this position, TASK channels as well as TWIK-1 bear a histidine. Notably, this histidine comprises the extracellular proton sensor of these channels, thus protonation of the histidine lead to a conformational change of the selectivity filter into a non-conductive state (Morton et al. 2003; Plant et al. 2012; Rajan et al. 2000).

Due to the lack of an intracellular gate in TREK channels, the SF gate was proposed as primary gate in K2P channels (Piechotta et al. 2011; Rapedius et al. 2012). It was hypothesised that the voltage sensitivity of the channels originates from the movement of three to four ions into the electric field of an inactive SF, resulting in a conformational change that allows ion conductance (Schewe et al. 2016). This mechanism is tightly coupled to the electrochemical potential. Upon all voltages negative to the reversal potential the SF is ion-depleted and therefore inactive. At voltages positive to the reversal potential an increasing fraction of the ion channels adopt the inactive, but now ion occupied state. This ion occupied state rapidly converts into the active outwardly permeating state. Upon inversion of the driving force, the SF only transiently conducts currents as this state is not stable due to a distinct SF occupancy, and finally adopts the initial, structurally distinct, ion depleted and inactive state. This model of a check valve system allows an ion flux only in the outward direction and prevents ion conduction to the intracellular site.

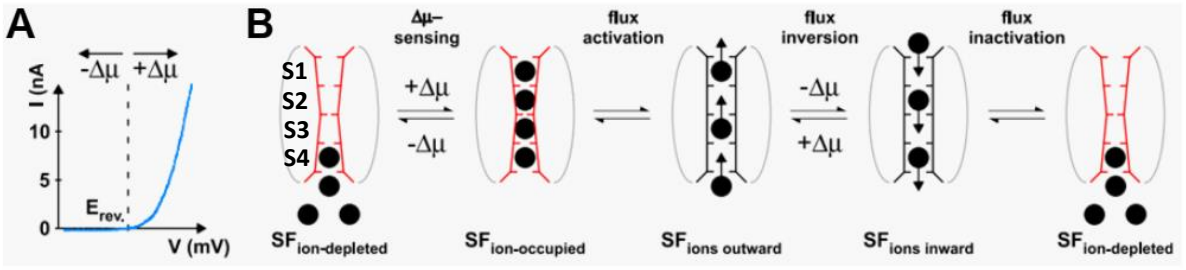

Figure 4 – Model of voltage gating in K2P channels (Schewe et al. 2016)**. '**[…] **A)** Illustration of the electrochemical driving force (i.e., Δμ = V_m $E_{rev.}$) dependence of K2P gating with a positive Δμ, leading to activation but inactivation for a negative Δμ. **B)** Cartoon of the proposed mechanism of flux coupled gating depicting that for a negative Δμ (i.e., all voltages negative to the Erev.) the filter is ion-depleted and inactive (SFion-depleted). For voltages positive to Erev., the channels start to activate as an increasing fraction of the channels populate the inactive but now ion occupied state (SFion-occupied) that rapidly converts into the active outwardly permeating state (SFions-outward). Upon inversion of the driving force (i.e., for potentials negative to the $E_{rev.}$), the SF only transiently conducts inward currents as this state is not stable (SFions-inward) and finally adopts the initial, structurally distinct, iondepleted, and inactive state (SFion-depleted)' (Figure 6, E, F, letters exchanged for A, B, description S1-S4 was added) (Schewe et al. 2016).

Thereby, mutation of the SF motif threonine (TXGXXX) that presents the S4 binding site for K^+ ions, leads to a reduction of the ion occupancy at the S1 and S4 site of the selectivity filter, resulting in a loss of voltage gating.

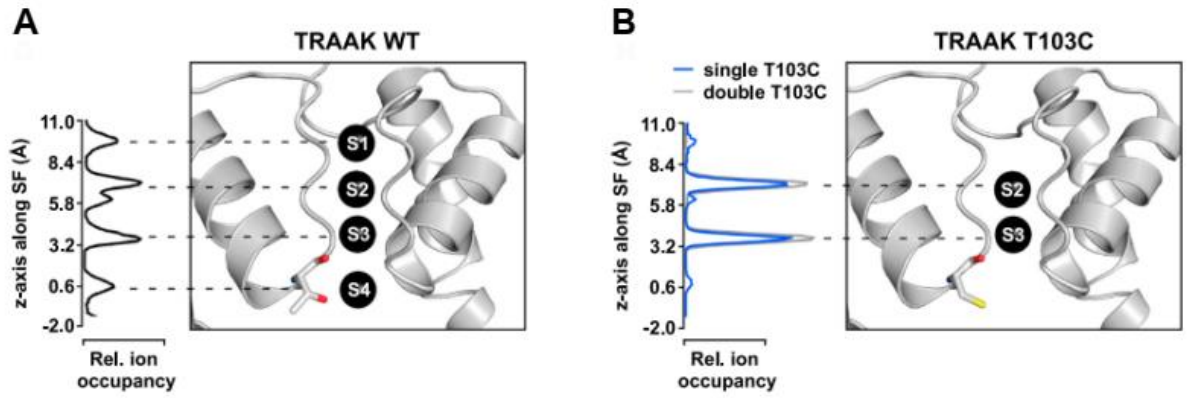

Figure 5 – Selectivity Filter occupancy in TRAAK K2P channel (Schewe et al. 2016)**.** '[…] **A-B)** MD simulations performed on TRAAK show relative ion occupancies for the ion binding sites S1–S4 (A) and their change (B) upon mutation of either one (single T103C) or both positions (double T103C), leading to a loss of binding to S1 and S4' (Figure 2 G, H, letters exchanged for A, B) (Schewe et al. 2016).

By contrast, replacement of K^+ by Rb^+ or Cs^+ ions increase the ion occupancy at the S1, S3 and S4 sites, and thus, accelerate voltage dependence of the channels. This becomes visible by the voltage dependent increase of the tail current amplitudes that are reflecting the slope of a rising P_o, depicted in figure 6. Also shown in figure 6 (C), this increase of ion occupancy observed in MD simulations, is reflected by a competition of the QA ion TPA and Rb^+ ions for the same (S4 – threonine) binding site.

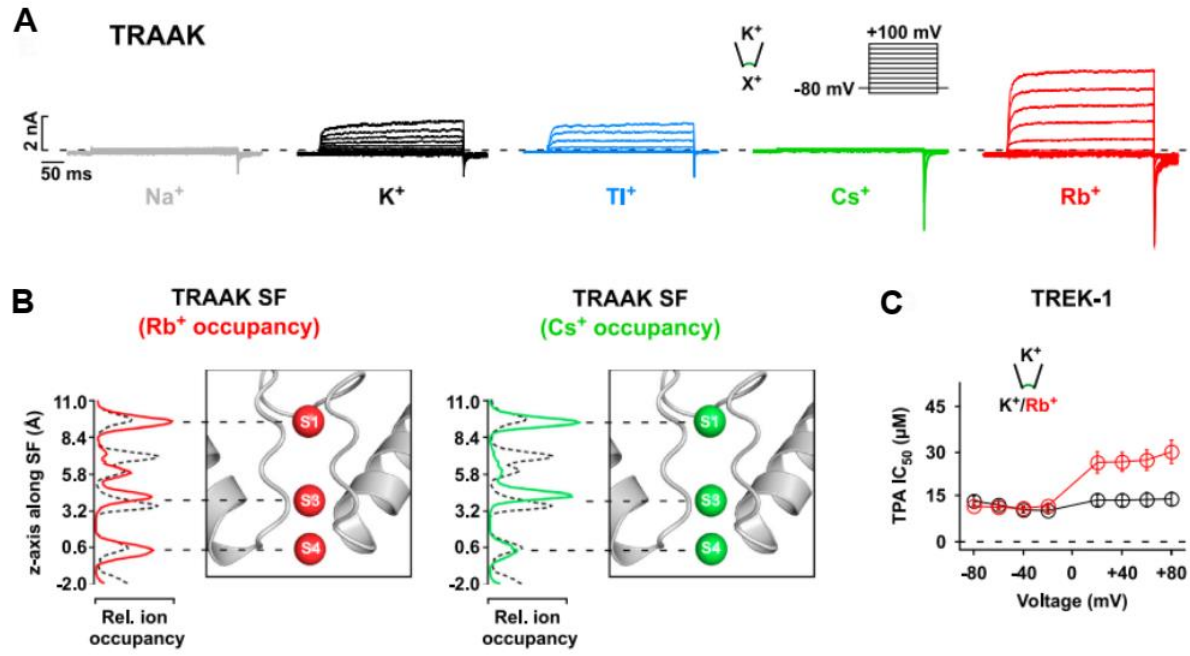

Figure 6 – Ion-Flux gating is sensitive to the permeant ion species. '[…] **A)** Voltage-evoked TRAAK currents with 120 mM $K^+_{ext.}$ and various intracellular ions (120 mM) as indicated. **B)** MD simulations

performed on TRAAK show the relative ion occupancies for the S1–S4 sites with Rb^+ and Cs^+ permeation in comparison to K+ permeation (black dotted line). **C)** The IC_{50} for TREK-1 channel inhibition by TPA was determined for the respective voltages in symmetrical K^+ and with intracellular Rb^+ replacing K^+; data are as mean ± SEM' (publication Figure 3 E, F, G – exchanged for letters A, B, C) (Schewe et al. 2016).

However, it was shown frequently that TREK/TRAAK channels convert from strict outward rectification to a leak mode upon channel activation (i.e. by cellular lipids such as arachidonic acid or upon acidification) suggesting that those stimuli somehow converge to the selectivity filter (Schewe et al. 2016). How this conversion exactly takes place among the different K2P channel members is still illusive. However, crystallographic studies suggest intracellular movements of the TM2 and TM4 as well as the proximal C-terminal domain to be highly important for gating regulation in K2P channels, which will be discussed in the following section.

1.2.2 Intracellular gating mechanisms

As mentioned in the previous section, potassium channels possess a central cavity, right below the selectivity filter facing the cytoplasm. In many K^+ channels the access of water and molecules to this pore cavity is regulated by a second gate made from flexible pore lining transmembrane helices. This 'helix-bundle-crossing' gate is controlled by a hinge glycine that allows the inner helices to bend and thus to constrict or delate the pore entrance. In contrast to the fourfold symmetric Kv or Kir channels, K2P channels only form bilateral symmetric pore cavities upon dimerization, due to their overall structure with 4 TMs and 2 pore loops in tandem. Hence, the pore lining helices TM2 and TM4 are asymmetrical and share only low amino acid identity. However, the hinge glycine (controlling the helix-bundle-crossing gate in other channels) is present as well in both pore lining helices TM2 and TM4, but with a shifted position in TM4 by two residues. This suggests the presence of a similar mechanism in K2P channels and indeed, TASK-3 channels show a reduction in channel activity if this residue is replaced by alanine (Ashmole et al. 2009). Furthermore, mutations of conserved residues at TM2 and TM4 (N133, A237) in TASK channels lead to an increase (or decrease, respectively) of the open probability (P_o) of the channel. Therefore, these residues are believed to play an important role for intracellular gating mechanisms, and thus, the functionality in TASK channels

(Ashmole et al. 2009). Consistently, a genetic mutation of the TM4 residue (A237N) within the KCNK9 gene (TASK-3), causes a loss-of-function of the channel and is associated with the development of the Birk-Barel syndrome, causing mental retardation, hypertonia, hyperactivity and syndromic facies (Šedivá et al. 2020). In addition, the amino acid stretch VLRFLT in TASK-3 (VLRFMT in TASK-1, respectively) that is located between the lower pore entrance in TM4 and the cytoplasmatic C-terminal domain was identified as regulation site for gating stimuli such as anaesthetics or GPCR induced inhibition and is often referred as halothane response element (HRE) (Talley and Bayliss 2002; Wilke et al. 2014). Interestingly, the recently published crystal structure of the TASK-1 K2P channel reveals a closed intracellular gate that is formed by this amino acid stretch on TM4 (VLRFMT) of each subunit, which lies across the entrance of the pore cavity. In accordance, mutations to alanine within this gate at any position (except for valine) lead to an increase of channel activity, indicating that these mutations lead to an opening of the lower constriction of the so called 'x-gate'. This constriction (if not mutated) exhibits a radius of 0.8 Å (Rödström et al. 2020). This structure is quite unusual, when compared to the crystal structure of other K2P channels. For example TREK-2 comprises a large radius of 7.5 Å at the entrance to its vestibule, even when the channel is found in its inactive state (Dong et al. 2015).

This unusual conformation is suggested to be caused by bends of TM4 (at the residues L241 and N250) on both sites of the HRE, resulting in this narrow x shaped constriction. The interface of this constriction is lined by the residues L244, M247 and the methyl group of T248. The stabilization of the bended helices is thought to be a result of the interaction of the hinge residue L241 that is pulled away from the helical axis due to the insertion of its sidechain into a hydrophobic pocket and its interaction with the residue R245. As previously indicated, mutations of either residues to alanine lead to a destabilisation of the x-gate (Rödström et al. 2020). Interestingly, the residues N133 and A237, that were found to be critical for channel activity in TASK-3 channels (see above, (Ashmole et al. 2009)), were also identified in the crystal structure as stabilizing elements of the x-gate, thus a mutation of N133 to alanine, leads to an increase of channel activity in TASK-1 as well. The opening of the constriction supposedly involves a relaxation of the x-gate extended helix, resulting in a straightening of the M4 helix, adopting a similar conformation as it is found in other K2P channels (Figure 8, (Rödström et al. 2020)). However, this was not verified in experiments, yet.

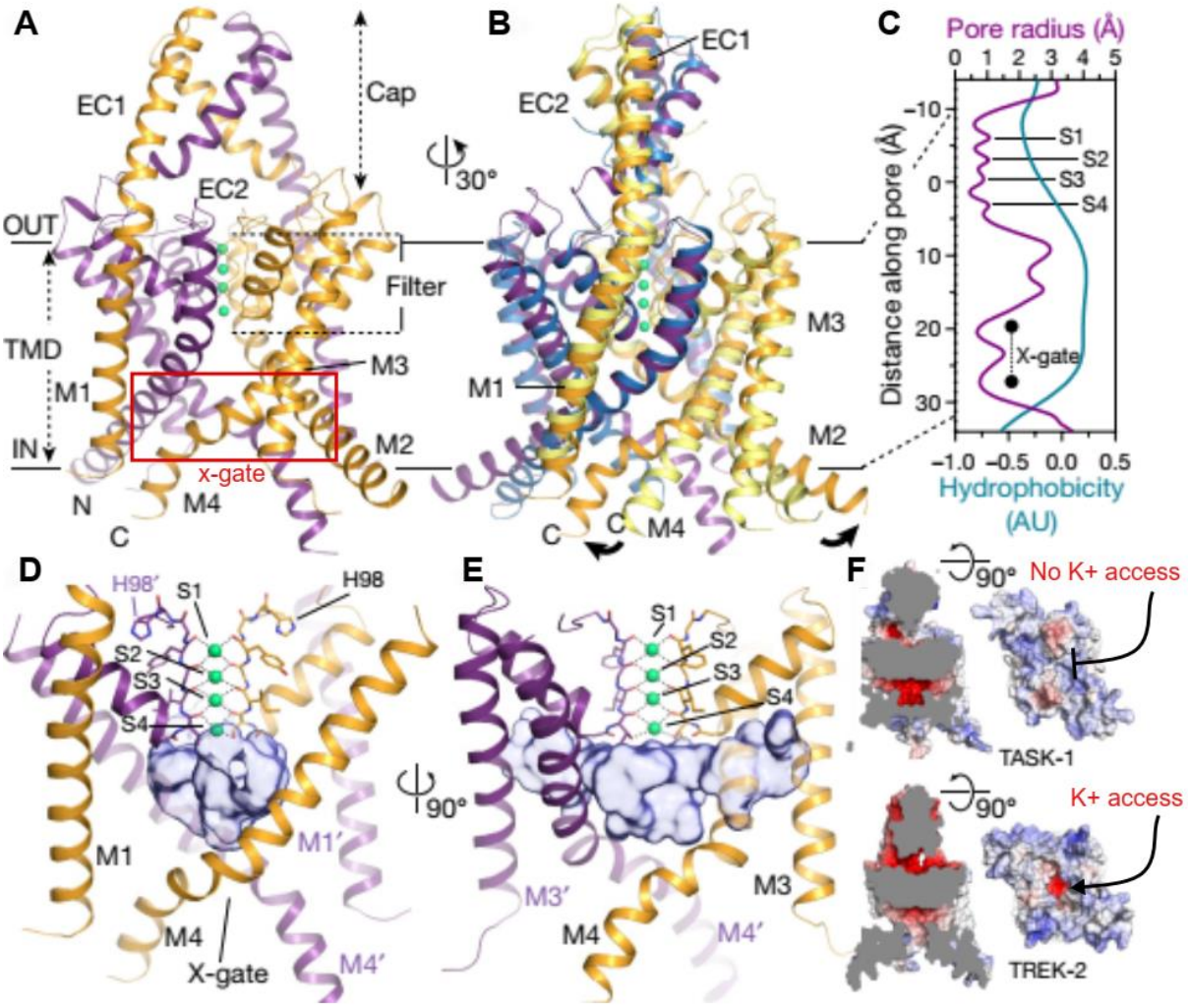

Figure 7 – TASK-1 K2P channel structure with intracellular x-gate (Rödström et al. 2020)**. 'A)** Cartoon showing the structure of TASK-1, with chain A in gold, chain B in purple and potassium ions in green, viewed from the membrane. **B)** Superposition of the structures of TASK-1 (gold and purple) and TREK-2 (down state (PDB: 4XDJ)) (yellow and blue). **C)** Radius and hydrophobicity of the TASK-1 pore25. AU, arbitrary units. **D - E)** The X-gate enclosing the vestibule and fenestrations (depicted with semi-transparent surfaces), viewed from the membrane plane (**D**) and rotated 90° (**E**). **F)** Electrostatic surfaces of TASK-1 and TREK-2 (PDB: 4XDJ) shown as a cross-section perpendicular to the membrane and seen from below […]' (Figure 1, a – f, letters exchanged by capital letters A-F) **(Rödström et al. 2020)**. X-gate and the resulting constriction, that is not found in TREK-2 is highlighted in red.

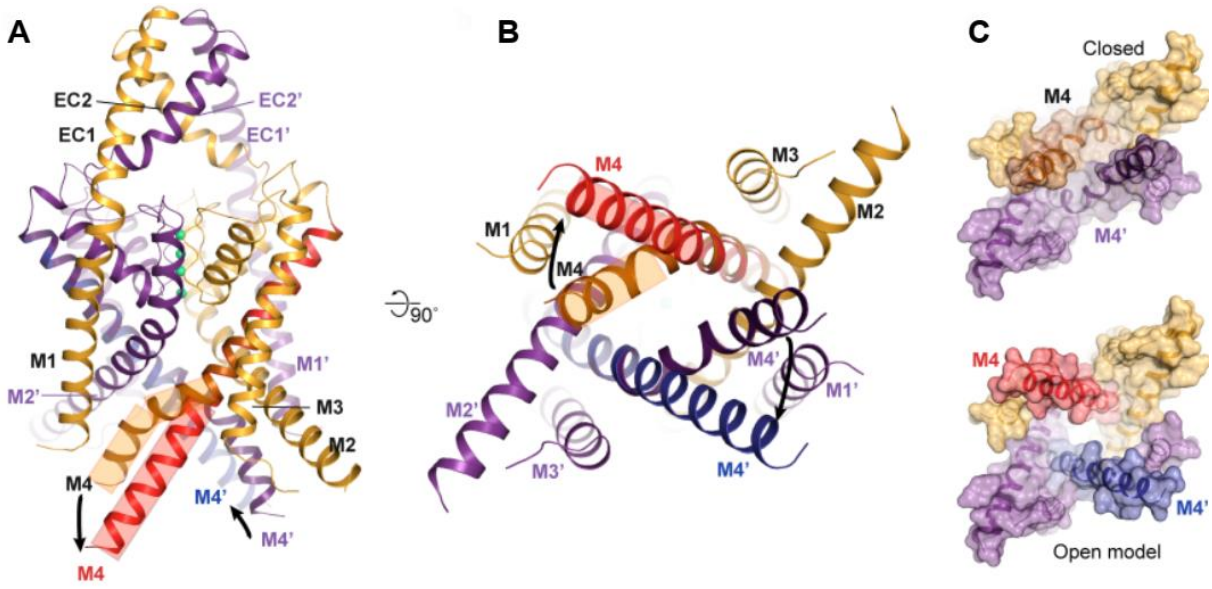

Figure 8 – Model of conformational change to the open structure in TASK-1 channels (Rödström et al. 2020). '**A-B)** Model of TASK-1 with M4 adopting a straight α-helical conformation (in red and blue) aligned with the TASK-1 structure shown from the side (A) and below the membrane (B). **C**) Open and closed models of TASK-1 viewed from below the membrane […]' (Extended data figure 7 a-c, letters have been exchanged by capital letters)**(Rödström et al. 2020).**

As already implied, the TREK/TRAAK channel family is believed to possess a widely open vestibule entrance, independently of the state of channel activity. This was probed in TREK-1 channels by pore accessibility assays, where open channel blockers like quaternary ammonium ions (QAs), were proven to have a state independent access to the channel pore cavity (Piechotta et al. 2011). This was supported by the introduction of a pore cysteine that was then consequently modified independently to the state of channel activity by the reactive QA 8-(Tributylammonium)octyl methanethiosulfonate (MTS-TBAO) compound. This reagent covalently binds to the pore cysteine, thus permanently blocks ion flux. The rate of this permanent MTS-TBAO block was very similar in the open and closed state of the channel, suggesting that the pore lining helices do not constrict or dilate during channel gating (Rapedius et al. 2012). This suggests, that there is no lower gate found in TREK-1 channels and that all stimuli altering the channel activity converge directly to the selectivity filter. Up to date, this conversion is poorly understood. Currently, it might be best explained by the model of an up- and down state conformation, were movements of TM4 and possibly the proximal C-terminal domain (CTD) towards the membrane lead to a stabilisation of the SF gate and enhance channel activity, whereas movements away from the membrane into the cytosol lead to channel closure (Brohawn, Campbell, and MacKinnon 2014; Lolicato et al. 2014). Still, the involvement of the

CTD in this membrane interaction was not experimentally verified yet. The involvement of the TM2 and TM4, however, is backed by the crystal structures of the TREK-2 K2P channel, that were produced with and without the TREK channel inhibitor Fluoxetine, also known as the antidepressant Prozac (Dong et al. 2015).

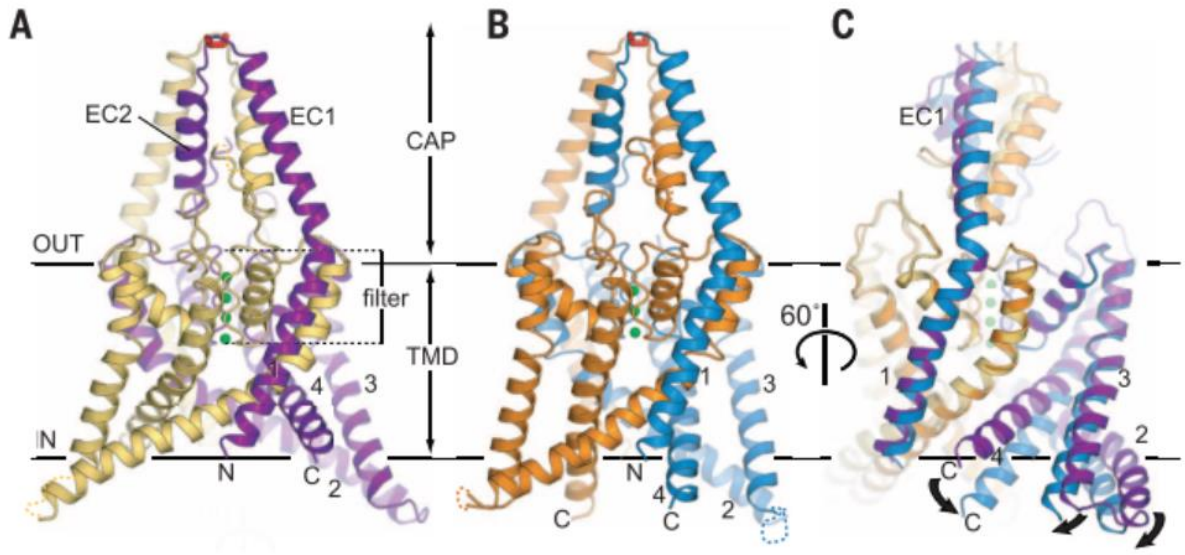

Figure 9 – Up- and down structure of TREK-2 K2P channels (Dong et al. 2015). '**A)** TREK-2 overall fold viewed parallel to the plane of the membrane, with views of (A) the up-state 3.4 Å structure, with chains A and B in yellow and purple; **B)** the down-state 3.9 Å structure, with chains A and B in orange and blue; **C)** a superposition of the states […]' (Figure 1 A-C) **(Dong et al. 2015).**

This study revealed, that the lower sections of the TM2, TM3 and TM4 helices are projecting further into the cytoplasm in the down-state and move upwards to the membrane engaging the conductive up-state conformation. Furthermore, the inhibitor Fluoxetine (indicated in Figure 10 A), binds within a side fenestration that is only accessible in the downstate conformation. Thus, it stabilizes the non-conductive state of the channel when it is bound within the fenestration, preventing an upward movement of the TMs (Dong et al. 2015). These side fenestrations, are lateral openings at the interface between TM2 of one subunit and TM4 of the other subunit of the dimer and are found so far in all crystallised K2P channels (Brohawn et al. 2012; Dong et al. 2015; Li, Rietmeijer, and Brohawn 2020; Lolicato et al. 2017; Miller and Long 2012; Rödström et al. 2020).

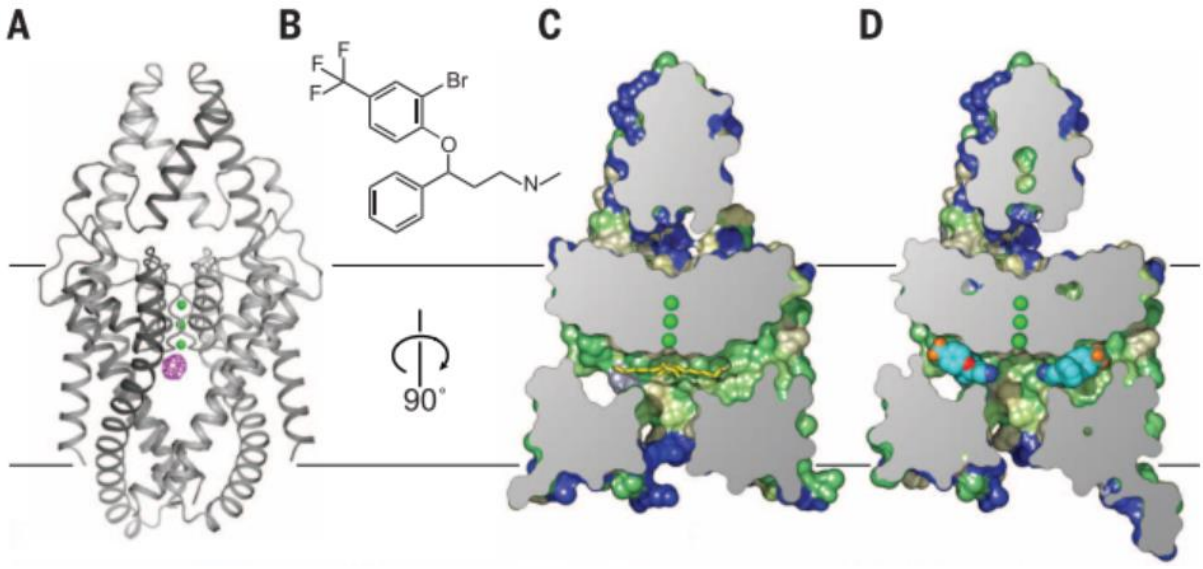

Figure 10 – Norfluoxetine binding site within the TREK-2 site fenestration (Dong et al. 2015). '**A)** Overall fold of the TREK-2 down state shown with the 5 Å anomalous difference map for the Br-fluoxetine/TREK-2 complex shown in pink (contoured at 4.5s), indicating the location of Brfluoxetine in the fenestration. **B)** Chemical structure of Br-fluoxetine. Norfluoxetine lacks the methyl group on the nitrogen. **C)** Cross section of a surface view of TREK-2 in the down state, colored by hydrophobicity [green (most hydrophobic) through yellow to blue (least hydrophobic)]. Yellow sticks represent Lip3. **D)** Complex of TREK-2 with norfluoxetine. Norfluoxetine is shown in light blue, dark blue, red, and orange for carbon, nitrogen, oxygen, and fluorine atoms, respectively […]' (Figure 2 A - D) **(Dong et al. 2015).**

Further, it was proposed that the fenestrations are filled with the hydrophobic tails of membrane phospholipids and that their interaction with the cleft lining helices TM4 and TM2 might specifically influence channel gating (Brohawn, Campbell, et al. 2014; Lolicato et al. 2014). Interestingly, it was shown that the (earlier mentioned) hinge glycine residue, that is found in most potassium channels plays an important role for the establishment of an up- or down configuration, respectively. Thereby, it has been suggested, that the TM2 and TM4 helices are able to bend around this glycine residue, shifting the TM4 from the down to the up state configuration (Dong et al. 2015; Lolicato et al. 2014).

In contrast to the findings that support a lack of a lower gate within the TREK subfamily, the recently published cryo-electron microscopy structure of the TASK-2 channels suggest the existence of a gateable lower constriction (Li et al. 2020). The key role in this study plays a lysine residue (K245) at TM4, that reportedly changes its conformation in response to pH alterations (more section 1.3.1.1, Figure 13). Thereby, it is suggested that it is blocking ion permeation by pointing into the entrance of the intracellular vestibule under acidic conditions.

The resolved structure, that was produced under alkalic conditions, however, comprises the lysine in an upward facing position, that is rotated in an angle of 90°, thus clearing the K^+ pathway (Li et al. 2020).

However, even though crystallographic as well as experimental data strongly suggest especially the involvement of the TM2 and TM4 helices in channel gating of all K2P channels, it is still unclear how their movements are regulated and how they are transducing those structural changes to the selectivity filter gate. However, until now, the experimental and computational data suggest two distinct mechanisms that are mainly characterised by the lack or existence of a lower pore constriction in TREK or TASK-1 and TASK-2 channels, respectively.

1.3 Regulation of K2P channels

The distribution of homo- and heteromeric K2P channels within the human body is ubiquitous and in accordance their regulation is remarkably versatile. K2P channels of the TREK/TRAAK subfamily that are i.e. expressed in nociceptive neurons of the dorsal root ganglia (DRG), respond to mechanical stretch and membrane pressure (Aryal et al. 2017; Brohawn, Campbell, et al. 2014; Clausen et al. 2017). Furthermore, they are sensitive to thermal stimuli and activated by internal and external acidification. The letter is thought to play a role in neuroprotection during ischemia. Additionally, studies in knockout-mice suggest that TREK channels are involved in pain perception and the regulation of neural activity as it is important for patients suffering under depression (Bayliss and Barrett 2008; Honoré 2007; Maingret et al. 2000; Noël et al. 2009; Pereira et al. 2014; Schneider et al. 2014). TASK-1 and TASK-3 are oxygen sensing, acid inhibited channels found in chemoreceptor cells of the carotid body (Buckler 2015). Furthermore, mutations within the KCNK3 gene encoding for TASK-1 were identified in patients suffering from pulmonary arterial hypertension (PAH), promoting their role in systemic and pulmonary vasculature by controlling i.e. the Ca^{2+} homeostasis, vascular tone or cellular proliferation (Ma et al. 2013). The pancreatic TALK-1 channels that is alkaline activated, like its subfamily members TALK-2 and TASK-2, are associated with β-cell glucose-stimulated insulin secretion, thus its malfunction is thought to play a key role in diabetes (Graff et al. 2020). The halothane sensitive channels of the THIK subfamily are found in the kidney, trigeminal ganglion (TG) neurons, microglia, as well as in the heart and atrial. They are proposed as novel drug targets for patients with atrial fibrillation or heat failure, as their down

regulation was observed within the tissue of such patients (Blin et al. 2014; Kang, Hogan, and Kim 2014). The Ca^{2+} activated TRESK channel also found in TG neurones as well as in sensory ganglion neurons are thought to be involved in sensory transduction and nociception. In example a frame shift mutation (F139WfsX24) within the KCNK18 gene leads to a loss of function of the encoded TRESK channel and was identified to cause severe migraine (Andres-Bilbe et al. 2020; Lafrenière et al. 2010). However, all dose outlined regulation mechanisms and their consequent implications for the well function of the human body only cover a little proportion of the versatile stimuli that regulate this diverse channel family. Physiological and pharmacological stimuli that are examined in this present study are discussed in more detail in the following sections.

1.3.1 Physiological regulation of K2P channels

This section outlines the physiological stimuli acting on potassium channels that are studied experimentally in this work. First the regulation of K2P channels by changes in pH and second the distribution of signalling lipids such as PIP_2 and Oleoyl-CoA and their impact on channel activity.

1.3.1.1 pH regulation

Except for THIK-1 and THIK-2 all remaining 10 K2P channels that are measurable in heterologous expression systems show pronounced sensitivity to alterations in pH values of their surroundings (Lesage and Barhanin 2011; Rajan et al. 2001).

TREK-1, TREK-2, TRAAK

Extracellular pH (pH_o) changes to more acidic pH values leads to a current decrease in TREK-1 channels. The apparent *pK*a recorded at 0 mV is 7.35 and 7.32 at 50 mV, showing that the inhibiting effect of H^+ is not voltage dependent. In contrast intracellular acidification promotes channel activation. Thereby, the residue E306 (in this study, due to different sequence counting referred as E321) was proposed as intracellular proton sensor and the residue H126 as extracellular sensor (Sandoz et al. 2009). A replacement by alanine, mimicking the protonated

state, renders the channel activation. Interestingly, TREK-2 is activated by both, intracellular as well as extracellular acidification, with a *pK*a of 7.3. The conserved histidine 151 (TREK-1 H126) functions also as pH sensing domain, however with the opposite effect on channel activity. This oppositional effect was explained by Sandoz et al. (2009) by the differential electrostatic interaction partners of the H^+ sensing histidine in TREK-1 and TREK-2. While in TREK-1 two of the interacting residues are negatively charged (D263, E265) and therefor attracted by the protonated histidine upon acidification, the corresponding residue in TREK-2 is positively charged (R293) and probably undergoes electrostatic repulsion. Crystallographic studies of TREK-2 by Dong et al. (2015) also confirm H151 (in this study counted as H156) as proton sensor that is located between the ECD and pore helix 1 of the transmembrane domain next to the pore region. However, they propose the residues E98 (E103, resp.) and A174 (A179, resp.) as interacting partners, shown in Figure 11 (Dong et al. 2015). TRAAK is inhibited by acidic pH_o and the histidine found in TREK-1 and TREK-2 is also conserved in this channel (here H85) and was equally identified as proton sensor (Sandoz et al. 2009). In contrast to TREK-1, TRAAK channels are opened by intracellular alkalinisation and the homolog residue of the intracellular TREK-1 proton sensor (TRAAK: E286, TREK-1: E321 (E306)) was shown to be not involved in pH regulation (Kim et al. 2001).

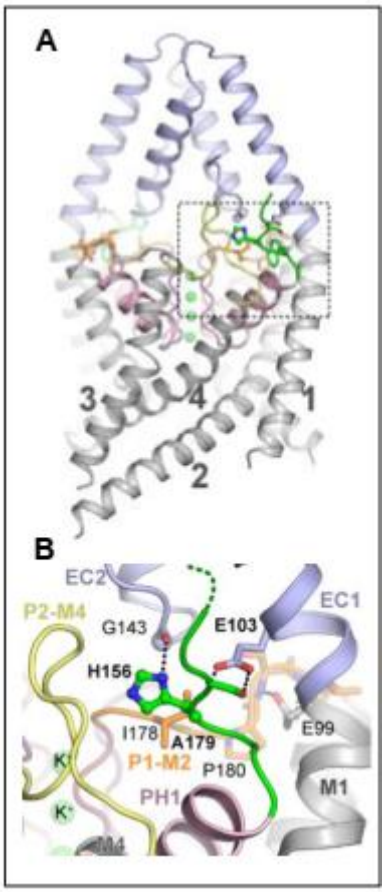

Figure 11 – The extracellular pH sensor in TREK-2. A) The external pH sensor region centered on His156. **B)** The sensor histidine (His156, green) is located between the extracellular domain (EC) (pale blue) and pore helix 1 (PH1) of the TMD adjacent to the pore region (Figure S12 A, B. in **Dong et al. 2015**, PDB Entry: 4BW5)

TASK-1, TASK-3

TASK-1 and TASK-3 channels are strongly inhibited by external acidification. TASK-1 has a *pK*a value of 7.3, as well as the equally inhibited TASK-1/TASK-3 heterodimers (Czirják and Enyedi 2002; Duprat et al. 1997). TASK-3 has a lower *pK*a of 6.0 – 6.7 and is fully active at pH 7.4 (Rajan et al. 2000). 90 % of the TASK-1 current is recorded at a pH_o 7.7 and less than 10 % of the current remains at pH_o 6.7.

A voltage dependence of the pH sensitivity was not observed, however a *pK*a shift to 6.8 was observed in high K^+ solution (100 mM) for TASK-1 channels, suggesting a competition of H^+ and K^+ ions for the same binding side (Morton et al. 2003). Shown in crystal structure, histidine 98 and its interaction partner Q209 were proposed as proton sensor, both extracellularly adjacent to the selectivity filter, shown in Figure 12 (Rödström et al. 2020). Intracellular sensitivity to pH changes is not yet reported.

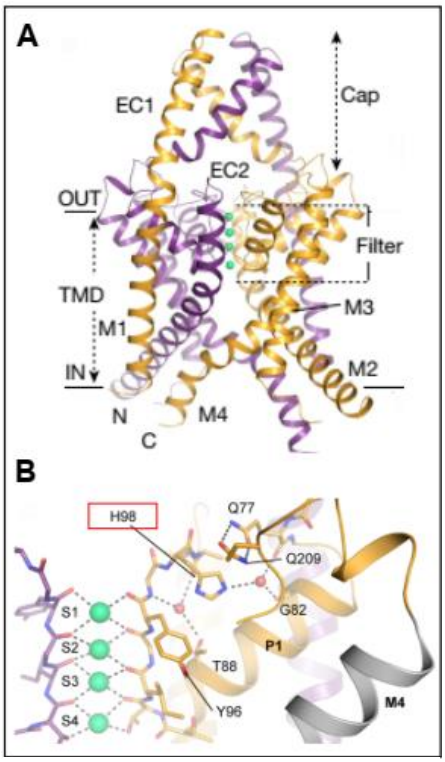

Figure 12 – The extracellular pH sensor in TASK-1. A) TASK-1, with chain A in gold, chain B in purple, K^+ ions in green. **B)** The pH-sensor residue, His98, the surrounding residues and the selectivity filter. Figure 1A and S2c**, Rödström et al. 2020,** PDB entry: 6RV2

TASK-2, TALK-1, TALK-2

TASK-2, despite of its name, belongs to the alkaline activated TALK subfamily. Accordingly, all three channels are activated by extracellular alkalisation. The *pK*a of TASK-2 was determined for extracellular pH changes at 8. TALK-1 and TALK-2 show a maximal channel activity at pH_o >10, thus their sensitivity is even more shifted to alkalic values (Decher et al. 2001; Girard et al. 2001; Reyes et al. 1998). TALK-2 and TASK-2 are also activated by alkaline pH_i values. Thereby, the residue K245 in TASK-2 was identified as putative pH sensor, as its mutation to alanine supposedly abolishes its sensitivity towards alkaline stimuli (Niemeyer et al. 2016). Crystallographic studies supported this hypothesis, as this residue was observed to undergo a conformational change upon alkalisation. As shown in Figure 4, the residue faces into the intracellular mouth of the channel at acidic pH 6.5 and rotates by ~90° upon intracellular alkalisation at pH 8.5. In this position it is pointing towards a proline at TM2, resembling the deprotonated state of the lysine. Supposedly, the *pK*a shift from 10.5 to lower values necessary for a deprotonation of the residue, is facilitated by the hydrophobic bottom face of TM2. Extracellularly, the residues R224 and N82 were further identified as pH sensing domain, depicted in Figure 13 (Li et al. 2020).

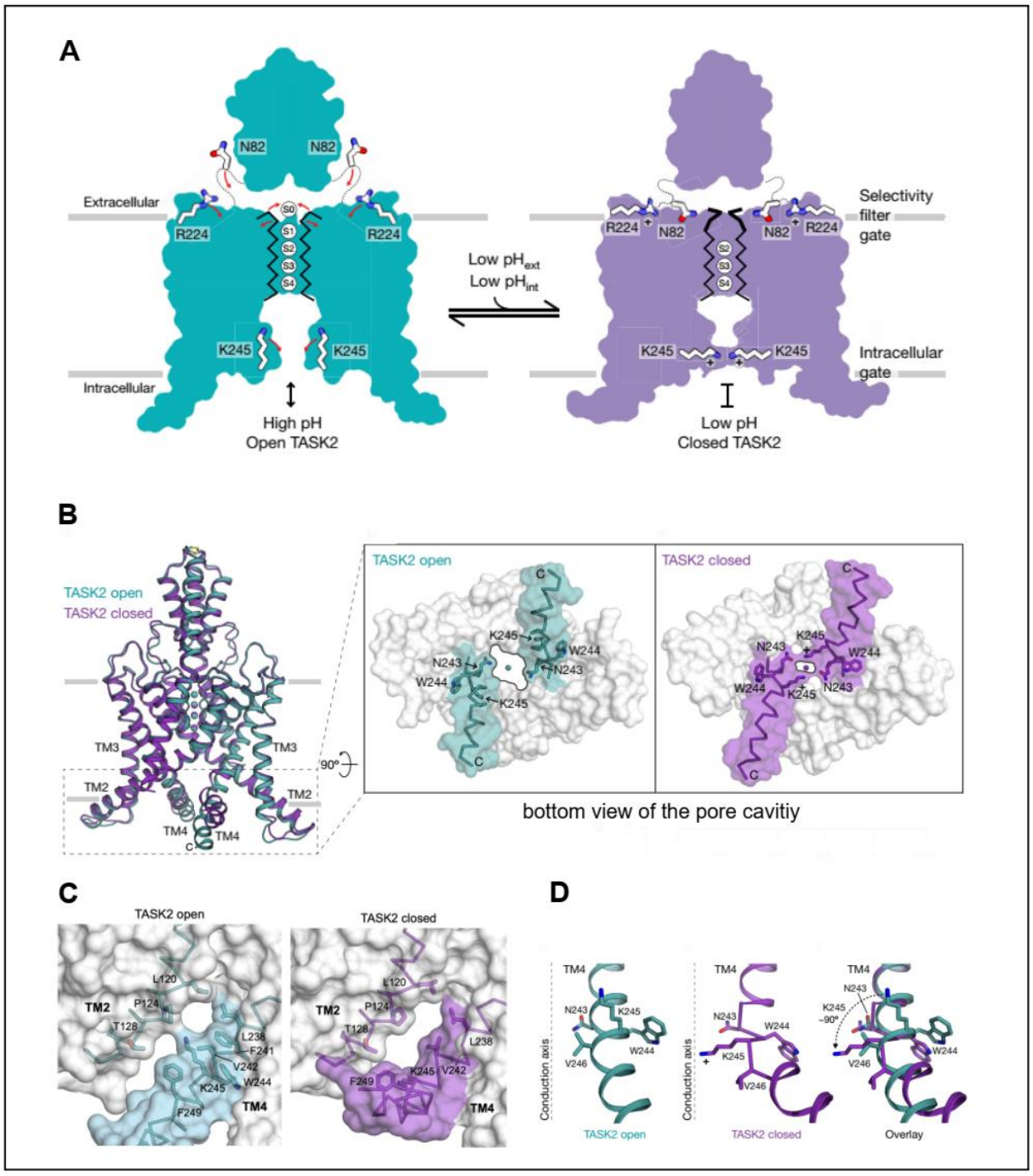

Figure 13 – The pH sensor in TASK-2 channels. A) Cartoon depicting the conformational changes of the extracellular pH sensing residues (R224, N82) and the intracellular K245 under high pH (turquoise, open channel) and low pH (purple, closed channel). **B)** TASK-2 channel structure at the open (turquoise) and closed (purple) state. The inset shows the bottom view of the pore cavity, that is narrowed upon acidification and widened upon alkalization, due to conformational changes of K245. **C)** Higher resolution of TM2 and TM4, depicting the interaction of K245 and P124 at TM4. D) Conformation of the residues 243-246 at the open and closed state, and shown as overlay. Figures are copied from Figure 5 (A) Figures 3 a-f (B, D) and Extended Data Figure 6 (C) from (Li et al. 2020).

TWIK-1

Within the TWIK channel family only TWIK-1 shows sensitivity towards external pH changes. Due to sumoylation of the lysine 274, TWIK-1 channels expressed in the granule cell layer are silent at the cell surface. Upon desumoylation, TWIK-1 becomes active and becomes sensitive to pH changes, similar to the TASK channels (Plant et al. 2012; Rajan et al. 2005). Thereby, extracellular acidification leads to current inhibition with a *pK*a of 6.7 underlying the same histidine dependent mechanism as it is observed for TASK-1 and TASK-3 (Lesage, Guillemare, et al. 1996; Lopes et al. 2001; Rajan et al. 2000, 2005). Accordingly, a replacement of the histidine 122 residing within the first P-loop to asparagine leads to pH insensitivity of the channel. Notably, TWIK-1/TASK-1 heteromeric channels expressed in cerebellar granule neurons were shown to be silenced due to sumoylation of the TWIK-1 subunit. A desumoylation also leads to channel activation that is yet again inhibited by external acidification (Plant et al. 2012). Interestingly, it was observed that under subphysiological extracellular potassium concentrations, that i.e. occur during pathological hypokalaemia, TWIK-1 channels switch their ion selectivity and become permeable to external Na^+ ions. Similarly, an inward Na^+ conductance by TWIK-1 was also observed upon external acidification which may contributes to cardiac arrythmias (Ma et al. 2011).

TRESK

TRESK channels are sensitive to external and internal pH changes. However, their activity changes by external pH variation is not as pronounced as observed for other K2P channels (i.e. TREK or TASK). Thereby, extracellular acidification leads to channel inhibition of about 20 % at pH 5.6, while alkalisation to 8.9 results in channel activation by 20 % when compared to a basal current at pH 7.3. By contrast, intracellular acidification results in a potent channel inhibition (60 % at pH 5.6) and alkalisation to a current increase in respect to the physiological pH at 7.3. Thus, the TRESK channel is more sensitive to intracellular than to extracellular pH changes (Sano et al. 2003).

1.3.1.2 Regulation of K2P channels by lipids

Membrane proteins such as ion channels are often regulated by lipids. This regulation occurs to be either linked to changes of the physical characteristics of the lipid bilayer in which the

proteins are incorporated or by changes of the hydrophobic interaction between the membrane protein and the lipid bilayer. Additionally, the binding of the lipid to a specific site of the ion channel might also alter the gating properties of an ion channel or leads to an increase or decrease of ion permeability. Finally, a regulation might also occur indirectly by the activation of signalling pathways (i.e. PKC signalling pathway), where arising metabolites than act on the gating mechanisms of an ion channel (Chemin et al. 2007; Decher et al. 2010; Meves 2008; Wilke et al. 2014). It was shown, that the mechanosensitive TREK/TRAAK subfamily is sensitive to lipids such as phospholipid phosphatidylionositol-4,5-bisphosphate (PIP_2) or arachidonic acid (Chemin et al. 2005; Lesage, Terrenoire, et al. 2000), however a systematic study of all K2P channels is still missing. Within this study the effect on K2P channel activity upon intracellular exposure to polyanionic lipids such as PIP_2 and the long-chain coenzyme A (CoA) ester Oleoyl-CoA was examined and are therefore discussed in more detail in the following section.

PIP_2

Polyphosphoinositides such as PIP_2, are derivatives of the phospholipid phosphatidylinositol (PI) that are reversibly phosphorylated. This phosphorylation occurs at the inositol ring of the amphiphilic molecule mediated by several cytoplasmatic lipid kinases adding phosphates to the hydroxyl groups on the inositol positions 3, 4 or 5. Accordingly, dephosphorylations at those sites are mediated by lipid phosphatases. In lipid bilayers, the negatively charged headgroup faces towards the cytoplasm and the nonpolar hydrophobic fatty acid tails are embedded in the cytoplasmatic leaflet of the lipid bilayer (Dickson and Hille 2019). Despite its relatively low abundance of about 1 % in cellular membranes compared to other phospholipids, PIP_2 plays an important role in cell signalling. Present in all eukaryotic plasma membranes it is involved in a variety of essential cellular processes such as endo- and exocytosis, the adhesion of the actin cytoskeleton and the lipid bilayer, as well as the here discussed regulation of ion channels (Aikawa and Martin 2003; Huang 2007; Logan and Mandato 2006; Raucher et al. 2000; Shukla et al. 2019). Characteristically, PIP_2 possesses two hydrophobic tails that are usually stearic and arachidonic fatty acids, however they are variable in different species or tissues. The highly negative headgroup with an electrostatic charge of -3 at physiological pH 7.2 (van Paridon et al. 1986; Toner et al. 1988) is especially important for the interaction with membrane proteins, were i.e. a cluster of basic residues can bind the phospholipid (McLaughlin and Murray 2005). Usually, PIP_2 is found restrictedly within the inner leaflet of the plasma membrane, where it is

often found clustered, thus increasing the local concentration of the phospholipid (Ingólfsson et al. 2014). Down regulation of PIP_2 at the plasma membrane is mediated by two main pathways (i) by phospholipase C (PLC) mediated hydrolysis and (ii) by dephosphorylation through PI(4,5)P2-5-phosphatases (Dickson and Hille 2019; Liu and Bankaitis 2010).

Within the K2P channel family several members are regulated by either PIP_2 directly or by a metabolite emerging from the PLC mediated PIP_2 depletion. I.e. members of the TREK/TRAAK as well as the TASK subfamily have been shown to be regulated by the intracellular application of PIP_2 as well as by its endogenous appearance within the cytoplasmatic leaflet of the examined cells (Chemin et al. 2005; Lopes et al. 2005).

Oleoyl-CoA

Long-chain acyl-CoA esters (LC-CoA) such as Oleoyl-CoA play a key role within the cellular fatty acid metabolism. Thereby, LC-CoA represents the metabolizable form of cellular long chain fatty acids. Via carnitine, acyl-CoA esters are transferred into the mitochondrial matrix, were they serve as substrates for the β-oxidation. Within the heart long-chain fatty acids represent the main metabolic substrates. An accumulation of LC-CoA esters within the cytosol was described under hypoxic conditions, were its further metabolization is impaired due to a reduced β-oxidation (Larsson et al. 1996). Furthermore, LC-CoA plays an important role as signalling molecule. It was shown in previous studies, that elevated concentrations of Oleoyl-CoA regulate ion channel activity (Liu et al. 2001; Rapedius et al. 2005; Shumilina et al. 2006). As indicated in Figure 14, cardiac K_{ATP} channels show a potent channel activation by Oleoyl-CoA and an inhibition by free fatty acids, linking the myocardial energy metabolism to changes in electrical activity of the heart (Liu et al. 2001). Similarly, K2P channels might be regulated by Oleoyl-CoA, which is studied in greater detail in this work (see section 3.1.3).

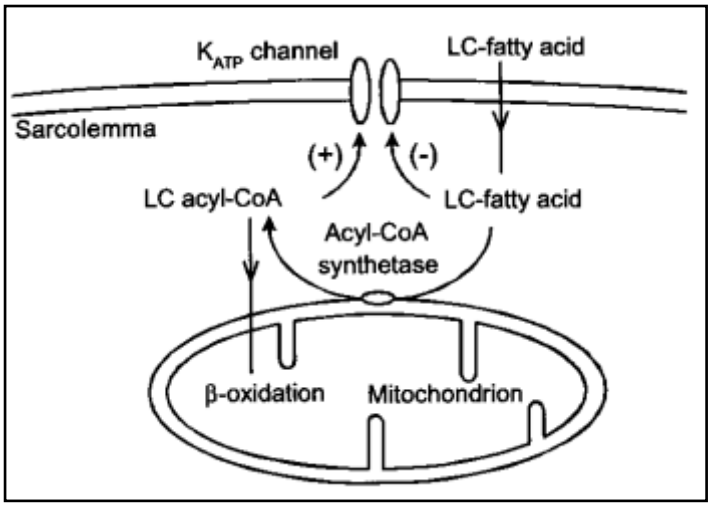

Figure 14 – Schematic diagram of the long chain fatty acid metabolim and KATP channel activity in cardiac tissue (Liu et al. 2001, Figure 7). CoA = Co enzyme A, LC = long chain, (+) activation, (-) inhibtion

1.3.2 Pharmacological regulation of K2P channels

Since their discovery 25 years ago, the role of K2P channels has emerged from poorly gated leak channels to highly regulated, voltage dependent K^+ channels. Due to their versatile regulation and function in physiological and pathophysiological processes within the human body, K2P channels have gained recognition as pharmacological targets. Thereby, several drugs have been identified to act on the different family members in a very versatile manner. This includes general and local anaesthetics, neuroprotectants, antidepressants as well as antipsychotics or cytostatic drugs. While i.e. TREK-1, TREK-2 as well as TASK-1, TASK-3 and TRESK channels are activated by volatile anaesthetics such as halothane or isoflurane (Heurteaux et al. 2004; Huang, Yu, and Fan 2008; Patel et al. 1999; Talley and Bayliss 2002), THIK-1 and THIK-2 channels show current inhibition by those substances (Rajan et al. 2001). In addition, the local anaesthetics lidocaine and bupivacaine were proven to inhibit TREK-1, TASK-1 as well as TASK-2 channels (Kindler et al. 2003; Nayak et al. 2009; Punke et al. 2003). Psychoactive substances such as the antidepressants fluoxetine (registered as 'Prozac') and its derivative norfluoxetine (NFx), chlorpromazine or haloperidol, that is i.e. deployed as therapeutic for acute and chronic schizophrenia are TREK-1 inhibitors (Kennard et al. 2005; Thümmler, Duprat, and Lazdunski 2007). By contrast, the mood stabilizers Lithium chloride, gabapentin, valproate and carbamazepine were shown to be TREK-1 activators, but ineffective for the closely related TREK-2 channels (Kim et al. 2017).

As already discussed, K2P channels are expressed within several tissues among the human body. Therefore, it is from great importance to determine their sensitivity not only to new developed substances, but also to already registered drugs. I.e. major side effects that are typically triggered by antipsychotics are symptoms such as parkinsonism or dystonia as well as weight gain, diabetes or cardiovascular disorders (Miyamoto et al. 2005). As K2P channels were shown to play an important role in a number of those disease (i.e. TALK-1 in diabetes or TASK-1 in PAH (Graff et al. 2020; Ma et al. 2013)) it is highly important to determine not only the effect of therapeutics, but also to study their cross reactivity among ion channels.

For instance, a group of small molecules (i.e. BL-1249, ML33-66, NS11021) all of which are carrying a negatively charged tetrazole or carboxyl group were shown to potently activate not only most of the K2P channels, but also voltage gated hERG channels and Ca^{2+}-activated BK_{Ca} channels (Bentzen et al. 2007; Pope et al. 2018; Schewe et al. 2019; Zhou et al. 2005). Interestingly, it was hypothesized that this cross-reactivity occurs due to a shared gating

mechanism among those channels. It was shown that these negatively charged activators (NCAs) bind below the selectivity filter (SF) and thereby attract K^+ ions to bind within the pore cavity. This increases the ion occupancy at the S1 and S4 site of the SF, altering the conformation of the filter into its active, ion conductive state (Schewe et al. 2016, 2019). This mechanism was supported by the observation, that all NCA responsive channels, were also activated by Rb^+ ions, which are as well increasing the ion occupancy at those SF sites. Accordingly, mutations known to reduce the S1 and S4 occupancy, abolish the Rb^+ as well as the NCA activation of these channels. Furthermore, this observed current increase (due to the NCA binding) was antagonised by quaternary ammonium ions (QAs), such as tetrapentyl- (TPA) or tetrahexylammonium (Schewe et al. 2019). Those compounds were proven to block the ionic current by their binding deep within the inner pore cavity of potassium channels. As their binding site resides directly under the SF, the pore cavity must be freely accessible to this blocker (Armstrong 1971). Therefore, QAs, often referred as open channel blockers, have emerged as important tools to study the inner pore structure of ion channels. In example, QA ions have been deployed to study the pore structure of K2P channels. Thereby, TREK-1 channels show a state independent block by TPA via the permeation pathway, thus the inner pore of the channel allows the binding of TPA even in the closed state (i.e. at alkalic pH) of the channel (Piechotta et al. 2011; Rapedius et al. 2012) (see section 1.2.2). These observations point out, that pharmacological studies do not only serve for medical applications, but also allow an insight into gating mechanisms of the targeted channel.

In this work, the antidepressant NFx, the spasmolysant 2-aminoethoxydiphenylborat (2-APB), which was proven to activate TREK/TRAAK channels (Beltrán et al. 2013), ONO-RS-082 a registered antidote for pulmonary arterial hypertension that is i.e. acting on TASK-1 channels (Ma et al. 2013) as well as the NCAs (like BL1249) and the QA (TPA) were used to study the relationship between gating stimuli and the structural regulation of K2P channels.

2. Material and Methods

2.1 Materials

2.1.1 Chemicals

All used chemicals were obtained from Merck ((Sigma Aldrich) Darmstadt, DE), Roth (Karlsruhe, DE), Serra (Heidelberg, DE), Tocris (Bristol, UK), Cayman Chemicals (Michigan USA), Axon Medchem (Groningen, NL), Toronto research chemicals (Toronto, Canada), Biomol (Hamburg, DE) or were synthesized by Marc Nazaré (FMP, Berlin, DE). If not indicated otherwise all solutions were prepared in deionized water (ddH_2O).

2.1.2 Buffers and Solutions

Frequently used buffers and solutions used for oocyte preparation and electrophysiological experiments were listed in the table below:

Table 2 – Composition of buffers and solutions

Solution	Composition
DNA, RNA synthesis	
LB (SOC) medium	2 % trypton, 0,5 % yeast extract, 10 mM NaCl, 2.5 mM KCl, 10 mM $MgCl_2$, 10 mM $MgSO_4$ und 20 mM glucose (Thermo Fisher Scientific)
LB plates	1 L LB (SOC) medium + 15 g agar and 100 µg µl-1 ampicillin
1 x TEA buffer	40 mM Tris-acetate, 1 mM EDTA (pH 8)
DNA-loading buffer	90 % formamide, 10 mM EDTA (pH 8), 0.05 % bromphenol blue, 0.05 % xylene cynol FF
Oocyte preparation	
Narcotic solution	6.25 g Tricaine, 250 mL $NaHCO_3$ 0.5 M, 5 L H_2O
OR2	82.5 mM NaCl, 2 mM KCl, 1 mM $MgCl_2x6H_2O$, 5 mM HEPES, pH 7.2
ND96	96 mM NaCl, 2 mM KCl, 1.8 mM $CaCl_2$, 1mM $MgCl_2$, 5 mM HEPES
Oocyte storage solution	54 mM NaCl, 30 mM KCl, 2.4 mM $NaHCO_3$, 0.82 mM $MgSO_4$, 0.41 mM $CaCl_2$, 0.33 mM $Ca(NO_3)2$, 7.5 mM TRIS, pH 7.2 adjusted with NaOH/HCl (+100 µg/mL Strep/100U/ml Pen)
Electrophysiology	
K^+ pipette solution	120 mM KCl, 10 mM HEPES, 3.6 mM $CaCl_2$, pH adjustment with KOH/HCl (pH 7.4, pH 10)
Rb^+ pipette solution	120 mM RbCl, 10 mM HEPES, 3.6 mM $CaCl_2$, pH adjustment with RbOH/HCl (pH 7.4)
K^+ bath solution	120 mM KCl, 10 mM HEPES, 2 mM EGTA, 1 mM Pyrophosphat, pH adjustment with KOH/HCl (pH 5 to pH 10)
Rb^+ bath solution	120 mM RbCl, 10 mM HEPES, 2 mM EGTA, 1 mM Pyrophosphat, pH adjustment with RbOH/HCl, (pH 7.4)

2.2.3 Compounds and reagents

Used compounds and reagents, as well as storage and usage information were listed in the following table:

Table 3 - used compounds and reagents

Abbreviation	Storage	Stock concentration	Final concentration, usage	Provider
channel regulation (physiological)				
Oleoyl-CoA (18:1)	- 20 °C	2 mM, DMSO	10 µM, K^+ bath solution, RT (room temperature)	Merck (Sigma Aldrich)
PIP_2	- 20 °C	1 mM, DMSO	10 µM, K^+ bath solution, RT	Merck (Sigma Aldrich)
Poly Lysine	- 20 °C	30 mg / ml	30 µg / µl, K^+ bath solution, RT	Merck (Sigma Aldrich)
BSA	RT	-	5 mg / ml, K^+ bath solution, RT	Merck (Sigma Aldrich)
DiC8 DAG	- 20 °C	10 mM, DMSO	20 µM, K^+ bath solution, RT	Merck (Sigma Aldrich)
channel regulation (pharmacological)				
2-APB	- 20 °C	100 mM, DMSO	1 - 2000 µM, K^+ bath solution, RT	Merck (Sigma Aldrich)
Drofenine	- 20 °C	20 mM, DMSO	1 - 2000 µM, K^+ bath solution, RT	Merck (Sigma Aldrich)
BL-1249	- 20 °C	50 mM, DMSO	50 µM, K^+ bath solution, RT	Tocris
NS11021	- 20 °C	50 mM, DMSO	50 µM, K^+ bath solution, RT	Tocris
ML67-33	- 20 °C	50 mM, DMSO	50 µM, K^+ bath solution, RT	FMP (Marc Nazaré)
DCPIB	- 20 °C	50 mM, DMSO	10 µM, 50 µM, K^+ bath solution, RT	Tocris
ONO-RS-082	- 20 °C	50 mM, DMSO	0.1 - 50 µM, K^+ bath solution, RT	Cayman Chemicals
NFx	- 20 °C	10 mM, DMSO	0.01 - 100 µM, K^+ bath solution, RT	Merck (Sigma Aldrich)
open channel blocker				
TPA	- 20 °C	100 mM, H2O	0.001 - 1 mM, K^+ bath solution pH 5, 7.4 and 10, Rb^+ bath solution, 0.2, 0.5, 1 mM 2-APB solution, K^+ pipette solution pH 10, RT	Merck (Sigma Aldrich)
TbutA	- 20 °C	100 mM, H2O	0.001 - 1 mM, K^+ bath solution, RT	Merck (Sigma Aldrich)
A1899	- 20 °C	10 mM, DMSO	10 µM, K^+ bath solution, RT	Tocris
AVE0118	- 20 °C	20 mM, DMSO	10 µM, K^+ bath solution, RT	Axon Medchem
cystein modification				
MTS-ET	- 20 °C	-	20 µM in K^+ bath solution, 20 µM DiC8 solution **or** 1 mM in K^+ / Rb^+ bath solution, 0.2, 0.5, 1, 2 mM 2-APB, 50 µM BL-1249, 3 µM ONO-RS-082, 4 µM Oleoyl-CoA solution. RT, **use within 5 minutes!**	Toronto Reasearch Chemicals & Biomol

MTS-TBAO	- 20 °C	20 mM, DMSO	100 µM, K^+ / Rb^+ bath solution, 1 mM 2-APB solution, RT	Toronto Reasearch Chemicals
Decyl-MTS	- 20 °C	200 mM, DMSO	50 µM in K^+ bath solution, 10 µM DCPIB solution or 100 µM in K^+ bath solution pH 5 and pH 7.4	Toronto Reasearch Chemicals

2.1.4 DNA templates, mutations and plasmid vectors

The used vectors and DNA templates as well as the introduced mutations that were examined within this study are listed in the table below:

Table 4 – Used DNA templates, mutations and vectors

Gene name	Protein Name	NCBI Reference Sequence	Organism	Mutation	Vector
KCNK2	TREK-1	NM_172042.2	human	WT	pFAW
		NM_172041.2	rat	WT	pSGEM
				G186C	pSGEM
				K316C	pSGEM
				K317C	pSGEM
				T318C	pSGEM
				K319C	pSGEM
				E320C	pSGEM
				E321C	pSGEM
				V322C	pSGEM
				F325C	pSGEM
				R326C	pSGEM
				S348C	pSGEM
KCNK10	TREK-2	NM_138318.2	human	WT	pFAW
KCNK4	TRAAK	AF_247042.1	human	WT	pFAW
				T264C	pFAW
				M268C	pFAW
				L271C	pFAW
KCNK3	TASK-1	NM_002246.2	human	WT	pFAW
KCNK5	TASK-2	NM_003740.3	human	WT	pFAW
				K245A	pFAW
				K245C	pFAW
KCNK9	TASK-3	XM_011517102.1	human	WT	pFAW
KCNK17	TASK-4 / TALK-2	NM_031460.3	human	WT, transcript variant 1	pSGEM
				L264A	pSGEM
				L145C / L264A	pSGEM
	TALK-2	EU978944.1	human	WT, transcript variant 2	pFAW
				L145C	pFAW

				Q266C	pFAW
				F285C	pFAW
				K261E	pFAW
				K261C	pFAW
KCNK16	TALK-1	NM_032115.4	human	WT	pFAW
KCNK13	THIK-1	NM_022054	human	WT	pFAW
KCNK12	THIK-2	NM_022055.1	human	R11A / R12A / R14A / R15A / R16A / A155P / A383P	pFAW
KCNK18	TRESK	NM_181840.1	human	WT	pFAW
KCNK1	TWIK-1	NM_002245.3	human	I293A / I294A	pFAW

pFAW	pSGEM
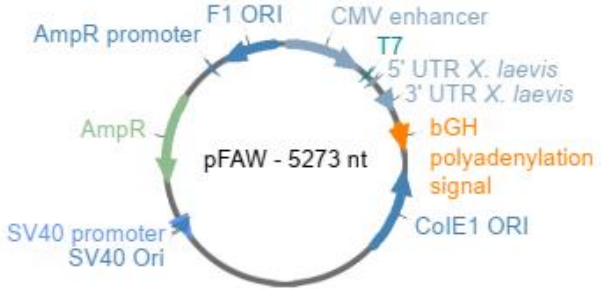	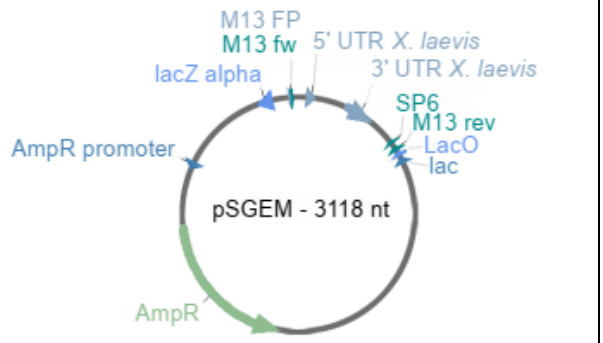

AmpR: Ampicillin resistance, ORI Origin of replication, UTR untranslated region, fw: forward, rev reverse, LacO: Lac operon, bGH: bovine growth hormone polyadenylation signal, ColE1: colicin E1, SV40 (MmPV1): Macaca mulatta polyomavirus1, CMV: cytomegalovirus, nt nucleotides

Notably, the channels THIK-2 and TWIK-1 were not expressed as WT channels as their cell surface expression is reduced due to ER retention signal sequences within their gene. Therefore, those genes were mutated as indicated in the upper table 4, were these residues were replaced by alanine or proline, resulting in an increase of measurable currents in inside out patches.

2.2 Methods

2.2.1 DNA amplification, mutagenesis and cRNA synthesis

A list of DNA templates, plasmid vectors and solutions used in this study is found in the section 2.1 Materials. DNA amplification, mutagenesis and cRNA synthesis was primarily performed by our lab technicians Michaela Unmark and Dr. Hariolf Fritzenschaft. The mutant TASK-4 L26A and TASK-4 L264A / L145C were provided by Susanne Rinné (Institute of Physiology and Pathophysiology, Vegetative Physiology, Philipps-University of Marburg, 35037 Marburg, Germany).

2.2.1.1 Polymerase chain reaction (PCR)

Amplification of DNA sequences *in vitro* was performed by polymerase chain reaction (PCR) with the settings presented in the following table:

Table 5 – PCR settings and sample composition

Step	Process	Temperature [°C]	Time [s]	Repeats		Sample composition	For 50 µl [µl]
1	Initial denaturation	95	120			DNA-template	0.2 (~0.2 - 1 ng μl^{-1})
2	Denaturation	95	30	18 to 30 cycles of step 2 – 4		Primer fw & rev	(each) 1.5 (~0.05 – 0.1 µM)
3	Annealing	50 - 58	30 - 45			Pfu-polymerase	1 (0.025 U μl^{-1})
4	Elongation	72	120 / kb			1x Pfu reaction buffer (from provider)	5
5	Final elongation	72	300			dNTPs	1.5
6	Storage	4				H_2O	39,3

Amplification products were controlled for correct chain length by agarose gel electrophoresis and purified using the NucleoSpin purification kit (Macherey-Nagel, Düren, DE).

2.2.1.2 Site-directed mutagenesis

In particular, the introduction of point mutations into K2P channel sequences was performed by site-directed mutagenesis using the 'QuickChange' protocol (QuickChange II, Stratagene, La Jolla CA, USA). Thereby, two complementary primers carrying the desired mutation at their center were designed for the full PCR amplification of the circular template plasmid using Pfu polymerase (Promega, Madison, WI, USA). A following digest using the *Dpn*I restriction enzyme that cuts only the methylated parental template DNA was performed for one hour. For inactivation of *Dpn*I, samples were kept at 80°C for 15 min. 5 µl of the unmethylated DNA carrying the point mutation was then used for transformation.

2.2.1.3 Transformation of *Escherichia coli* (*E. coli*)

For the transformation 5 µl of the DNA sample were added to 50 µl of competent *E. coli* (DH5α) cells and incubated on ice for 10 minutes. A heat shock was performed for 45 s at 42°C and then returned on ice. Next, 500 µl of SOC liquid medium was added and cells were incubated for one hour at 37°C on a shaker. Subsequently, cells were sedimented at 8000 g for 5 min. 400 µl of the supernatant was discarded and cells were resuspended in the remaining 100 µl SOC medium. Following, they were plated on Luria-Bertani (LB) plates supplemented with 100 µg ml^{-1} ampicillin and incubated over night at 37°C.

2.2.1.4 Plasmid preparation

For plasmid preparation 5 to 15 single clones were harvested from the LB plate obtained from the transformation. Single clones were picked and transferred to 5 mL LB medium to obtain 10 – 25 µg DNA ('Mini prep') or to 50 mL LB medium supplemented with ampicillin (100 µg mL^{-1} to obtain 125 – 500 µg plasmid DNA ('Midi-Prep'). Following, samples were incubated overnight (~16 hours).

DNA isolation by alkaline lysis and following purification was performed using commercial DNA extraction kits (NucleoSpin, Macherey-Nagel, Düren, DE). Finally, the plasmid length and integrity were controlled by agarose-gel electrophoresis and DNA-concentration was determined photometrically (NanoDrop, Thermofisher Scientific, Waltham, MA, USA).

2.2.1.5 Complementary RNA (cRNA) synthesis

Complementary RNA containing a 7-methylguanosincap (cRNA / m^7g-RNA) was generated following the instruction of the AmpliCap-Max T7 (pFAW vector) and SP6 (pSGEM vector) High Yield Message Maker Kits (Cellscript, Madison, WI, USA). The plasmid DNA was linearized by MluI digestion and purified by the DNA purification kit (NucleoSpin, Macherey-Nagel, Düren, DE). Thereby, the DNA-sequence is transcribed complementary into RNA and polyadenylated at the 3'UTR of the linearized vector. Following a phenol-chloroform precipitation RNA was stored in ddH_2O at -20 °C (long term storage at -80 °C). cRNA-concentration was determined photometrically at 260 nm (NanoDrop, Thermofisher Scientific, Waltham, MA, USA) and verified by agarose gel electrophoresis.

2.2.1.6 Agarose gel electrophoresis

Analysis and control of the generated DNA or cRNA products used in this study was done by agarose gel electrophoresis. Therefore, 0.8 - 1 % agarose (w/v) was solved in boiling TEA buffer. For subsequent visualization of the separation, Roti gel stain (1:10'000, Carl Roth, Karlsruhe, DE), was added to the solution before gel polymerization. The fluorescent Roti gel stain intercalates in the DNA and allows their visualization via UV illumination (360 nm, ChemiDoc, Biorad, Hercules, CA, USA. DNA samples were mixed with 6x loading buffer, to the RNA samples and formamide was added for denaturation (Ambion Gel Loading Buffer II, Thermo Fischer Scientific, Waltham, MA, USA). Subsequently, the agarose gel was placed in a TEA buffer filled gel chamber and loaded with the samples that were then electrophoretically separated applying constant 120 mV. To predict the fragment length of the separated samples a 1 kB DNA ladder was loaded additionally to the gel (GeneRuler 1 kb DNA Ladder, Thermo Fischer Scientific, Waltham, MA, USA).

2.2.2 Electrophysiology

All electrophysiological experiments in this thesis were done using inside out macro size patches of stage V-VI oocytes (Dumont 1972) of the South African clawed toad, *Xenopus laevis*, purchased from Fort Atkinson, WI, USA and accommodated at the animal breeding of the Christian-Albrechts University.

2.2.2.1 *Xenopus laevis* oocyte preparation and RNA expression

For the egg extraction, adult females were anesthetized using Tricain (0.2 % in 50 mM $NaHCO_3$) and kept on ice. After the extraction of around 2 cm^3 of ovary tissue animals were stitched up using sterile absorbable surgical strings (Glycolon, Resorba Medical GmbH, Nürnberg) and kept in a shaded box until they recovered from the narcotic. Afterwards they were returned to the animal breeding.

Meanwhile, the ovary tissue was reduced to smaller pieces and incubated at RT for one hour with 2 µg ml^{-1} collagenase type II (Biochrom GmbH, Berlin) solved in OR2 solution (table 2). Subsequently, eggs were washed several times using ND96 solution (table 2) to stop the collagenase reaction and stored at 17°C.

For the heterologous protein expression oocytes were defolliculated manually using fine forceps and injected with about 50 nl of the K2P channel specific cRNA [2 – 4 ng μL^{-1}]. Glass capillaries for the injection were pulled using a Sutter Instrument P-1000 micropipette puller (Novato, CA, USA) and broken sharply at the platin filament of a micro forge (Narishige Scientific instrument, Tokyo, Japan). After the injection oocytes were kept separated in 24-well plates at 17°C for 2 to 14 days.

2.2.2.2 Patch clamp

All electrophysiological measurements were obtained from macro size inside out patches using an EPC10 amplifier (HEKA electronics, Lamprecht, DE). A bath electrode was installed as reference electrode and currents were sampled at 10 kHz and filtered at 3 kHz. Therefore, thick walled borosilicate glass pipettes were pulled in a Sutter Instrument P-1000 micropipette puller (Novato, CA, USA) and their tip was melted using a micro forge (Narishige Scientific instrument, Tokyo, Japan). Subsequently, the pipette resistance was about 0.2 – 0.6 MΩ. Pipettes were filled with pipette solution (Table 2) containing in all measurements 120 mM potassium and was adjusted to pH 7.2, if not indicated otherwise. The intracellular solution was applied using a multi barrel pipette (Figure 15) that was made from 6 double barrel theta glass capillaries stuck together. This allows the exchange of 12 different (bath)solutions to the same patch. At standard conditions the bath solutions contained 120 mM potassium and was adjusted to pH 7.4. If necessary, pH was adjusted (pH 5 – pH 10) and / or compounds and modifying reagents (Table 3) were added.

If not indicated otherwise, measurements in this study were done using either ramp protocols pulsing voltages from -80 to +80 mV with a duration of 1 s and in intervals of 9 s, continuous pulses at +40 mV or rectangle pulses with a duration of 0.3 s from a holing potential at -80 mV ranging from -100 to +100 mV in 20 mV steps.

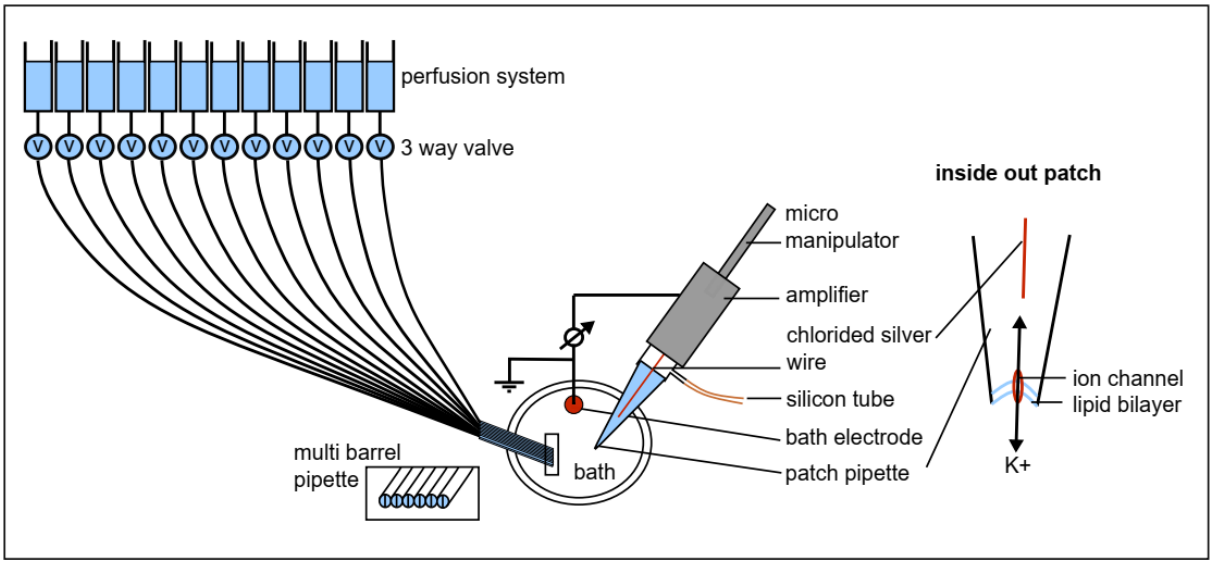

Figure 15 – Patch clamp experimental setup. The perfusion system to the left is connected to a multi barrel pipette, that allows a quick solution exchange. The bath electrode is connected to the patch clamp amplifier and functions as reference electrode to the chloride silver wire within the patch pipette. The silicon tube allows the application of pressure for patch sealing, after the attachment of the patch pipette to the cell membrane. Subsequently, inside out patches are generated by a rapid up movement using the micro manipulator that is connected to the amplifier.

Some figures presented in this study are planned to be published within this year and include experimental measurements of former and current lab members. The concerning Figures and the contribution of other authors is listed in the following table:

Table 6 – Experimental contribution of other lab members

Figure	channel, number of experiments	Experimenter
19 A - PIP_2 regulation of K2P channels	TALK-2: 6	Dr. Marcus Schewe
21 A - Oleoyl-CoA regulation of K2P channels	TALK-2: 13 (incl. Figure 21 B), TRESK: 5, TREK-1: 4 (incl. Figure 22 A)	Björn Jürs
23A - 2-Aminoethoxydiphenyl borate regulation of K2P channels	TREK-1: 21 (incl. Figure 23 B), TREK-2:12, TALK-2: 4 (incl. Figure 23 B), TASK-1: 4, TASK-2: 11, TASK-1: 4, THIK-1: 13, THIK-2: 10, TRESK:10	Dr. Marcus Schewe
	TALK-2: 9 (incl. Figure 23 B)	Björn Jürs
27 B - Tetrapentylammonium (TPA) accessibility in K2P channels.	TREK-1: 50, TREK-2: 16, TRAAK: 17, TALK-1: 7, TALK-2: 6, TASK-2: 4, TASK-1: 10, TASK-3: 50, TWIK-1: 5, THIK-1: 11, THIK-2: 11, TRESK: 50	Dr. Marcus Schewe, Jan Langer, Björn Jürs
27 F - Tetrapentylammonium (TPA) accessibility in K2P channels.	TALK-2: TPA in K+: 6, TPA in 2-APB 1 mM: 4, TPA in 2-APB 0.2 mM: 7, TPA in 2-APB 0.5 mM: 5, TPA in Rb+: 6	Björn Jürs
38 C - ONO-RS-082 dose response curve of TASK-1	TASK-1: 9	Marcus Schewe

2.2.3 Data recording and analysis

Electrophysiological data were recorded using PatchMaster (Version: v2x73.5, 21.05.2015) from HEKA Elektronik Dr. Schulze GmbH, Lambrecht Germany and were further analyzed using the belonging FitMaster tool (Version: v2x73.5, 21.05.2015). Data were than exported as itx files and statistically and graphically processed using Igor Pro 6.3.7.2 (32-bit release). The relative activation or inhibition of a channel current is shown relative to the basal current $I_{0:}$

Fold change (relative activation %): $\frac{I}{I_0}\ (\cdot 100)$

Inhibition (%): $\left(100 - \left(\frac{I}{I_o}\right) \cdot 100\ \right)$

Dose-response curves were analyzed using the implemented fit function (HillEquation) in Igor.

Hill Equation: $f(x) = base + \frac{(max-base)}{\left\{\frac{xhalf}{x}\right\}^{rate}}$

Where max: the control current in ampere, base: the inhibited current in ampere, X: the concentration of the inhibitor, xhalf: the concentration of half-inhibition and rate: is the Hill coefficient.

The Pymol Molecular Graphic System (Version 2.4.1, Schrödinger, LLC, https://pymol.org) was used for visualization of crystal structures and flagging of relevant amino acids. Image processing was done using the Inkscape vector graphic program (Version 1.0.1 (3bc2e813f5, 2020-09-07, https://.inkscape.org, open source).

3. Results

This section presents first the physiological and pharmacological regulations of K2P channels examined in this work and followingly, presents the results of the investigated gating mechanisms of these channels and their gating regulation by those stimuli.

Except for TWIK-2, TWIK-3 (KCNK7) and TASK-5, all K2P channels are measurable in heterologous expression systems. Notably, TWIK-1 and THIK-2 channels used in this study, do not reflect measurements of the original WT gene, but contain mutations that increase their surface expression (see section 3.1.5).

If not indicated otherwise, all measurements are done using inside out patches from *Xenopus laevis* oocytes and are recorded at room temperature under symmetric K^+ concentrations (120 mM), using the following pulse protocols: (i) Ramps -80 to +80 mV with a duration of 1 second and intervals of 9 s (ii) continues pulses of +40 or -80 mV or (iii) rectangle pulses -100 to +100 mV in 20 mV steps, starting from a holding potential at -80 mV with a duration of 300 ms.

3.1 Physiological regulation of K2P channels

Two pore domain potassium channels are widely distributed in human cellular tissues. Their activity is influenced by a broad range of physical and chemical stimuli like temperature, membrane stretch or pH alterations as well as cellular metabolites such as long chain fatty acids or membrane lipids. The latter (pH and lipids) are examined in this section.

3.1.1 Intracellular pH regulation

Regulation of K2P channels by alterations in pH is well known. Thereby, it was shown extensively that channels of the TREK/TRAAK subfamily, as well as the channels of the TASK and TALK families are inhibited by extracellular acidification (except for TREK-2 that is activated by acidic pH_o) (Decher et al. 2001; Dong et al. 2015; Duprat et al. 1997; Girard et al. 2001; Rajan et al. 2000; Reyes et al. 1998; Sandoz et al. 2009) (see section 1.2.2.1). Although, the regulation mechanisms by extracellular pH changes are well established, the pH regulation from the cytoplasmatic site stays illusive.

To further study the intracellular pH regulation in TASK and TALK channels, current responses to varying pH values ranging from pH 6 to pH 10 were measured in patch clamp experiments. Therefore, inside out patches of *Xenopus laevis* oocytes expressing either TASK-1, TASK-2 or TALK-2 WT channels were measured applying Ramp pulses from -80 to +80 mV, as shown in Figure 16 A to C. For comparison the TREK-1 current response to intracellular acidification at pH 5 is shown in Figure 16 D. As depicted in the pH response curves, TASK-1, TASK-2 as well as TALK-2 are predominantly closed at acidic pH and show a strong activation by intracellular alkalisation compared to physiological pH at 7.4. While, the current increase of the TASK-1 and TALK-2 channels show their highest slop between pH 9 and 10, currents of the TASK-2 channels seam to gradually saturate with increasing pH, yielding an EC_{50} at around pH 8.5.

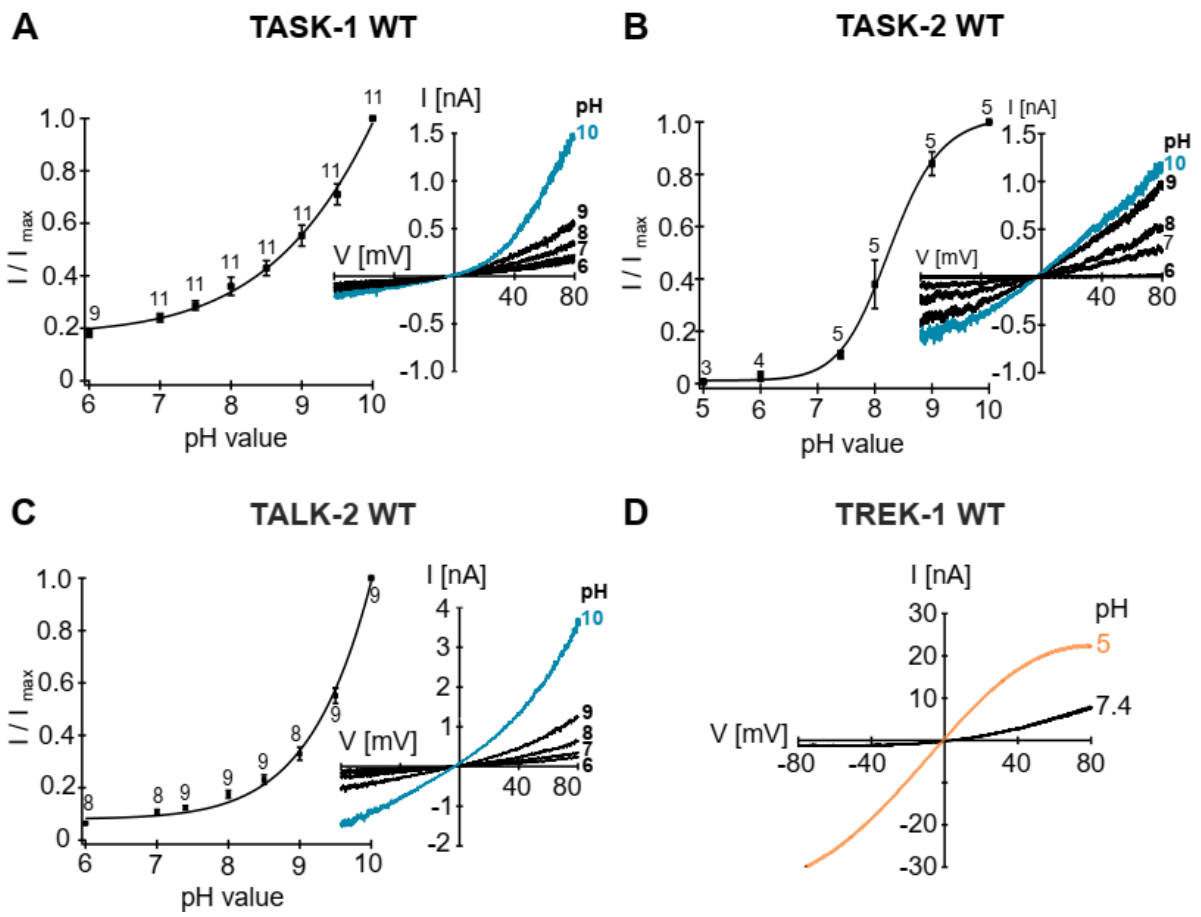

Figure 16 – Intracellular pH sensitivity of TASK and TALK channels. **A-C)** Activation of TASK-1, TASK-2 and TALK-2 channels by intracellular alkalisation shown as pH response curves of TASK-1 (A), TASK-2 **(B)** and TALK-2 **(C)** WT channels ranging from pH 6 to pH 10. Measured in Ramps from -80 to +80 mV with a duration of 1 s using inside out patches of *Xenopus laevis* oocytes under symmetrical K+

(120 mM) conditions (inset) and normalised to I max (at pH 10) at +40 mV. **D)** Example trace of TREK-1 WT currents at pH 7.4 (black) and pH 5 (orange). Measured as in A.

Since the residue K245 was recently proposed as intracellular proton sensor in TASK-2 channels (Bustos et al. 2020; Li et al. 2020) we mutated the putative proton sensing lysin to the residues alanine and cysteine and repeated the pH response experiment using these TASK-2 K245A and K245C mutants. Figure 17 A and B show the resulting pH response curves of the mutant channels (turquoise) compared to the wild type (black). Thereby, the response curves of both mutants show a shift to more acidic values with midpoints around pH 7. While the mutation to alanine also causes an overall decrease in pH sensitivity (visible as a flattening of the response curve and illustrated in the example traces in Figure 17 C), the cysteine mutant remains sensitive to acidification as well as to alkalisation (Figure 17 D), rising questions about the functionality of this residue as proton sensor in TASK-2 channels. Notably, basal currents at pH 7.4 of the mutant K245C and K245A currents are increased compared to the WT currents (Figure 17 E), indicating that this site, is important for channel gating.

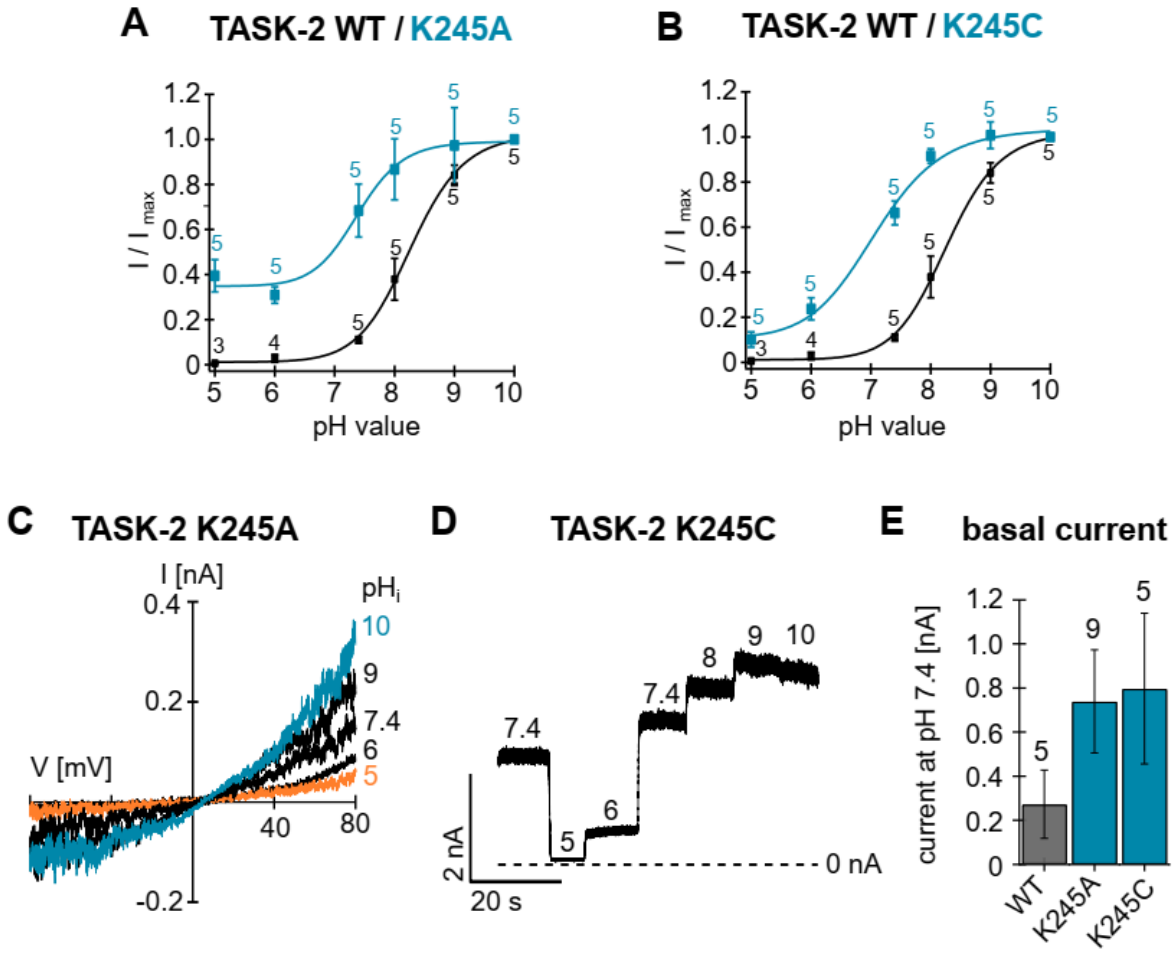

Figure 17 – Intracellular pH sensitivity of TASK-2 K245A and K245C mutant. **A)** Activation of TASK-2 K245A mutant (turquoise) and TASK-2 WT (black) channels by intracellular alkalisation shown as pH response curves ranging from pH 5 to pH 10. **(C)** Normalised current to I max (at pH 10) at +40 mV. **B)** TASK-2 K245C (turquoise) and WT (black) as in A). **D)** Example trace of TASK-2 K245C measured under increasing pH values as indicated. **E)** Bar plot (mean ± SEM) comparing the basal currents of WT, K245A and K245C at pH 7.4 and +40 mV, showing a current reduction for K245A (0.02 ± 0.005, nA, n = 5) and an increase for K245C (0.8 ± 0.34 nA, n = 5) compared to WT currents (0.74 ± 0.23, n = 9).

As TALK-2 is a close relative to the TASK-2 channel, we additionally mutated the homolog lysine at position 261 in the TALK-2 channel to the negatively charged glutamic acid to test weather this mutation would abolish or reduce the pH sensitivity in this related channel. As depicted in Figure 18 A and B, the pH sensitivity for the TALK-2 K261E mutant (turquoise) stays very similar to the wild type, suggesting that this residue is not the proton sensor in TALK-2 channels either. Interestingly, this mutation also causes a current increase in the TALK-2 channel, as shown in the bar plot (Figure 18 C) and therefore might be an important site for the regulation of channel activity.

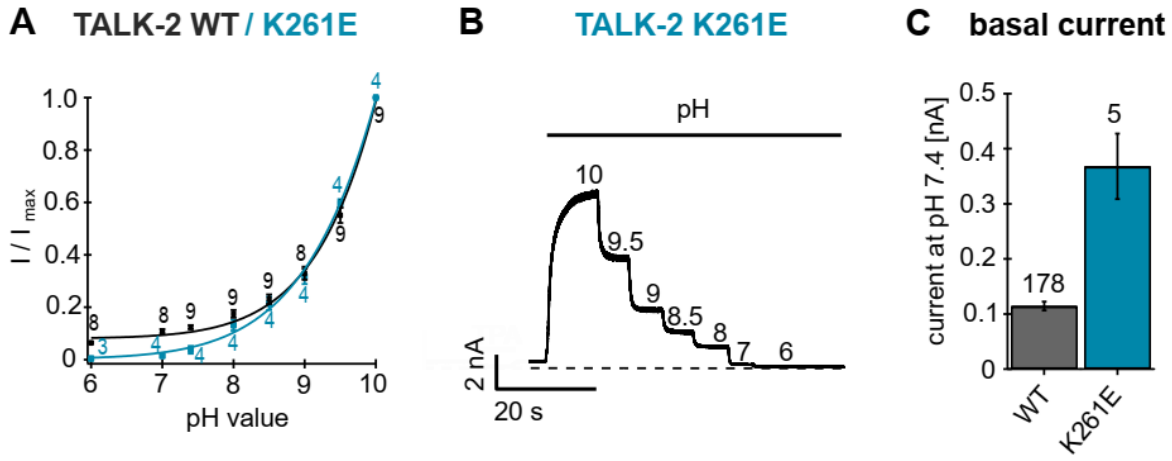

Figure 18 – Intracellular pH sensitivity of TALK-2 K261E mutant. **A)** Activation of TALK-2 K261E mutant (turquoise) and TALK-2 WT (black) channels by intracellular alkalisation shown as pH response curves ranging from pH 6 to pH 10. Measured in Ramps or cont. pulses under symmetrical K^+ (120 mM) conditions and normalised to I max (at pH 10) at +40 mV. **B)** Example trace of TALK-2 K261E mutant measured at cont. +40 mV under symmetrical K^+ concentrations and decreasing pH values from 10 to 6 as indicated. **E)** Bar plot (mean ± SEM) comparing the basal currents of WT and K261E at pH 7.4 and +40 mV, showing a current increase for K261E (0.37 ± 0.01 nA, n = 5) compared to WT currents (0.11 ± 0.06, n = 178).

3.1.2 Regulation of K2P channels by phosphatidylinositol 4,5-bisphosphate (PIP_2)

The phospholipid phosphatidylinositol 4,5-bisphosphate (PIP_2) plays a crucial role as physiological regulator of ion channel activity and therefore excitability of nerves (Chemin et al. 2005; Huang 2007; Lopes et al. 2005).

Here, we tested the direct effect of PIP_2 for 12 K2P channels applying 10 µM PIP_2 to the cytoplasmatic site of the channels in inside out patches. As depicted in Figure 19 A, the responses to this signalling lipid varied strongly within the K2P channel subfamilies, as well as in the efficacy on the particular subtype members. In accordance with previous reports, a very robust channel activation within the TREK/TRAAK subfamily was observed with a fold activation of 17.1 ± 2.85, 10.87 ± 2.85 and 113.56 ± 24.35 for TREK-1, TREK-2 and TRAAK, respectively. Thereby, the activated currents displayed a nearly linear current voltage (I-V) relationship (Figure 20, A / B / C). Members of the THIK subfamily were also activated by PIP_2, with a strong activation for THIK-1 (19.33 ± 2.32) and a weaker activation for THIK-2 (3.91 ± 0.60), however, both displaying again linear I-Vs (Figure 19 B and 20 H). Within the TALK subfamily PIP_2 caused only a ~2-fold activation for TALK-1 and TALK-2. However, the effect of the third subfamily member, TASK-2, was more complex, displaying a biphasic response to PIP_2. As shown in Figure 19 D, in many patches TASK-2 currents showed a strong rundown and the application of 10 µM PIP_2 caused initially a robust activation. However, the activation ceased and finally dropped below the starting level, resulting in 82.80 ± 2.77 % current inhibition. In patches lacking rundown, PIP_2 application caused an inhibition only. In contrast, application of a lower PIP_2 concentration (0.1 µM) did not produce inhibition, but reversed an observed rundown. These findings suggest two distinct regulatory mechanisms in TASK-2 with low PIP_2 concentrations stabilizing the basal channel activity via an activatory site and higher PIP_2 levels causing inhibition, possibly via a distinct inhibitory site.

In the TWIK subfamily only TWIK-1 expressed functionally, but lacked PIP_2 sensitivity and a similar outcome was observed for TRESK channels (Figure 20 F / I).

Finally, the TASK subfamily, were only TASK-1 and TASK-3 are expressed functionally, both channels show a marked inhibition (80.00 ± 1.95 % and 60.83 ± 10.36 %) by PIP_2 (Figure 20, C and Figure 20 G).

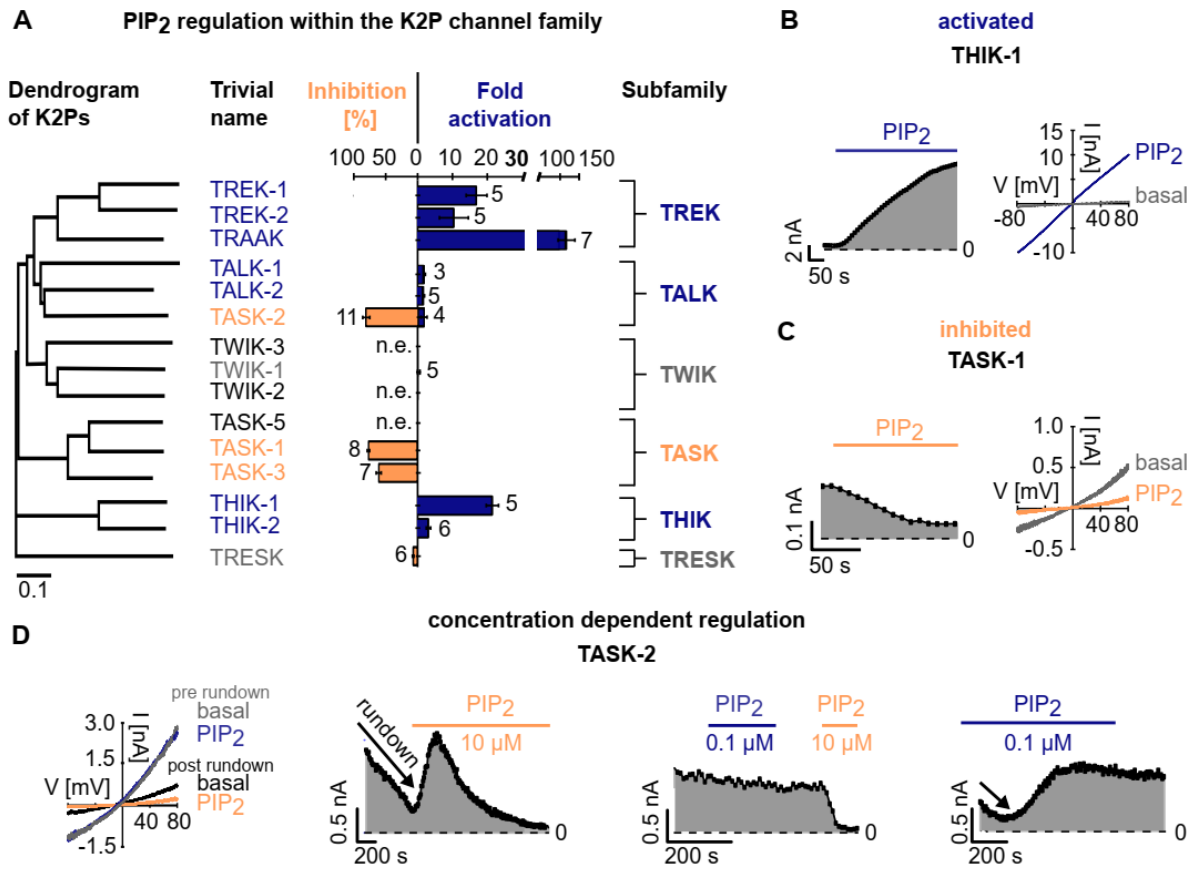

Figure 19 - PIP_2 regulation of K2P channels. A) Activation (blue) and inhibition (orange) of K2P channels (ordered in respect to the dendrogram (Enyedi and Czirják 2010)) by PIP_2 (10 µM) measured in Ramps as shown in B/C/D and analysed at +40 mV, as mean ± SEM, n as indicated above each bar. Fold activation: TREK-1: 17.07 ± 2.85, TREK-2: 10.87 ± 3.96, TRAAK: 113.56 ± 24.35, TALK-2: 1.5 ± 0.14, TALK-1: 2.03 ± 0.03, TASK-2: 2.44 ± 0.29 (initially) & 82.80 ± 2.77 % inhibition (followingly), THIK-1: 21.45 ± 1.67, THIK-2: 3.91 ± 0.60 WT channels. Current inhibition [%]: TASK-1: 80.0 ± 1.95 %, TASK-3: 60.83 ± 3.92 %, TWIK-1: 1.07 ± 0.31 and TRESK: 6.87 ± 1.14 % were not notably affected (grey). n.e. = no expression, channels showing insensitivity were marked in grey. **B-C)** Ramp traces (right) and time curse at +40 mV (left) of the PIP_2 (10 µM) activated THIK-1 (B) and PIP_2 inhibited TASK-1 (C) K2P channels. **D)** Ramp trace and analysed currents at +40 mV of TASK-2 channels showing either a current rundown (left/right) over time or not (middle). The application of low concentrated PIP_2 (0.1 µM) rescues channel rundown (right) but produces no inhibition (middle); 10 µM PIP_2 also rescues rundown if present (left), but leads to a following inhibition of the channel. If no rundown is present 10 µM lead to inhibition only (middle).

In summary, 10 of the 12 investigated K2P channels changed their activity in response to PIP_2, with only TWIK-1 and TRESK lacking a clear PIP_2 sensitivity. Members of the TREK, THIK and TALK subfamilies were activated, but with TASK-2 only initially, whereas members of the TASK subfamily were inhibited.

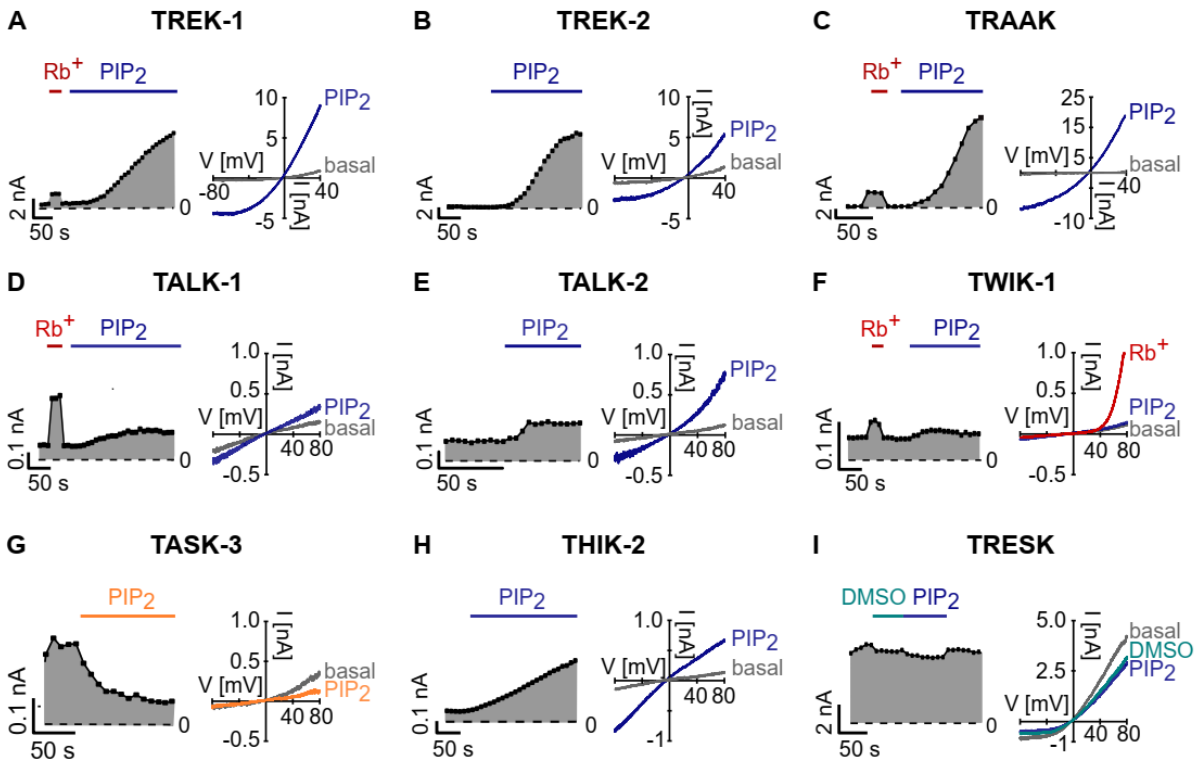

Figure 20 - PIP_2 regulation of K2P channels. A - I) Ramp traces (-80 to +80 mV) using inside out patches of *Xenopus laevis* oocytes (right) and corresponding time curse at +40 mV (left) of the PIP_2 (10 µM) activated TREK-1 (A), TREK-2 (B), TRAAK (c), TALK-1 (D), TALK-2 (E), THIK-2* (Mbr mutant), and PIP_2 inhibited TASK-3 (G) K2P channels. TWIK-1* (I293A/I294A mutant) (F) and TRESK (I) are not affected by PIP_2.

3.1.3 Regulation of K2P channels by Oleoyl-CoA

Further, the lipid sensitivity of the 12 expressed K2P channels was explored by testing the polyanionic lipid Oleoyl-CoA, that represents a common cellular long chain fatty acid metabolite.

Here, the effect of 10 µM Oleoyl-CoA (18:1) was applied to inside out patches from *Xenopus laevis* oocytes and the current response was recorded using a Ramps protocol, as shown in Figure 21 & 22. To demonstrate the time curse of the Oleoyl-CoA regulation and the performed washout (using bovine albumin serum (BSA)) measurements at +40 mV were plotted over time (Figure 21 & 22). For further comparison, regulation effects at +40 mV were normalised to the basal current, shown in Figure 21 A.

Similar to the PIP_2 application, 10 µM Oleoyl-CoA caused strong activation of the TREK subfamily members, with a fold activation of 14.64 ± 3.42, 6.17 ± 1.19 and 39.79 ± 15.46 for

TREK-1, TREK-2 and TRAAK, respectively. These effects were readily reversible upon extraction of Oleoyl-CA from the membrane (Figure 21 B, 22 A, B). THIK channels were also potently activated roughly comparable to the PIP_2 effect (THIK-1: 27.24 ± 2.31, THIK-2: 12.99 ± 0.42). Interestingly, in the TALK subfamily, a massive activation of about 95-fold was observed for the TALK-2 channel while TALK-1 was only moderately activated (4.35 ± 0.46) (Figure 21 B, 22 C). TASK-2 channels were inhibited by 10 µM Oleoyl-CoA by 89.91 ± 2.5 %. Notably, unlike PIP_2, Oleoyl-CoA did not reactivate TASK-2 channels after rundown. TWIK and TRESK channels, that were both insensitive to PIP_2, were inhibited by Oleoyl-CoA. Within the TASK subfamily, only TASK-3 was inhibited by 38.51 ± 5.45 % upon Oleoyl-CoA application, while TASK-1 was insensitive (Figure 21 A, 22).

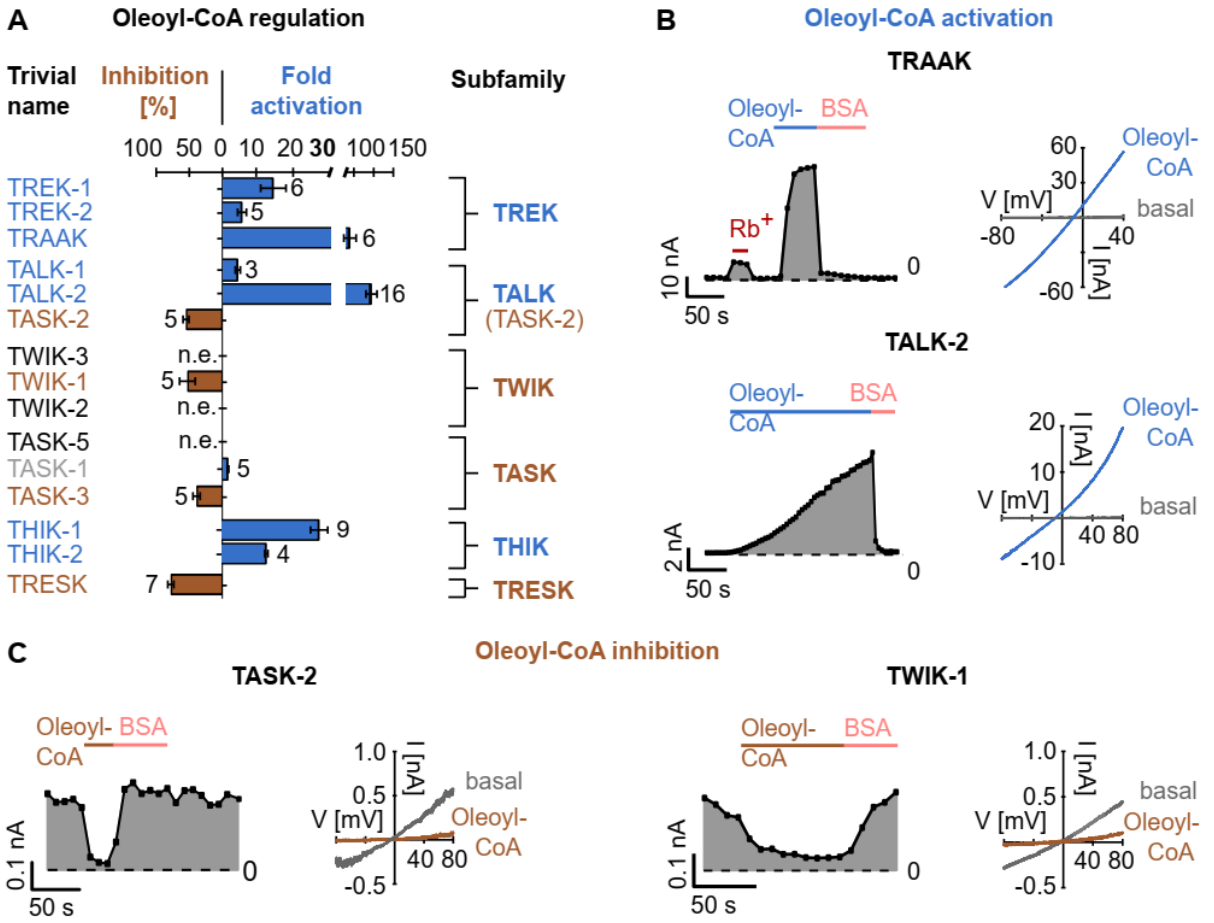

Figure 21 - Oleoyl-CoA regulation of K2P channels A) Activation (blue) and inhibition (brown) of K2P channels by Oleoyl-CoA (10 µM), measured in Ramps and analysed at +40 mV as shown in B/C (mean +/- SEM, n as indicated). Strong activation for TREK-1: 14.65 ± 3.42, TRAAK: 39.79 ± 15.46, TALK-2: 94.33 ± 13.82, THIK-1: 27.24 ± 2.31 and THIK-2: 12.99 ± 0.42. Weak activation for TREK-2: 6.17 ± 0.19 and TALK-1: 4.35 ± 0.46 and TASK-1: 2.3 ± 0.21. Current inhibition [%] for TWIK-1: 52.31 ± 11.88 %, TASK-2: 89.91 ± 2.50 %, TASK-3: 38.51 ± 5.45 % and TRESK: 73.11 ± 4.49 %. **B)** Example traces of Oleoyl-CoA activated TRAAK and TALK-2 channels. **C)** Example traces of Oleoyl-CoA inhibited TASK-

2 and TWIK-1 channels. Measured as described in A. Washout was performed using 5 mg/ml BSA. *measurements of other lab members were included in figure A and B. For more detail see Table 6.

In summary, with the exception of TASK-1, all tested K2P channels changed their activity upon Oleoyl-CoA application and the subfamily response profile (activation vs. inhibition) in general resembled that of PIP_2. However, exceptions to this notion were seen for the strongly Oleoyl-CoA activated TALK-2 channels, that only showed a rather weak PIP_2 response and TWIK-1 and TRESK channels that showed clear Oleoyl-CoA inhibition but lacked PIP_2 sensitivity.

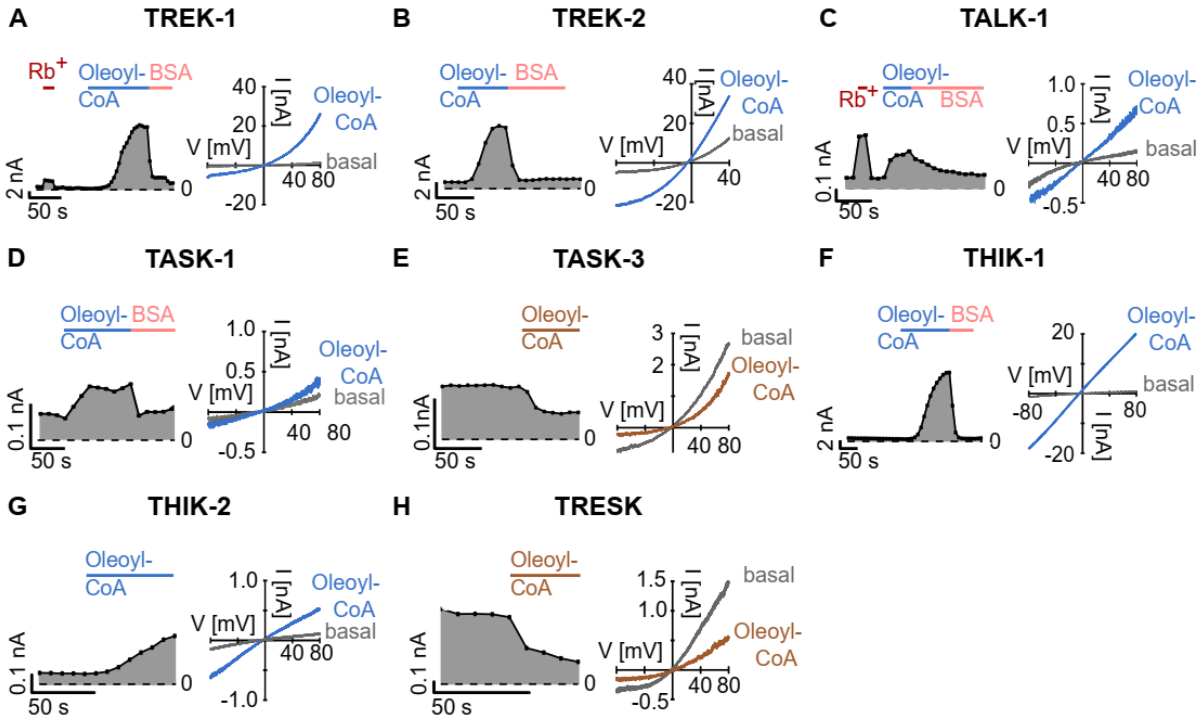

Figure 22 - Oleoyl-CoA regulation of K2P channels A-H) Example traces of K2P channels activated (blue) or inhibited (brown) by 10 µM Oleoyl-CoA, basal current is indicated in grey and washout was performed using 5 mg / ml BSA (orange). Measurements were done using inside out patches of *Xenopus laevis* oocytes and measured in Ramp protocols as shown on the right (A-H) and analysed at +40 mV and plotted over time (left, A-H).

3.2 Pharmacological regulation

3.2.1 2-Aminoethoxydiphenyl borate and Drofenine activate TALK-2 K2P channels

The compound 2-aminoethoxydiphenyl borate (2-APB) was shown to serve as an activator for several ion channels including the channels of the TREK/TRAAK K2P subfamily (Beltrán,

2013). Here, a similar behavior for the TALK-2 channel was observe that becomes potently activated in a dose-dependent manner by 2-APB yielding an EC_{50} of 648 ± 99 µM, shown in Figure 23 B and 23 C.

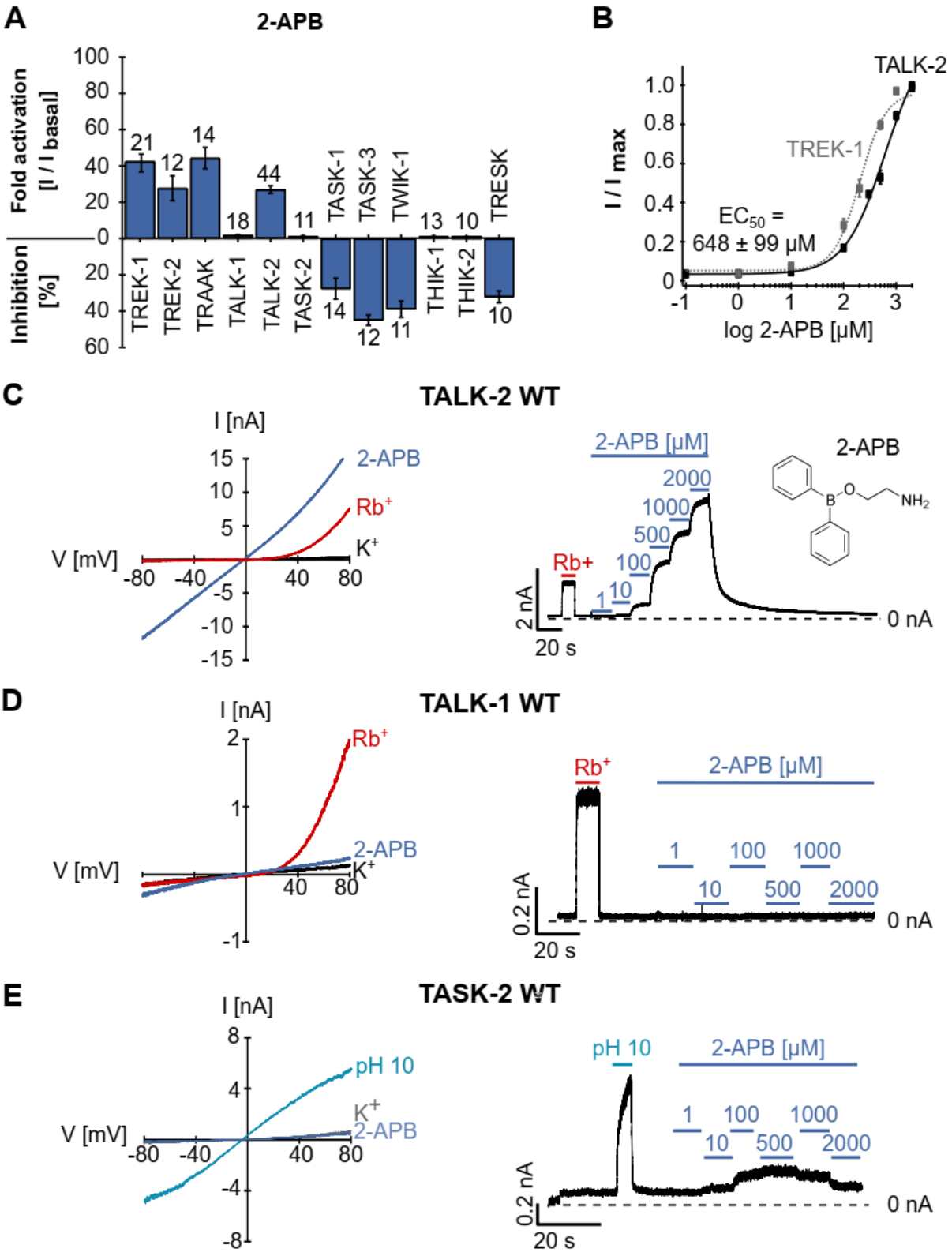

Figure 23 - 2-Aminoethoxydiphenyl borate regulation of K2P channels. A) Fold activation of K2P channels at +40 mV by 1 mM 2-Aminoethoxydiphenyl borate (2-APB, inset C) measured in Ramps and continues pulses at + 40 mV as shown i.e. in C, D, E. **B)** 2-APB dose response for TALK-2 (black) and TREK-1 (grey), yielding an EC_{50} for TALK-2 WT channels of 648 ± 99 µM. **C - E)** Example traces of 2-APB (blue) regulation in Ramps (left, 1 mM 2-APB) and continues pulses at +40 mV (right, 2-APB 1 – 2000 µM) of TALK-2 (C), TALK-1 (D) and TASK-2. For comparison Rb+ (120 mM, red) or pH 10 (turquoise) were applied as indicated. *****Measurements of other lab members were included in figure A and B, see Table 6.

As other K_2P channels were screened for current activation by 2-APB, shown as fold activation upon 1 mM 2-APB at +40 mV in Figure 23 A, we observed that this activating effect stayed restricted to the TREK/TRAAK subfamily and the examined TALK-2 channel. Whereas TWIK-1, TASK-1, TASK-3 and TRESK showed a current inhibition, THIK-1 and THIK-2 as well as the TALK subfamily members TALK-1 (Figure 23 D) and TASK-2 (Figure 23 E) showed none or only moderate activation. Interestingly, as shown in Figure 24, the spasmolysant Drofenine, a structurally related compound, also activated TALK-2 channels, whereas TALK-1 channels were unaffected. This observation suggests, that TALK-2 and TALK-1 are regulated differently, event though, they belong to the same subfamily. Especially in regard to the regulation of a potential intracellular gate, this becomes interesting. Therefore, see section 3.3.2.3.

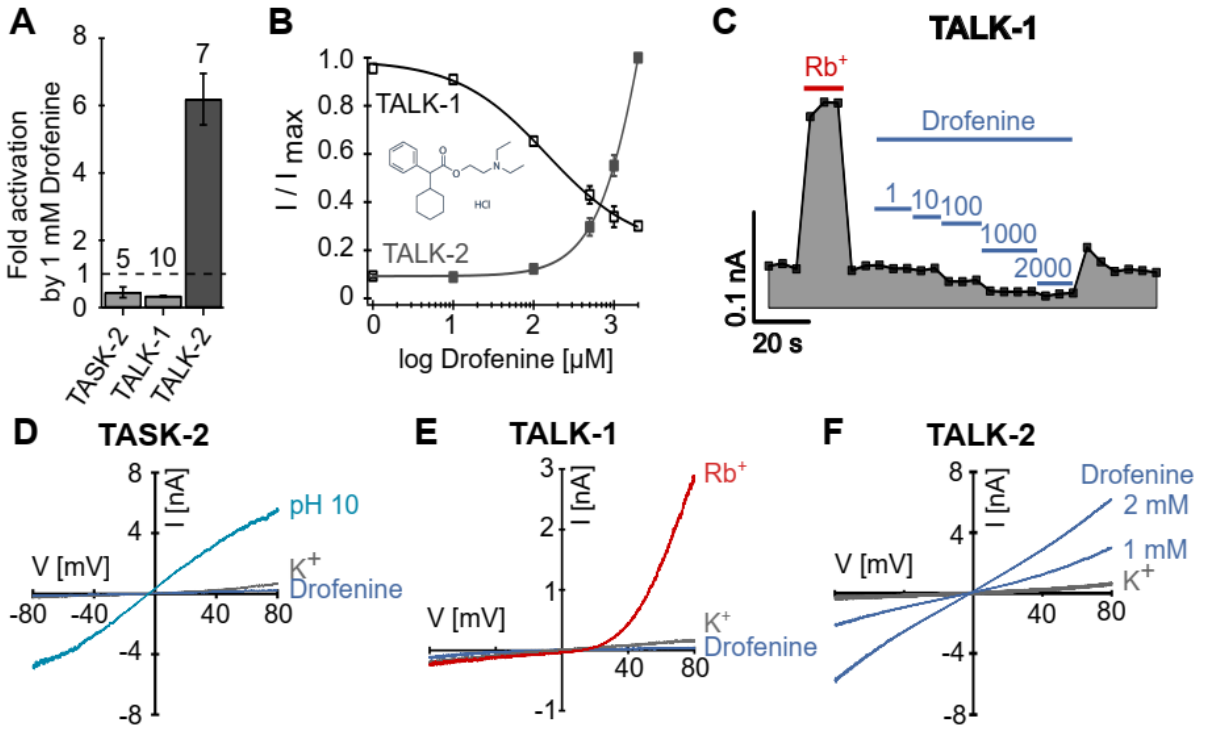

Figure 24 - Drofenine regulation of TALK channels. A) Fold activation of TASK-2, TALK-1 and TALK-2 channels at +40 mV by 1 mM Drofenine measured in Ramps as shown i.e. in D, E, F. **B)** Drofenine dose response curves for TALK-2 (grey, filled) and TALK-1 (black) showing an inhibiting effect for TALK-1, while TALK-2 is activated with rising concentrations. **C)** Plotted Drofenine dose response curve of TALK-1 at +40 mV, measured in Ramps as shown in E. **D - F)** Example traces of 2-APB (blue) regulation in Ramps using 1 mM Drofenine of TASK-2 (D), TALK-1 (E) and TALK-2 (F). For comparison Rb+ (120 mM, red) or pH 10 (turquoise) were applied as indicated.

3.2.2 Regulation of TALK channels by negatively charged activators

Negatively charges activators (NCAs) like BL-1249 are known to activate K2P and other ion channels by stabilizing the conductive state of the selectivity filter (Schewe et al. 2019). Figure 25 A demonstrates this large increase of current for the TALK-2 channel when treated with 50 µM BL-1249 (dark blue), that is even 6 times higher than the previously described activation by 1 mM 2-APB (light blue). In accordance, other NCAs like NS11021, ML67-33 or DCPIB also activate TALK-2 channels up to 110-fold when applied with a concentration of 50 µM. However, the related TALK-1 channel shows an overall weaker activation that is seen only as 5-fold current increase for NS11021 and DCPIB and a 30-fold increase for ML67-33 compared to the basal potassium current at pH 7.4 (Figure 25 B, C, D).

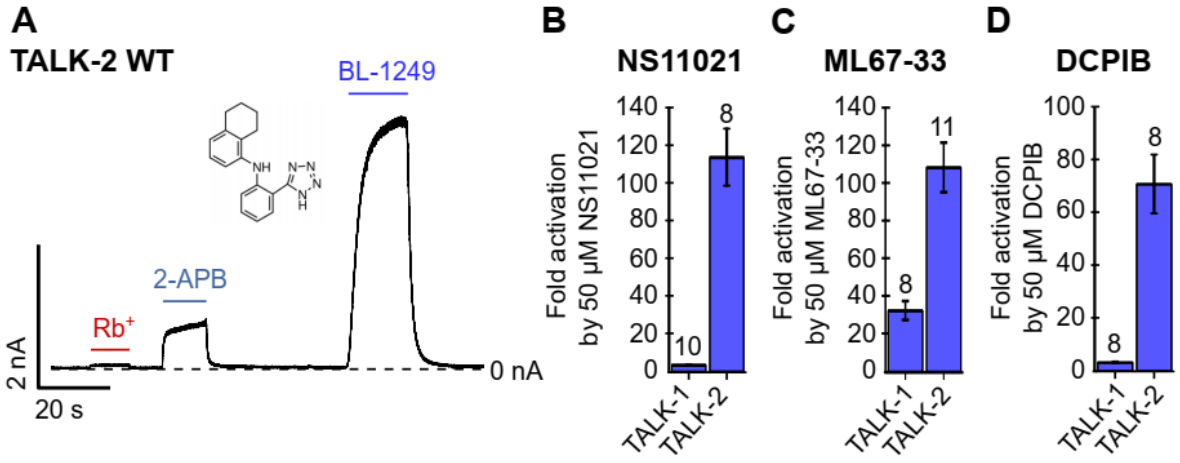

Figure 25 - Regulation of TALK channels by NCAs. A) Example trace of TALK-2 WT channels at +20 mV, activated by Rb+ (red) 1 mM 2-APB and 50 µM BL-1249. **B-D)** Fold activation of TALK-1 and TALK-2 channels at +40 mV by 50 µM of NS11021 (B), ML67-33 (C) and DCPIB (D), measured in Ramps -80 to +80 mV.

3.3 Gating mechanisms in K2P channels

3.3.1 Selectivity filter gating in TALK, TASK and THIK channels

As described in previous studies, TALK-2 channels are activated by rubidium ions (Rb^+) that are stabilizing the ion occupancy at the selectivity filter and thus evoke the opening of the ion flux gate (Schewe et al. 2019). Figure 26 A shows the resulting increase of the voltage dependent outward current as well as an increase in tail current amplitude that arises when Rb^+ is applied to the cytoplasmatic site of the channel. Thereby, rectangle pulses ranging from -100 to +100 mV where applied to an inside out patch and measured in symmetric potassium (black) or after intracellular substitution with Rb^+ (red). The voltage dependent increase of the tail current amplitude that is reflecting the slope of a rising open probability (P_o) is shown in Figure 26 F. Thereby, intracellular substitution with Rb^+ leads to a slightly stronger current rectification in comparison to symmetric K^+ concentrations. The deactivation time after repolarization from a rectangle pulse to +100 mV was analyzed as exponential fit of the tail current amplitude, yielding about 0.5 ms in symmetric K^+ and 2 ms upon intracellular Rb^+ substitution (Figure 26 D).

The observed potentiation of outward currents did only occur upon intracellular Rb^+ substitution. When applied extracellularly, voltage dependence was shifted slightly to more negative potentials and tail currents were diminished (Figure 26 A, black, right). A rise of inward currents was not observed when K^+ was substituted by Rb^+ (Figure 26 A, right, black, red) suggesting that only an outward ion-flux is possible, while inward movement of ions lead to channel closure.

The current response of TASK-1, TASK-2 and THIK-1 channels to intracellular Rb^+ substitution was characterized by a poor (or slower) ion conductance, where outward currents where decreased compared to K^+ currents (Figure 26 B, C). Furthermore, the tail current amplitude, shown in Figure D was not increased as it is observed for TALK-2. While the TALK-2 channels showed a 15-fold increase of their tail currents in response to Rb^+ at +100 mV, TASK-1, TASK-2 and THIK-1 channels showed an unaltered or reduced amplitude yielding a fold change of 0.6 ± 0.08 (n = 10), 0.33 ± 0.05 (n = 10) and 0.99 ± 0.05 (n = 3), respectively. The TASK-1 deactivation time (upon repolarization after a rectangle pulse to +100 mV (Figure 26 D) was about 2 ms in symmetric K^+ and slightly faster upon intracellular Rb^+ substitution (1 ms). As visible in the current voltage (I-V) curves TALK-2, TASK-1 and THIK-1 were all relatively open at negative potentials (Figure 26 F, G, H, grey).

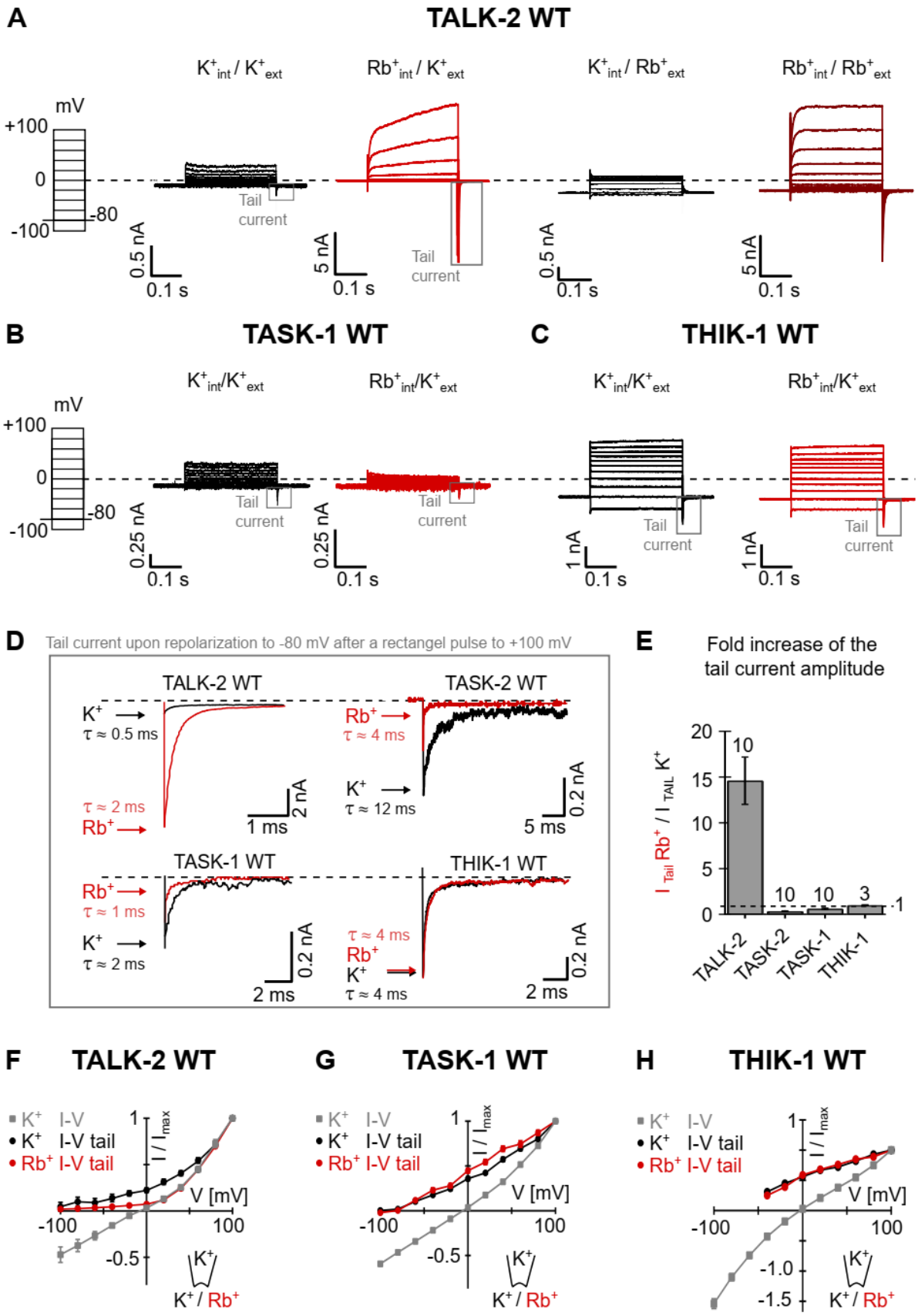

Figure 26 – Selectivity filter gating in K2P channels. A) TALK-2 current responses to rectangle pulses ranging from -100 to +100 mV in symmetrical K^+ (120 mM [Kint] / 120 mM [Kext]) (black) or after

K^+ replacement by Rb^+ at the intracellular (red), extracellular (black) or both sides (brown). **B)** TASK-1 current responses measured as in A, in symmetrical K^+ (black) or after intracellular K^+ replacement by Rb^+ (red). **C)** THIK-1 current responses measured as in A, in symmetrical K^+ (black) or after intracellular K^+ replacement by Rb^+ (red). **D)** Upscaled tail currents from measurements in A for TALK-2 and TASK-1, THIK-1 and TASK-2, indicated as grey box. **E)** Fold change of tail current amplitudes (mean ± SEM, n as indicated) after intracellular Rb^+ application at +100 mV of TASK-1 (0.6 ± 0.08, n = 10), TALK-2 (14.6 ± 2.58, n = 10) TASK-2 (0.33 ± 0.05, n = 10) and THIK-1 (0.99 ± 0.05, n = 3) channels. **F - H)** I-V curves of TALK-2 (F), TASK-1 (G) and THIK-1 (H) WT channels indicating currents at the end of a depolarizing step (-100 to +100mV, in 20 mV steps, gray boxes) and the corresponding tail current amplitude upon repolarization to -80 mV (black circles), red circles indicate tail currents upon intracellular Rb^+ substitution, values as mean ± SEM, n as in Figure E.

However, TALK-2 channels showed a pronounced rectification upon positive voltages. In contrast, the I-V curves of THIK-1 and TASK-1 channels were almost linear, with THIK-1 being even more open at negative potentials. The THIK-1 tail current amplitudes at negative voltages -100 to -60 mV were non-existent. Upon less negative (-40 to 0) and positive values, tail currents became visible and increased step wise, indicating that the open probability increased correspondingly with higher voltages. However, when compared to other K2P channels such as TALK-2 (Figure 26 F) or TASK-1 (Figure 26 G) this increase was quiet poor, indicating that THIK-1 currents are only weakly voltage dependent. The deactivation time upon repolarization was 4 ms in symmetric K^+ and upon intracellular Rb^+ substitution after a pulse to +100 mV. Thus, a Rb^+ substitution did not alter the size of the tail current amplitudes nor changed the time of deactivation. In respect to the Rb^+ conductance TASK-2 channels behaved very similarly to TASK-1 channels and are therefore not shown in detail. However, the tail current amplitude of these channels was larger and the deactivation time was slow (~12 ms) (Figure 26 D). After K^+ substitution with Rb^+ tail currents were strongly decreased and faster deactivated (~ 4 ms), shown in Figure 26 D. This suggest that the application of Rb^+ ions reduce the P_o of TASK-2 and enhance channel deactivation.

3.3.2. Intracellular gating mechanisms

3.3.2.1 Intracellular pore blocker accessibility

In order to study the inner pore structure of potassium channels, QA ions, such as Tetrapentlammonium (TPA), have been used extensively in the past (Camino et al. 2000;

Piechotta et al. 2011; Rapedius et al. 2012). Applied to an excised inside-out patch from *Xenopus laevis* oocytes TPA causes a fast, reversible current block of the TREK-1 and other K2P channels by the occupancy of their freely accessible inner pore cavity (Rapedius et al. 2012). As illustrated in Figure 27 B this approach holds true for eleven of the twelve tested K2P channels in this study. But to our surprise, the TALK-2 K2P channel showed an unexpected insensitivity towards this open channel blocker. Figure 27 A shows example traces measured in Ramps from -80 to +80 mV of TRAAK, TASK-3, TASK-2 and TALK-2 channels. While potassium currents of the TRAAK, TASK-3 and TASK-2 channels are blocked about 80 – 90 % by 1 mM TPA (grey), the TALK-2 channel shows no current alterations. As depicted in the Cartoon (Figure 27 C), this observation contrasts the common understanding of the state independent pore accessibility in K2P channels (such as TREK-1), suggesting the presence of a lower pore constriction or some other mechanism preventing the binding of TPA ions to the channel pore.

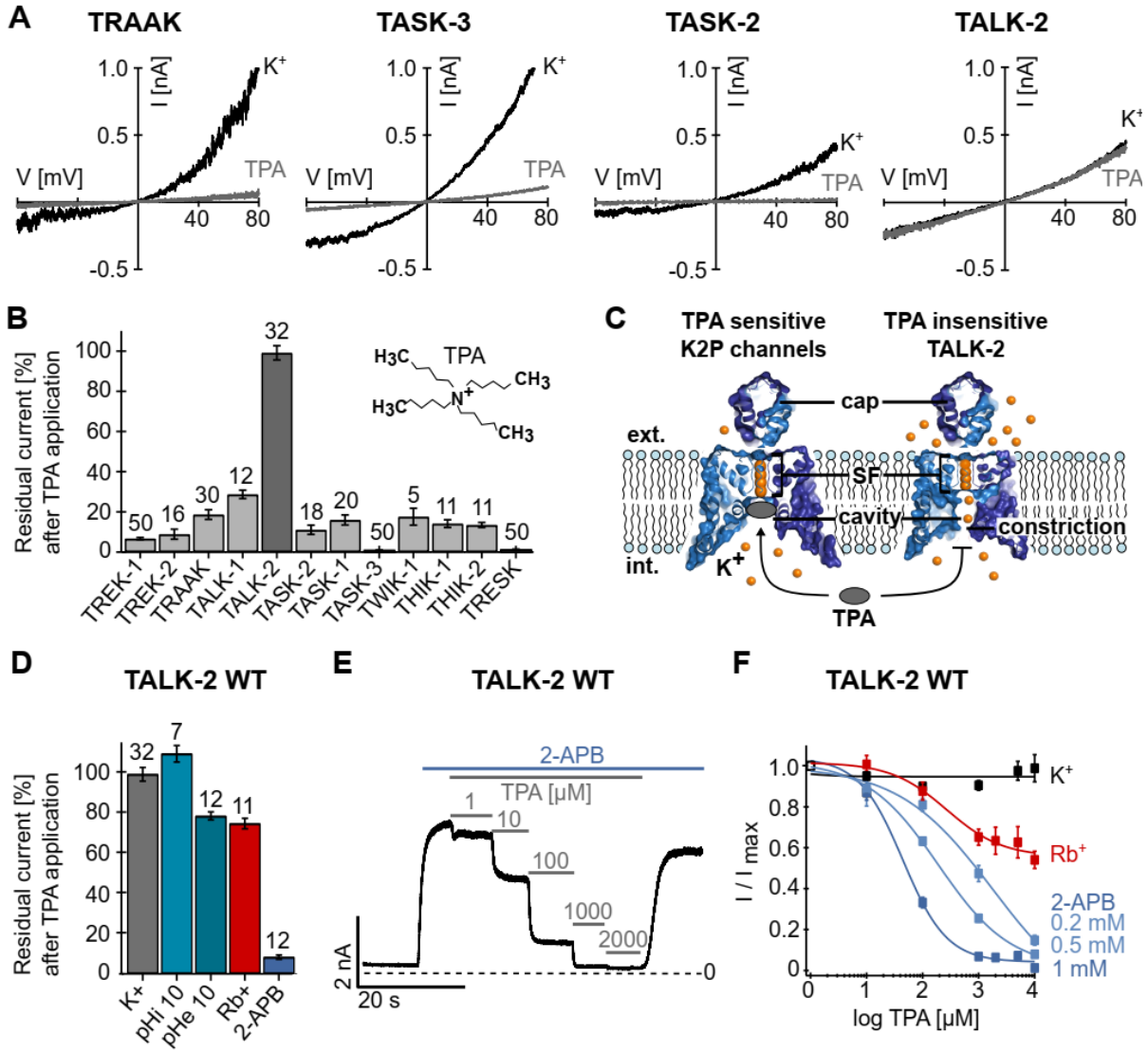

Figure 27 – Tetrapentylammonium (TPA) accessibility in K2P channels. A) Example traces measured in Ramps, showing a reduced current amplitude after application of 1 mM TPA (grey) compared to currents at pH 7.4 (black) for TRAAK, TASK-3 and TASK-2 channels. TALK-2 currents are unaltered. B) Residual current after 1 mM TPA application tested on 12 K2P channels, measured as in A. (TREK-1: 6.68 ± 0.62, n = 50; TREK-2: 8.9 ± 2.48, n = 16; TRAAK: 18.68 ± 2.41, n = 30; TALK-1: 28.7 ± 2.08, n = 12; TALK-2: 99.11 ± 3.56, n = 32; TASK-2: 11.12 ± 2.3, n = 18, TASK-1: 15.96 ± 2.48, n = 20, TASK-3: 0.84 ± 0.16, n = 50; TWIK-1 17.6 ± 4.18, n = 5; THIK-1 14.13 ± 1.93, n = 11, THIK-2 13.45 ± 1.28, n = 11, TRESK 1.17 ± 0.29, n = 50). D) TALK-2 residual current after TPA application at basal conditions (grey, 99.11 ± 3.56, n = 32), upon intra- and extracellular pH 10 activation (turquoise, 109.32 ± 4.25, n = 7; 78.39 ± 2.06, n = 12), Rb^+ activation (red, 74.63 ± 2.77, n = 11) and after channel activation by 1 mM 2-APB (8.30 ± 1.22, n = 12). E) Dose dependent TPA inhibition (gray, 1, 10, 100, 1000, 2000 µM) of TALK-2 upon previous 2-APB (1 mM) activation, measured at continuous +40 mV. F) TPA dose response curves of TALK-2 channels at basal conditions (sym. K^+, 120 mM, black), after Rb^+ activation (red) and upon activation by 2-APB applied in 3 concentrations (0.2, 0.5, and 1 mM, blue). *contribution of other lab members in figure B, F, more detail see table 6.

As described previously, TALK-2 channels are activated by Rubidium ions (Rb^+) that are stabilizing the ion occupancy at the selectivity filter and thus evoke the opening of the ion flux gate ((Schewe et al. 2016), Figure 26 A). Assuming, that this filter gate activation does not involve major structural changes of the inner channel pore, we observed with no surprise that the previously described TPA insensitivity remained at high levels (74,63 ± 2.77 %) after Rb^+ activation. Furthermore, previous activation of the TALK-2 channel by intra- and extracellular alkalization (pH 10) did also not increase TPA sensibility (Figure 27 D). In the very contrast, activation upon 1 mM 2-APB led to a highly increased TPA sensitivity comparable to other K2P channels (Figure 27 D). As shown in Figure 27 E, this gain of TPA sensitivity is dose dependent. Here, WT TALK-2 channels were activated previously by 1 mM 2-APB and then subsequently blocked by increasing TPA concentrations (0.001 – 2 mM). In Figure 27 F, we demonstrate that this dose dependence is shifted in correlation to the previously applied 2-APB concentration (0.2, 0.5 and 1 mM). The higher the applied 2-APB concentration, and thus the activation of the channel, the merrier is the TPA block.

3.3.2.2 Gating at the C-terminal domain in TREK channels

Due to the lack of an intracellular gate, gating stimuli in TREK-1 and other K2P channels are thought to converge directly to the selectivity filter. Yet, how this conversion is processed remains unclear. However, it is suggested in crystal structure studies (Dong et al. 2015) that

TREK-2 channels are found in at least two distinct states. A more conductive up-state and a less conductive downstate, as illustrated in Figure 28 A. Thereby, the lower sections of the M2, M3 and M4 helices are projecting further into the cytoplasm in the down-state and are moved further up into the membrane in the up-state conformation. Furthermore, Norfluoxetin (NFx), registered as the antidepressant Prozac (indicated in Figure 28 A), binds within a side fenestration that is only accessible in the downstate conformation. Thus, stabilizing the less conductive state of the channel, visible as a dose dependent NFx inhibition of TREK-1 WT channels in Figure 28 D.

However, the C-terminal domain, that was mostly removed for crystallization, is believed to play an important role for the modulation of channel activity. Thereby, protonation due to pH changes, lipid interactions (i.e. with PIP_2) or other posttranslational modifications could favor an incorporation of the C-terminus to the plasma membrane and by that stabilize the more active up state.

To test the involvement of the proximal C-terminal domain in TREK-1 channel activation, a cysteine modification assay was performed. Therefore, several mutants with introduced cysteine residues at the proximal C-terminal domain (K316C to V322C, F325, R326 and S348) were created and the lipophilic reagent Decyl-MTS was applied to the cytoplasmatic site of the channel. As illustrated in Figure 28 B, the lipophilic Decyl-MTS reagent was expected to seek an incorporation into the membrane. Thereby, it should function as anchor like structure, when bound to the modified cysteine residues, thus forcing the C-terminal domain to move upwards and thereby stabilize the conductive up state.

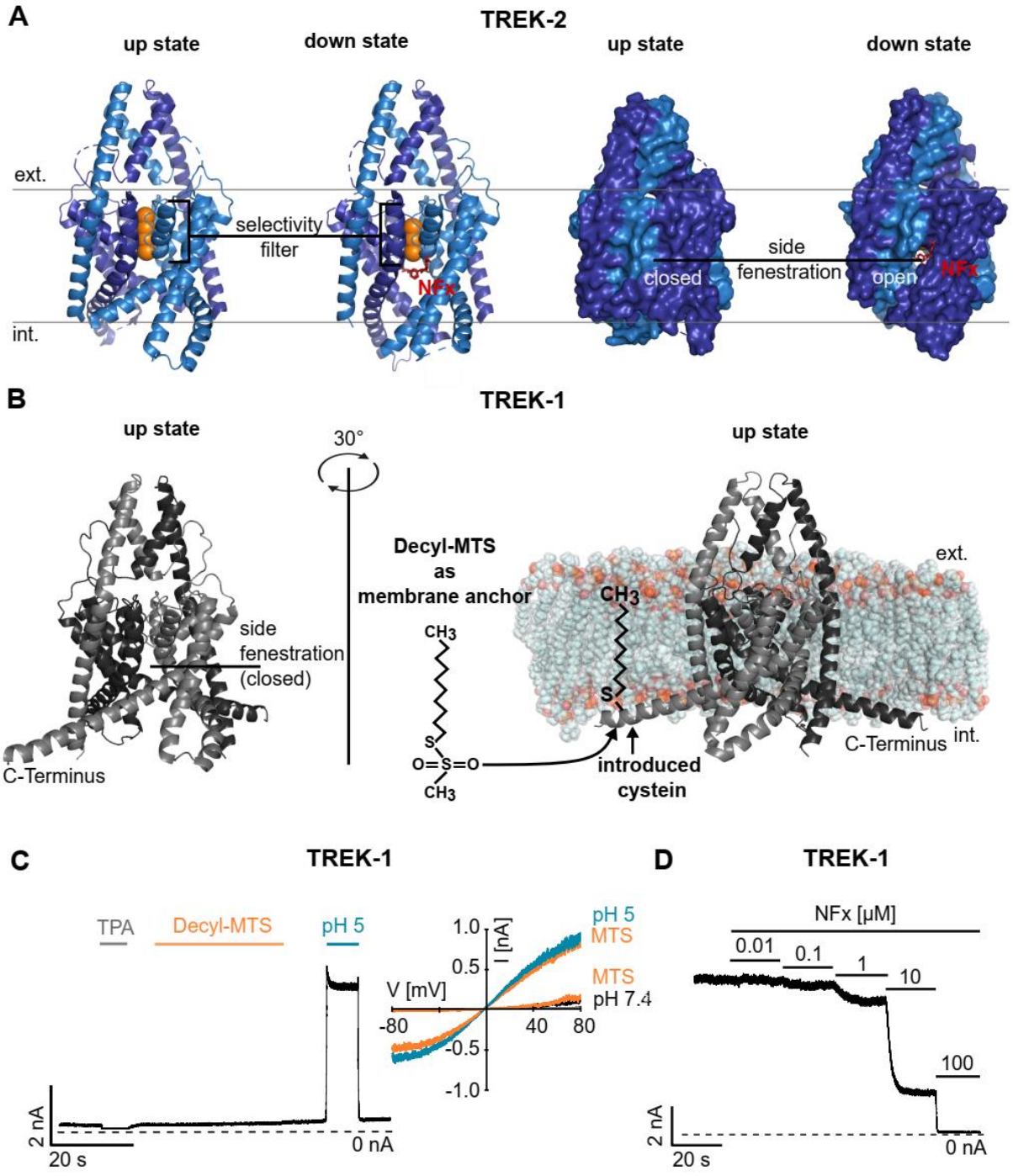

Figure 28 – Up- and down states in TREK channels. A) Christal structures of TREK-2 in the up (conductive) and down (non-conductive) state conformation (PDB Entry: 4BW5 and 4XDK). Binding of Norfluoxetin within the site fenestration, that is only accessible in the downstate conformation, visible in the surface illustration on the right, is shown in red. **B)** TREK-1 crystal structure (PDB Entry E306AX with membrane from Steven Tucker, Oxford University, UK) in its putative up state, orientated with direct view at the narrow side fenestration (left), embedded into a membrane and turned by 30° (right). The chemical structure of the cysteine modifying MTS-Decyl reagent and its expected anchor like behavior after its binding to an introduced cysteine at the C-terminal domain are indicated, (dimensions are enlarged for better visibility and do not reflect real proportions). **C)** TREK-1 WT, measured at continues + 40 mV or in Ramps, showing that 100 µM of Decyl-MTS (orange) does not alter currents at pH 7.4

(black) nor at pH 5 (turquoise). 1 mM TPA (gray) was applied to test the patch quality. **D)** Dose dependent inhibition of TREK-1 channels by Norfluoxetin (0.001 – 100 µM).

Strikingly, this was observed for 8 of the 10 tested residues. While WT channels showed no reaction to the reagent (Figure 28 C), the mutants K317C, T318C, K319C, E320, V322C, F325C, R326C and S348C were activated irreversibly (up to 150-fold) within seconds after Decyl-MTS was applied to the patch (Figure 29 A-H). Notably, application of the central cavity blocker tetrapentylammonium (TPA) led to a full current inhibition before and after activation with Decyl-MTS (Figure 29 A – F). However, activation by acidic pH 5 (turquoise, Figure 29 A, C, E, D, G) was altered, leading only for the mutant K317C (A) to a further current increase, whereas the decyl-MTS activated currents of the mutants K319C, E321C, V322C and R326C were decreased about 40 %. Interestingly, mutation at the putative proton sensor E321 (Honoré et al. 2002) and at the putative phosphorylation site S348 ((García et al. 2020), there referred as S333) led to a gain of function, thus further activation of the already highly conductive channels was only weak compared to the other mutants (Figure 29 E, H).

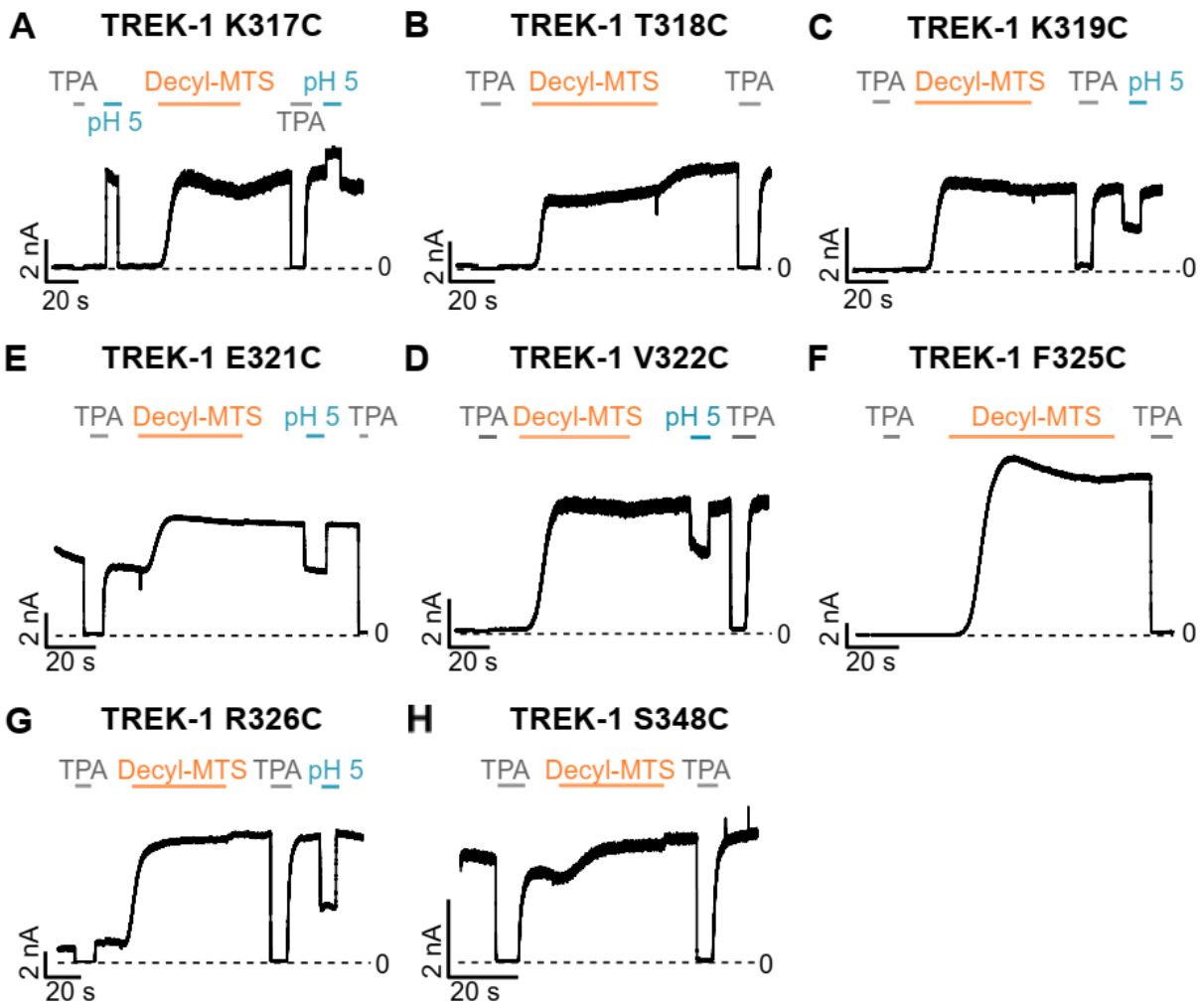

Figure 29 – C-terminal activation by Decyl-MTS modification in TREK-1 channels. A-H) Example traces of TREK-1 mutants K317C, T318C, K319C, E320C, V322C, F325C, R326C, S348C measured in inside out patches at continues +40 mV, in symmetric K^+ at pH 7.4. 1 mM TPA (gray) or K^+ solution exchange to pH 5 (turquoise). was applied before and after activation with 100 µM Decyl-MTS.

Interestingly, the residues K316C and E320C showed a current inhibition when treated with 100 µM Decyl-MTS (Figure 30 A, B). Thereby, the basal potassium current at pH 7.4 was not notably altered by Decyl-MTS application. The response to pH 5, however, was reduced after the modification (Figure 30 A and B, left current trace). This modification induced inhibition of the channel became more visible, shown in the right current trace, where Decyl-MTS was applied at previously pH 5 activated currents, measured in continues -80 mV and symmetric K^+ concentrations (Figure 30 A and B right current trace).

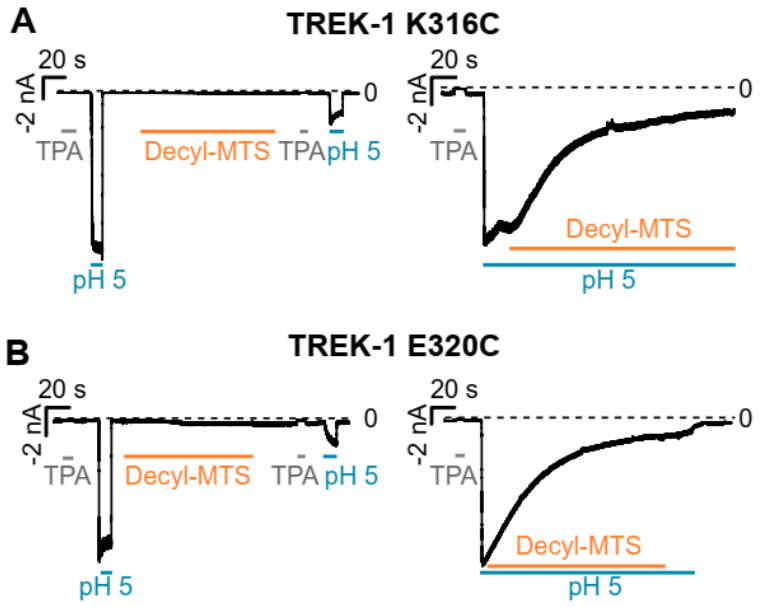

Figure 30 – Current inhibition by C-terminal Decyl-MTS modification in TREK-1 channels. A-B) Example traces of TREK 1 K316C (A) and E320C (B) mutants. Measured in inside out patches at continuous -80 mV in symmetric K^+ concentrations at pH 7.4 if not indicated otherwise. 1 mM TPA (grey) and K+ solution at pH 5 (turquoise) were applied previously and after Modification with Decyl-MTS (orange) (left side). On the right, channels were activated by pH 5 and Decyl-MTS modification was performed at pH 5, leading to a current inhibition.

For better comparison, the fold activation (orange) and the relative inhibition (blue) respectively, were shown in Figure 31 B. Notably, residues facing the membrane phase shown in the crystal structure (Figure 31 A) where activated (orange), while residues facing the cytosol where inhibited (blue). As indicated in Figure 28, the transition of the TREK-2 channel from the open to the closed state evokes the closing of a side fenestration (Dong et al. 2015). As shown in Figure 28 D, TREK-1 channels are also inhibited by NFx that binds within this fenestration and accordingly stabilizes the non-conductive down state of the channel. To further address this suggestion, NFx dose response curves were made under (i) physiological pH 7.4 (black) and (ii) intracellular acidification (turquoise) using the TREK-1 WT channel (Figure 31 D). Additionally, the TREK-1 F325C mutant was also tested under physiological conditions as well as upon Decyl-MTS modification. The response to NFx in physiological pH, was very similar for the WT (IC_{50} = 3.9 ± 0.5 µM) and the F325C mutant (IC_{50} 4.6 ± 0.7 µM). Strikingly, the IC_{50} of the WT activated by intracellular pH 5 as well as the F325C mutant activated by Decyl-MTS, was shifted by several fold to 12.9 ± 1.1 and 44.2 ± 8.9, respectively. This observation supports the proposed gating mechanism presented by Dong et al. 2015 and confirms this approach of membrane tethering (leading to activation) by the introduction of a lipid anchor.

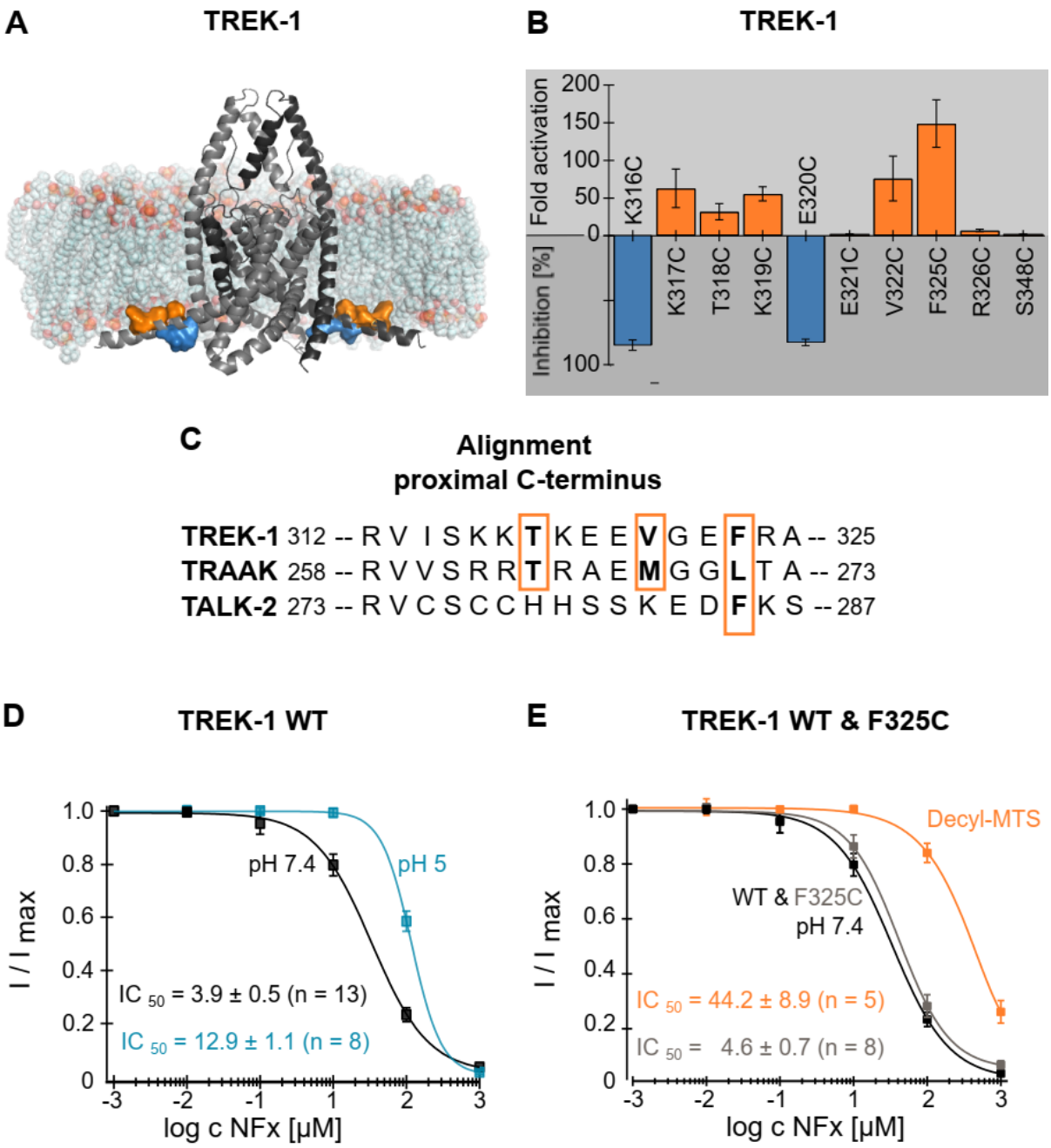

Figure 31 – Comparison of Decyl-MTS modifications of TREK-1 C-terminal mutants. A) Crystal structure of TREK-1, embedded in a phospholipid membrane (PDB Entry E306AX with modeled membrane from Steven Tucker, Oxford University, UK). To cysteine mutated residues at the C-terminal domain activated by 100 µM Decyl-MTS are coloured orange and those inhibited in blue, respectively. **B)** Fold activation or relative Inhibition in % by 100 µM Decyl-MTS (measured as in Figures 29 and 30) of TREK-1 mutants. K317C (63.02 ± 25.69, n = 4), K318C (31.90 ± 10.66, n = 5), K319C (55.64 ± 9.28, n = 8), E321C (1.81 ± 0.22, n = 5), V322C (75.93 ± 29.64, n = 8), F325C (148.77 ± 31.55, n = 13), R326C (7.03 ± 1.49, n = 7) and S348C (1.73 ± 0.25, n = 8) were activated, while K316C (85.29 ± 4.06 %, n = 4) and E320C (82.77 ± 2.4 %, n = 5) were inhibited (in pH 5). (mean ± SEM). **C)** Alignment of the proximal C-terminus of TREK-1, TRAAK and TALK-2 channels. Homolog residues, mutated in the 3 channels were boxed in orange. **D-E)** Norfluoxetine (NFx) dose response curve of WT TREK-1 channels

(D) and F325C mutants (E) under standard physiological conditions (pH 7.4) and pH 5 activated (D) or Decyl-MTS activated (E) channels.

To test whether this gating mechanism is transferable to other channels, homolog residues (Alignment, Figure 31 C) to the TREK-1 F325C and V322C yielding the greatest activation (148.77 ± 31.55 and 75.93 ± 29.64, respectively), as well as the intermediately activated T318C mutant (31.90 ± 10.66) were created in TRAAK K2P channels.

Strikingly, as shown in Figure 32 the Decyl-MTS modification of the three mutants T264C (C), M268C (D) and L271C (E) led to channel activation, compared to the WT, that was not affected (A). The overall fold activation (5 – 30-fold, Figure 32 B) of the TRAAK mutants was lower compared to those for the TREK-1 channels. However, the mutant L271C, that is the homolog of the strongest activated F325C mutant in TREK-1, was also the mutant strongest activated by Decyl-MTS in TRAAK.

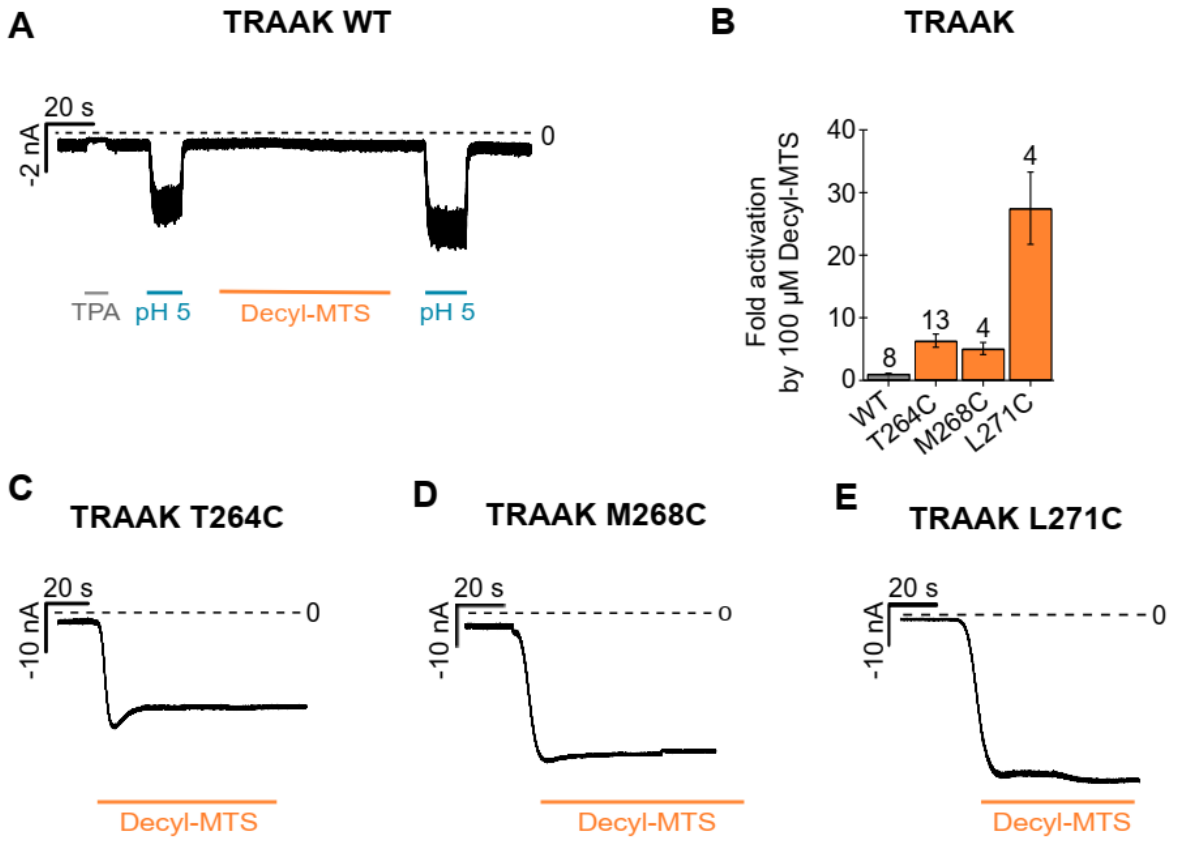

Figure 32 - C-terminal activation by Decyl-MTS modification in TRAAK channels. A) Example trace of TRAAK WT at continuous -80 mV. 1 mM TPA (gray) fully blocked the channel and a pH change to 5 (turquoise) led to channel activation before and after Decyl-MTS (100 µM, orange) application. **B)** Fold activation by 100 µM Decyl MTS of WT (1.04 ± 0.07), T264C (6.36 ± 1.04), M268C (5.09 ± 0.96) and L271C (27.51 ± 5.78) mutants. **C-F)** Example traces of TRAAK T264C (C), TRAAK M268C (D) and TRAAK L271C (E) mutants, measured as in A.

Therefore, we created the homolog to the F325C mutant in TREK-1 (or L271C in TRAAK, respectively) also in TALK-2 channels, here at position F285, and repeated the experiment. In contrast to the previous observations in TREK-1 and TRAAK channels, where Decyl-MTS modification led to a quick channel activation within seconds, an activation of the TALK-2 F285C only occurred over a long period of time (> 2 minutes (Figure 33 B). Due to this long activation time, measurements were carried out in Ramps -80 to +80 mV to secure better patch stability and plotted at +40 mV. As shown in Figure 33, TALK-2 WT channels (A) were unaffected by 100 µM Decyl-MTS, while the F285C mutant (B) shows a weak, but slowly generated activation of 6.68 ± 2.35-fold (mean ± SEM). Interestingly, application of 1 mM of the central cavity blocker TPA (grey) did not lead to a full current block after Decyl-MTS modification, as it was shown previously upon activation with 2-APB. These observations suggest, that gating regulation in TALK-2 channels potentially differs from that observed in TREK and TRAAK channels.

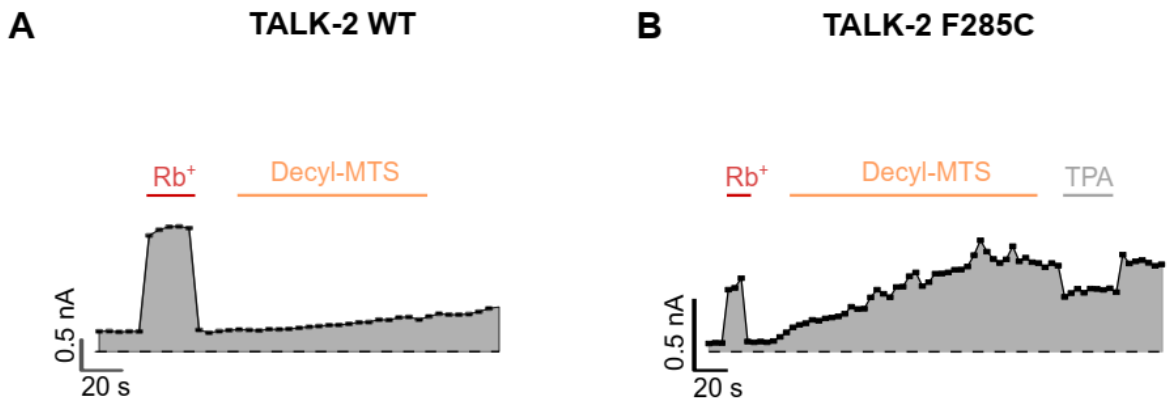

Figure 33 – Decyl-MTS modification in TALK-2 channels. A) Representative TALK-2 WT current trace measured in Ramps -80 to +80 mV analyzed at +40 mV and plotted over time. Rb^+ (red) was applied to test patch quality. Application of 100 µM Decyl-MTS had no effect on the channel. **B)** Current trace of TALK-2 F285C mutant measured as in A. Rb^+ activates the channel comparable to the WT (red). Decyl-MTS leads to a slow activation. Application of TPA (1 mM) leads to a ~20 % inhibition of the Decyl-MTS activated channel.

3.3.2.3 Probing for cytoplasmatic gates in TREK-1 and TALK-2 channels using MTS-reagents

Another approach to test the existence of an intracellular gate is by assaying the accessibility of MTS-reagents to the central cavity at different states, illustrated in Figure 34. Therefore, we mutated pore cavity residues to cysteine in TREK-1 (G186C) and TALK-2 (L145C) channels

and performed an accessibility assay using MTS-TBAO. The latter, is an MTS reagent with a tetrabutylammonium moiety, that is expected to block the channel current, when introduced to the pore.

As shown in Figure 34, TREK-1 WT currents were unaffected by 100 µM MTS-TBAO applied to basal potassium currents at pH 7.4. The pH 5 response, however, was reduced by 50 % after the application (A). Yet, upon pH 5 (B) or 2-APB (C) activation, currents were inhibited reversibly. In contrast, currents of TREK-1 G186C mutants where inhibited irreversibly. Thereby, we tested the mutant for modification upon pH 5, Rb^+ as well as 2-APB activation, yielding a similar time curse of modification beneath 0.4 s for all three conditions (Figure 34 D, E, F, Figure 35 H).

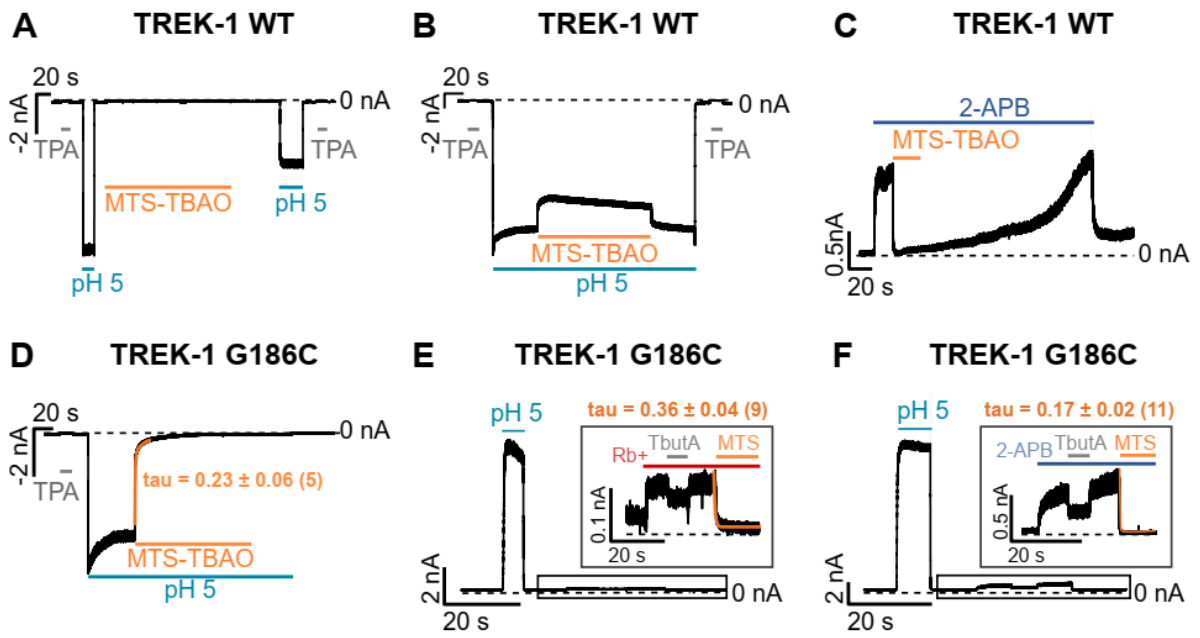

Figure 34 – Pore accessibility for MTS-TBAO in TREK-1 channels. A - C) Example traces of WT TREK-1 channels measured at continuous -80 mV (A, B) or continuous +40 mV (C). 100 µM MTS-TBAO was applied in K^+ pH 7.4 (A) or after activation with pH 5 (B) or 1 mM 2-APB (C), (1 mM TPA was used to test the patch stability). **D - F)** Example traces of TREK-1 G186C mutants measured at continuous -80 mV (A) or continuous +40 mV (E, F). 100 µM MTS-TBAO (MTS) was applied after activation with pH 5 (D), Rb^+ (E) or 1 mM 2-APB (F). For better visibility, modification was enlarged in figure E, F (box), 100 µM Tetrabutylammonium (TbutA) was applied to test sensibility towards the blocker.

As shown in Figure 35 A and B, application of MTS-TBAO led to a weak current increase when applied to TALK-2 WT channels at basal K^+ conditions and upon Rb^+ activation. 100 µM

Tetrabutylammonium, shown in B, failed to block WT currents. Application of MTS-TBAO to the pore cavity mutant L145C, shown in Figure 35 C, led to a stepwise inhibition of the basal and Rb^+ current, when applied repeatedly for 1 s. Applied for at least 15 s, potassium currents as well as Rb^+ or 2-APB activated currents were inhibited irreversibly. However, in contrast to the TREK-1 G186C mutant, the time curse of modification (tau) was 10 times slower when applied in K^+ and Rb^+ (both gating stimuli that are acting directly at the selectivity filter) solution (3.61 ± 0.16 s; 3.3 ± 0.16 s), than upon 2-APB activation (0.27 ± 0.02 s) (Figure 35 G, H). Notably, the mutated residue L145 is part of the homolog binding site for quaternary ammonium ions in TREK-1 channels (Piechotta et al. 2011). As shown in Figure 35 I, mutation at this position to cysteine increases the sensitivity for Tetrabutylammonium in TALK-2 channels.

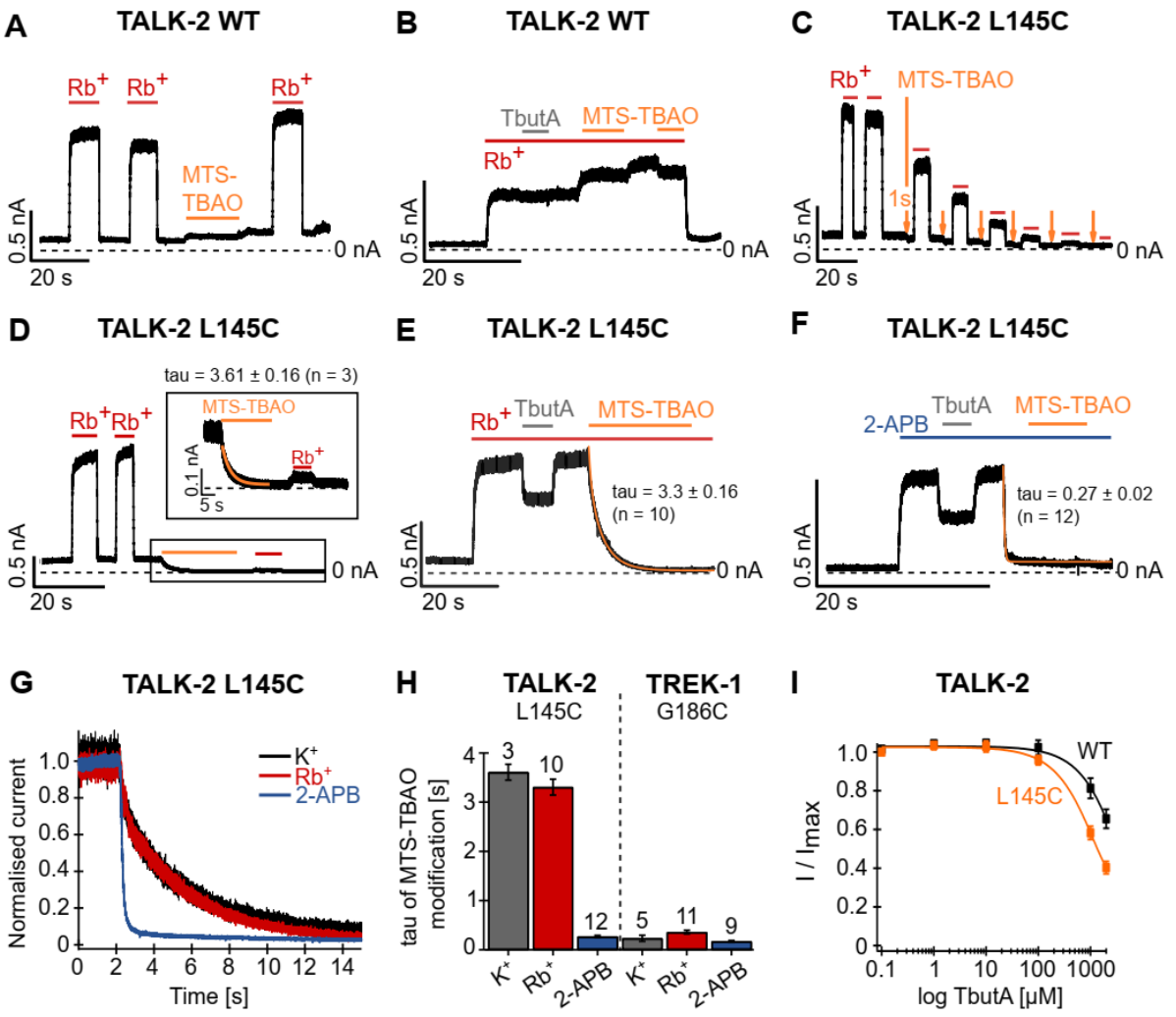

Figure 35 – Pore accessibility of MTS-TBAO reagents in TALK-2 channels. A-B) Example traces of WT TALK-2 channels measured at continuous +40 mV. 100 µM MTS-TBAO (orange) was applied in K^+ pH 7.4 (A) or after activation with Rb^+ (B, red), leading to a slight current increase. Tetrabutylammonium (TbutA, 100 µM, gray) did not lead to a current decrease (B). **C)** Example trace of

the TALK-2 L145C mutant, measured as in A. MTS-TBAO was applied repeatedly for 1 s in K+ pH 7.4 solution and Rb^+ activation was tested after each MTS-TBAO step. **D - F)** Example traces of TALK-2 L145C mutants, measured as in A. MTS-TBAO (MTS) was applied at basal K^+ conditions (D), upon Rb^+ activation (E) and upon 2-APB (1 mM) activation (F). For better visibility, modification was enlarged in figure D (box), 100 µM Tetrabutylammonium (TbutA, gray) led to a 30 - 40 % current decrease in E, F. **G)** Current, normalized to the maximal current before MTS-TBAO modification, measured as in D, E, F showing a slow time curse of modification in K^+ (black) and Rb^+ (red) solution compared to the modification in 2-APB (blue). **H)** Time curse of MTS-TBAO modification at + 40 mV for TALK-2 L145C mutant and TREK-1 G186C mutant in potassium pH 7.4 (or pH 5 for TREK-1), upon Rb^+ activation and after 2-APB activation. Modification of TREK-1 G186 C were similar under all three conditions (K+: 0.23 ± 0.06 s, Rb+: 0.36 ± 0.04 s, 2-APB: 0.17 ± 0.02 s), while TALK-2 modification was slower in K+ or upon Rb+ modification (K+: 3.61 ± 0.16 s, Rb+: 3.31 ± 0.16 s, 2-APB: 0.27 ± 0.02 s). **I)** TbutA dose response of TALK-2 WT and TALK-2 L145C mutant at +40 mV.

To further explore this observed state dependent pore accessibility of TALK-2 channels and to rule out potential side effects of the MTS-TBAO reagent (i.e. by an increased QA sensibility of the TALK-2 L145C mutant) we repeated the cysteine accessibility assay replacing MTS-TBAO by the positively charged MTS-ET (1 mM) reagent. Furthermore, we created a homology model of TALK-2 mapped on the recently solved TASK-1 channel structure that suggests a lower constriction under the selectivity filter, referred as x-gate (Rödström et al. 2020), shown in Figure 36 A. From this, we introduced (apart from the pore cavity L145C mutant) another cysteine mutant at position Q266 localized at the x-gate, facing downwards into the cytosol (Figure 36 A), that is expected to be state independently modified.

A comparison of the WT, L145C and Q266C basal currents, upon Rb^+ activation as well as 1 mM 2-APB activation is shown in Figure 36 B and C. Thereby, basal currents of the L145C mutant is increased by 0.08 nA, while the basal current of the Q266C mutant is slightly decreased (0.02 nA) compared to WT currents. In accordance fold activation upon 2-APB application, was reduced for the L145C mutant and slightly increased for the Q266C mutant compared to WT. Rb^+ activation was very similar for WT, the L145C and Q266C mutants.

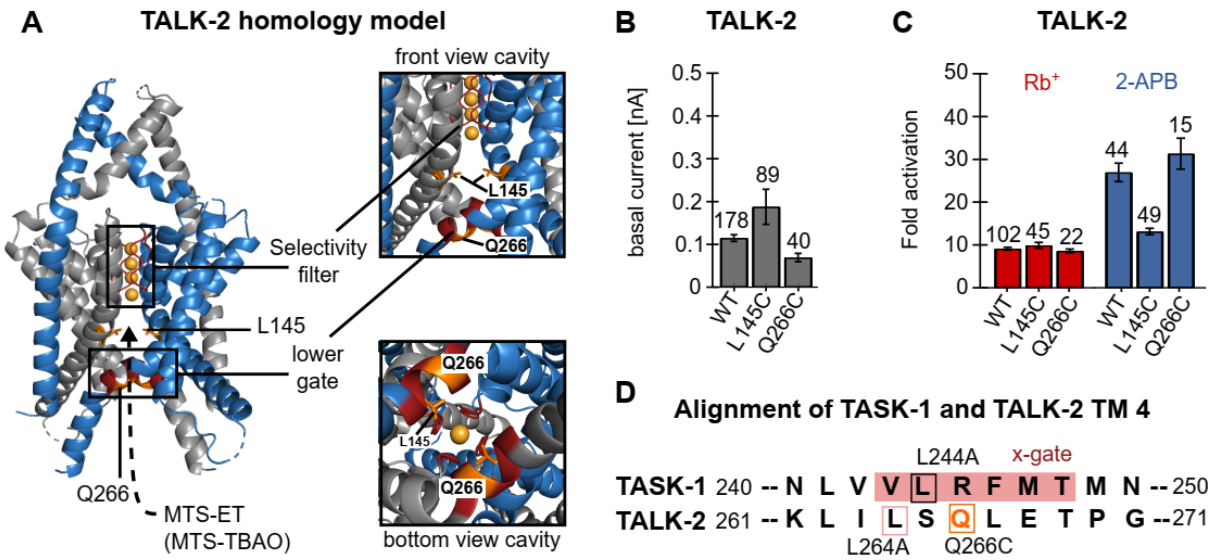

Figure 36 – Homology model of TALK-2 mapped on TASK-1 crystal structure. A) Homology model of TALK-2 mapped on TASK-1 crystal structure (PDB Entry: 6RV3, created by Wendy González, Universidad de Talca, Chile), illustrating an upper selectivity filter gate and a lower (x-) gate. Residues L145 within the central cavity and Q266 that resides within the x-gate region, were modified to cysteine (orange) for MTS modifications. **B-C)** Comparison of basal (B, WT: 0.11 ± 0.01 nA, n = 178; L145C: 0.19 ± 0.04 nA, n = 89; Q266C: 0.07 ± 0.01 nA, n = 40) and Rb^+ (Fold activation WT: 9.11 ± 0.34, n = 102; L145C: 9.9 ± 0.68, n = 45; Q266C: 8.6 ± 0.43, n = 22) or 2-APB (1 mM) activated currents of TALK-2 WT, L145C and Q266C mutants (2-APB: WT: 26.97 ± 2.15, n = 44; L145C: 13.15 ± 0.75, n = 49; Q266C: 31.34 ± 3.63, n = 15). **D)** Alignment of TASK-1 and TALK-2 TM4 x-gate region in TASK-1 (red). Gain-of-function mutation L244A in TASK-1 and analogue L264A mutant in TALK-2, as well as residue Q266C mutation for state independent modification are framed in black, red and orange, respectively.

Next, the accessibility under conditions affecting either the selectivity filter (K^+ and Rb^+) or using activators such as 2-APB, BL-1249, Oleoyl-CoA (that potentially open the lower constriction) was tested. Thereby, MTS-ET had no effect on TALK-2 WT currents upon basal potassium currents, shown in Figure 37 A (left). Upon Rb^+ or 2-APB activation MTS-ET had a small but reversible effect on WT currents (Figure 37 middle, right). In contrast, the L145C mutant showed a state dependent modification, characterized by a fast current inhibition by MTS-ET upon 2-APB (12.3 ± 1.2 s) activation, but not under basal nor Rubidium activated conditions (Figure 37 B). Interestingly, the time curse of MTS-ET modification (tau) for 2-APB activated channels is correlated to the fold activation of the activating compound. As depicted in Figure 38 A, MTS-ET modification speeds up upon an increasing 2-APB fold activation. In addition, an activation dependent modification was not observed for the Q266C mutant, where MTS-ET modification (leading here to a current increase) was possible in all experimental

settings (Figure 37 C). Notably, the time curse of modification was the same for all three conditions (Figure 38 B).

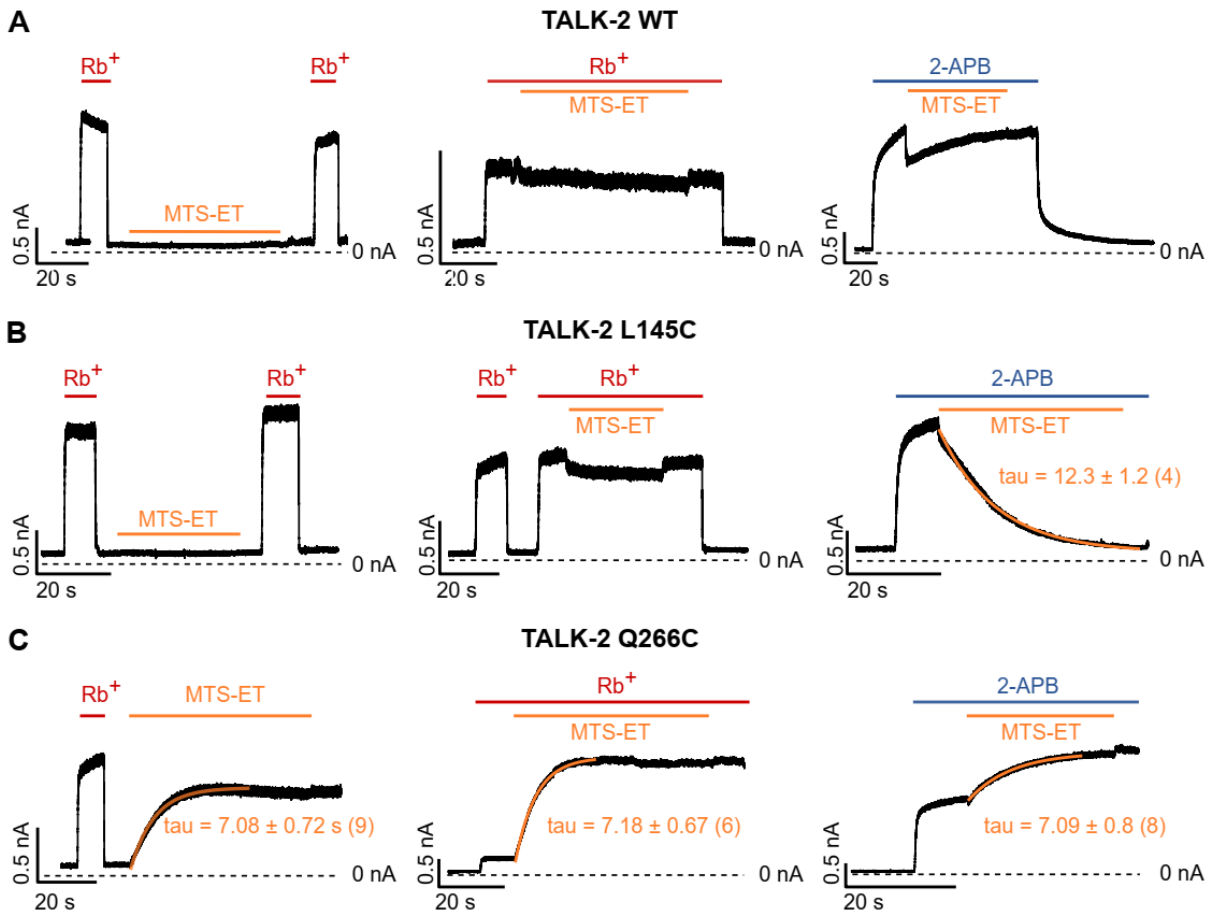

Figure 37 – MTS-ET modification of TALK-2 WT, L145C and Q266C mutants. A-C) Example traces, measured at +40 mV using inside out patches from *Xenopus laevis* oocytes expressing WT TALK-2 channels (**A**), the TALK-2 L145C mutant (**B**) or the Q266C mutant (**C**). 1 mM MTSET (orange) was applied for at least 30 s upon basal K^+ concentrations (symmetric, 120 mM) (left), upon Rb^+ (red) avtivation (middle) and 2-APB (blue) activation (right). While the WT was not modified by MTSET, the L145C mutant is inhibited irreversibly upon 2-APB activation (tau = 12.3 ± 1.2, n = 4) and the Q266C mutant is activated by MTSET under all three conditions with a similar time constant (K^+: 7.08 ± 0.72 s, n = 9; Rb^+: 7.18 ± 0.67 s, n = 6; 2-APB: 7.09 ± 0.8 s, n = 8).

Modification of TALK-2 L145C subsequently activated by BL-1249, Oleoyl-CoA or ONO-RS-082 led (similar to 2-APB) to a fast and irreversible current inhibition (Figure 38 D, E, F). The Q266C mutant was also modified upon BL-1249 and Oleoyl-CoA activation, in an activating manner as discribed before. Thereby, the time curse of modification upon BL-1249 was in the same range as modifications upon basal potassium, Rb^+ activated or 2-APB activated conditions (BL-1249: 7.29 ± 0.84 s). However, modification uppon Oleoyl-CoA activation was

slower, yielding a tau of 23.34 ± 2.48 s. Application of MTS-ET on the ONO-RS-082 activated Q266C mutant led to a weak current decrease during the time of application, that was reversed after the removal of the modifying reagent, shown in Figure 38 I.

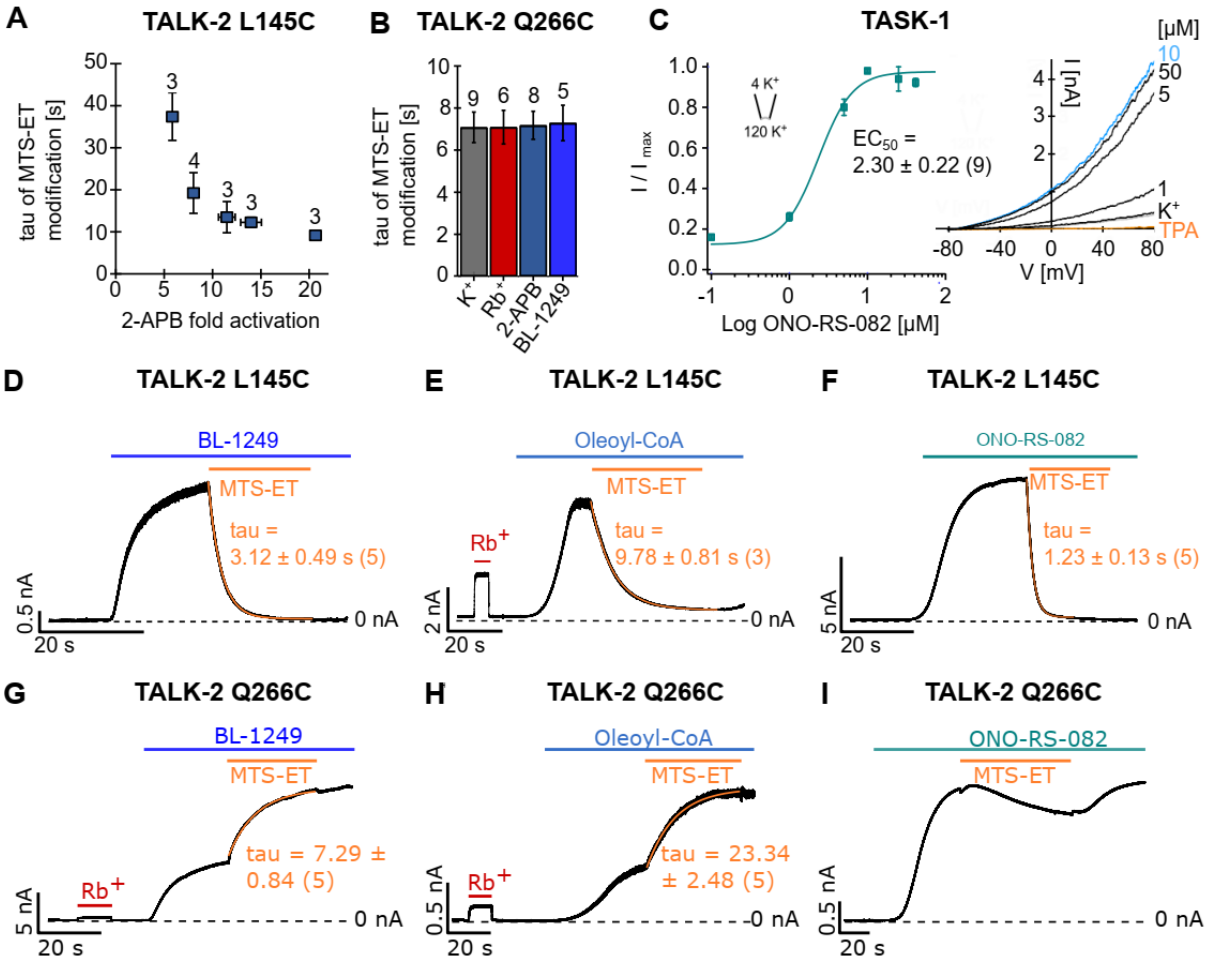

Figure 38 – MTS-ET modification of L145C and Q266C mutants upon activation. A) Tau of MTS-ET (1 mM) modification at varying 2-APB fold activations, measured in cont. +40 mV traces (as in Figure 25 B) using the following 2-APB concentrations: 0.1, 0.2, 0.5, 1 and 2 mM. **B)** tau of MTS-ET (1 mM) modification of TALK-2 Q266C mutants at +40 mV performed in basal K^+ solution (gray, 7.08 ± 0.72 s, n = 9), upon Rb^+ (red, 7.18 ± 0.67 s, n = 6), upon 2-APB (blue, 1 mM, 7.09 ± 0.8 s, n = 8), and upon BL-1249 (darkblue, 50 µM, 7.29 ± 0.84 s, n = 5) activation. **C)** ONO-RS-082 dose response curve of TASK-1 WT channels in asymmetric K+ concentrations (outside 4 mM / inside 120 mM). **D-F)** Example traces of MTS-ET modification of the TALK-2 L145C mutant at +40 mV (D, E) or +20 mV (F) upon activation by 50 µM BL-1249 (D), Oleoyl-CoA (for better patch stability channel was activated using 10 µM Oleoyl-CoA and than held at a constant activity level using 4 µM Oleoyl-CoA) and 3 µM ONO-RS-082. **G-I)** Example traces of TALK-2 Q266C measured as in D-F. *measurements of an other lab member were shown in figure C, see table 6.

In previous studies, it was shown for TASK-1 channels that the mutation of the residue L244A, which resides within the amino acid stretch forming the cytoplasmatic x-gate, increases the basal current of TASK-1 channels dramatically (Rödström et al. 2020). Therefore, it was suggested that these mutations impair the functionality of the x-gate, preventing channel closure (Rödström et al. 2020). Homolog to this residue, we created a TALK-2 mutant (L264A) indicated in the alignment in Figure 36 D.

As it is shown in Figure 39 A and B, the outward current (black) as well as tail current amplitude of this TALK-2 mutant L264A was enlarged compared to the WT. To test weather this mutation has an effect on the SF of the channel K^+ ions were substituted intracellularly by Rb^+ ions, that were thought to stabilize the SF and thus lead to a potentiation of the channel current (shown in section 3.3.1). Notably, the fold activation by Rb^+ substitution (Figure 39 A, red) was similar for the WT and L264A mutant channels, suggesting that the functionality of the filter gate is unaffected by this mutation. By contrast, 2-APB, that potentially acts on an intracellular gate, failed to activate the TALK-2 L264A mutants, but potently activated the WT channels (Figure 39 C). Furthermore, the TPA sensitivity rose dramatically for this mutant compared to the insensitive WT channel (Figure 39 D, E). As a further approach, we tested 2 more open channel blockers, namely A1899 and AVE0118 (Kiper et al. 2015) on the WT channel at basal potassium currents and upon 2-APB (1 mM) activation, as well as on the L264A mutant. Thereby, WT channels were (similarly to TPA) not affected by the application of 10 µM of both compounds. By contrast, upon 2-APB activation or using the L264A mutant, currents were blocked about 50 % by A1899 and AVE0118 (Figure 39 G, H, I). These observations suggest that the binding of open channel blockers is enhanced in the L264A mutant. To further test the pore accessibility of this mutant, an additional cysteine was introduced to the pore cavity of the mutant (TALK-2 L145C L264A). As shown in Figure 39 F, the double mutant L145C L264A was rapidly modified by 1 mM MTS-ET (0.48 ± 0.04 s) under physiological conditions at pH 7.4. This suggests that the L145C L264A mutant has an increased pore accessibility, compared to the WT that was not modified by MTS-ET under the same conditions (Figure 37 A).

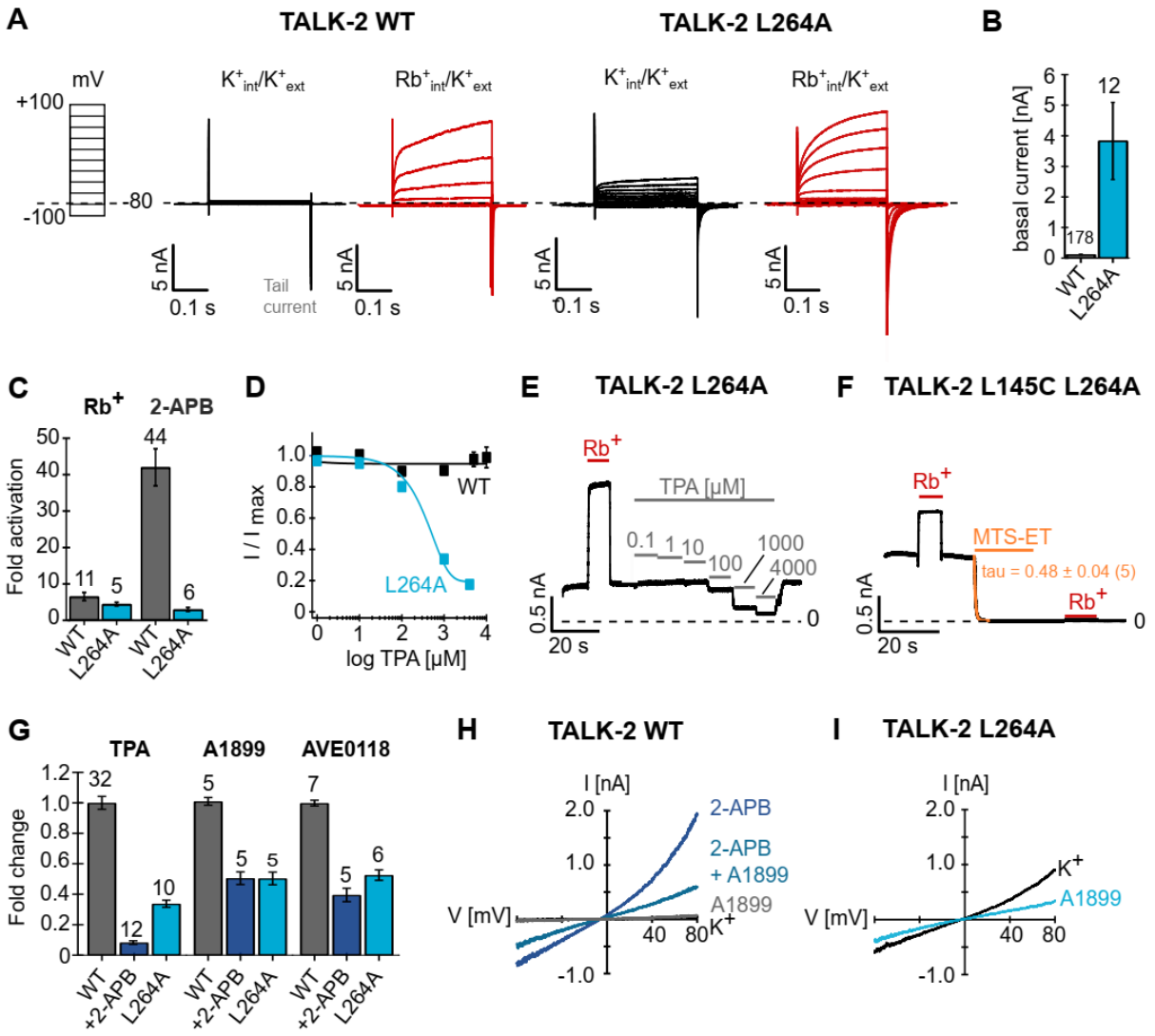

Figure 39 – Effects of the mutation L264A within the putative lower gate in TALK-2 channels. A) Current traces of TALK-2 WT and TALK-2 L264A mutant in symmetric K^+ (black) and after intracellular replacement by Rb^+ (red) measured in voltage families from -100 to +100 mV. **B)** Basal currents of the gain-of-function mutation L264A (3.83 ± 1.26 nA, n = 12) compared to WT channels (0.11 ± 0.01 nA, n = 178). **C)** Fold activation of WT (grey) and L264A mutant (light blue) by Rb^+ and 2-APB (1 mM). **D)** TPA dose response curve (1 – 4000 µM TPA) from WT (black) and L264A mutant (light blue) measured as in E). **E)** Example trace of the L264A mutant blocked by TPA (0.1 – 4000 µM) in a dose dependent manner. **F)** MTS-ET (1 mM) modification of L264A mutants measured at cont. +20 mV in inside out patches, yielding a time curse of modification of 0.48 ± 0.04 s. **G)** Fold change produced by the open channel blockers TPA (1 mM), A1899 (10 µM) and AVE0118 (10 µM) upon basal WT currents (gray), 2-APB (1 mM) activated WT currents and basal L264A mutant currents. Measured as shown in H, I. **H - I)** Example traces of WT (H) an L264A mutants (I) bevor and after application of A1899 and upon activation of the WT using 1 mM 2-APB.

3.3.2.4 Intracellular gates in TASK-1 and TASK-3 channels

As previously described, TASK-1 and TASK-3 channels show inhibition by PIP_2 (section 3.1.2) As depicted in Figure 40 A, a disruption of the intracellular x-gate in TASK-1 channels (see alignment in Figure 40 D) by an introduction of alanine mutations (L244A and R245A, (Rödström et al. 2020)) abolished the PIP_2 inhibition. Application of 10 µM PIP_2 led to an 80 % inhibition of WT TASK-1 channels (Figure 40 A left). By contrast, the x-gate mutants L244A and R245A show no (R245A) or only weak (L244A) sensitivity to PIP_2 (Figure 40 A, middle & right, Figure C). In comparison, 1 mM of the open channel blocker TPA led to a full current block in WT and mutant channels.

Since TASK-3 channels share high sequential similarities with its subfamily member TASK-1 (Figure 40 D), mutations at the homolog positions L244A and R245A were introduced in TASK-3. Strikingly, both TASK-3 mutants L224A and R245A were not inhibited by PIP_2 (they show a weak current increase) while the WT showed an inhibition of 60 % (Figure 40 C). This suggests a similar mechanism of PIP_2 regulation in TASK-1 and TASK-3 channels and indicates that TASK-3 might also exhibits an intracellular gate.

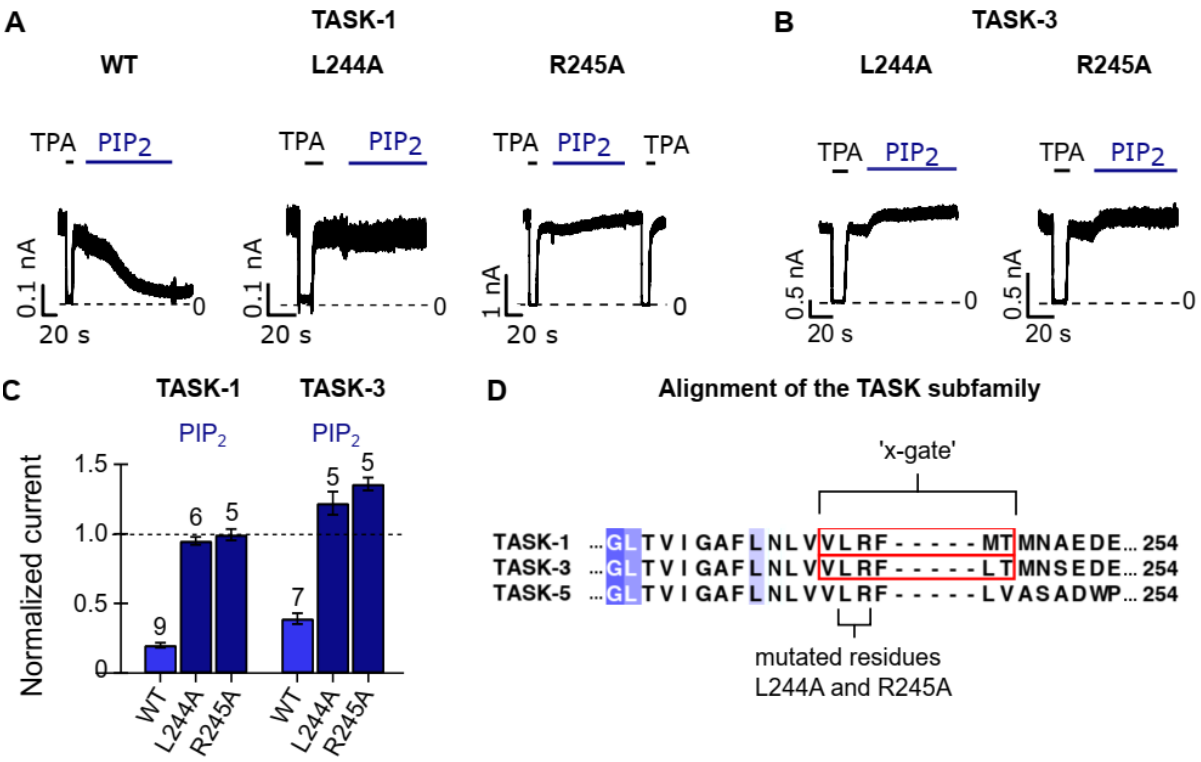

Figure 40 – Mechanism of the PIP_2 sensitivity in TASK-1 channels. A-B) Example traces of TASK-1 WT, L244A and R245A mutants (A) at continouse +40 mV and TASK-3 L244A and R245A mutants

(B) at pH 7.4. 1 mM TPA inhibits the current of all channels. 10 µM PIP_2 leads to an inhbition of the TASK-1 WT current, but not when applied to the TASK-1 and TASK-3 mutants L244A and R245A. **C)** Normalized current (I_{lipid} / I_{basal}) of PIP_2 sensitive TASK-1 and TASK-3 WT and PIP_2 insensitive L244A and R245C mutant channels (mean ± SEM, n as indicated above each bar. TASK-1: WT 0.2 ± 0.02, L244A 0.95 ± 0.03 and R245A 0.99 ± 0.04, TASK-3: WT 0.39 ± 0.04, L244A 1.22 ± 0.08, R245A 1.36 ± 0.05. **D)** Alignment (Brohawn et al. 2012) of the TASK subfamily members TASK-1, TASK-3 and TASK-5, showing striking similarities. The ‚x-gate' forming region is highlighted in red and mutated residues that disrupt the gate are indecated (black).

3.3.2.5 Pore accessibility in TRESK channels

Regulation of TRESK K2P channels plays a critical role in neuronal excitability in DRG neurons (Tulleuda et al. 2011). To study a potential gating mechanism at the intracellular mouth of the channel, we introduced a cysteine within the pore cavity (F352C) and probed for MTS modification under varying gating stimuli.

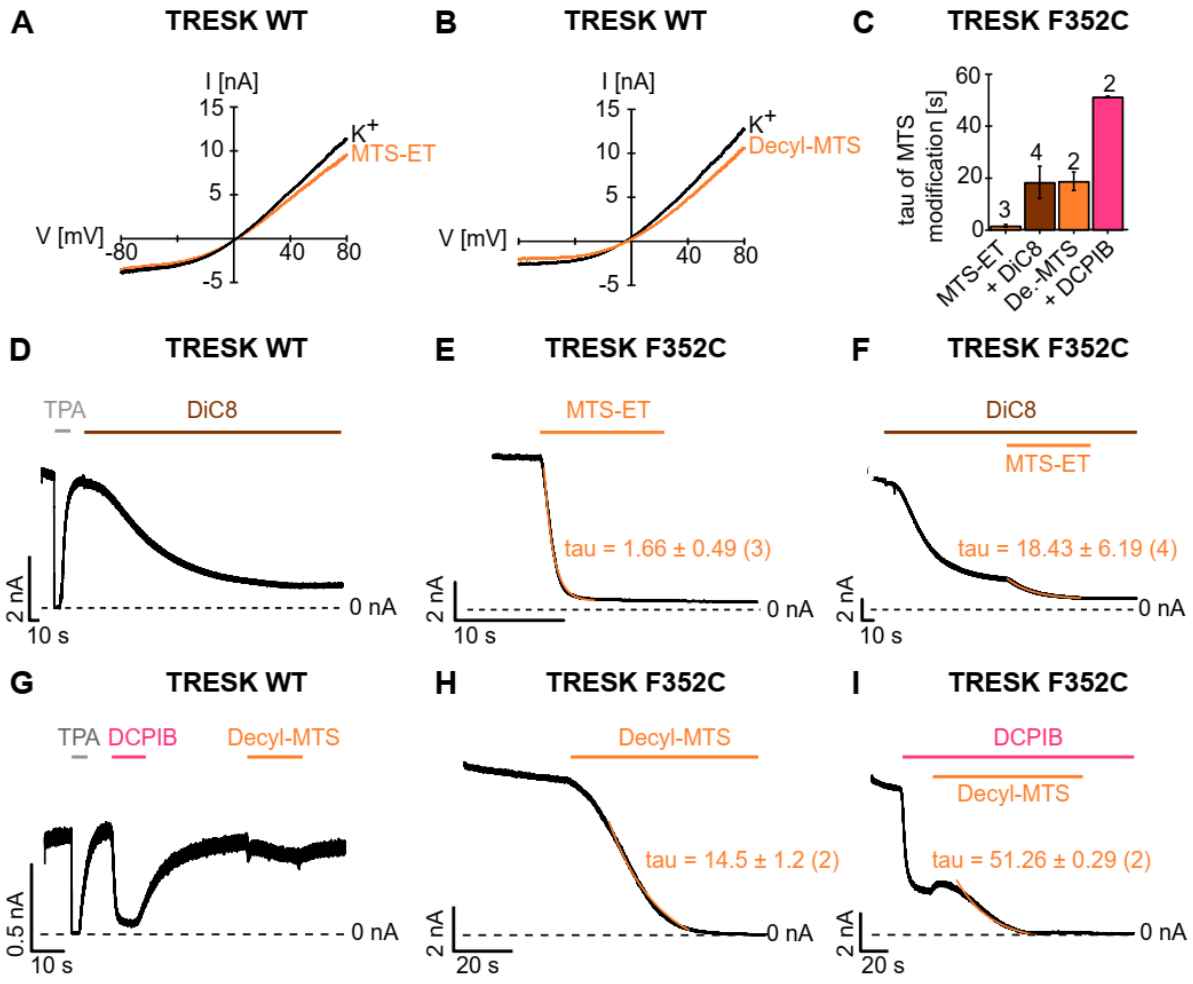

Figure 41 – Intracellular gating in TRESK channels. A-B) Ramp traces of WT TRESK channels measured in symmetric K+ (black) or upon MTS-ET (A) and Decyl-MTS (B) application. **C)** tau of MTS modification of 20 µM MTS-ET and 50 µM Decyl-MTS (orange, 1.66 ± 0.49 s and 14.5 ± 1.2 s, respectively) and upon channel inhibition by 20 µM DiC8 (brown) or 10 µM DCPIB (pink) 18.43 ± 6.19 s and 51.26 ± 0.29 s. **D)** Example trace of TRESK WT channels measured in inside out patches at +40 mV at basal K^+ conditions and upon inhibition by 1 mM TPA and 10 µM DiC8. **E)** TRESK F352C mutant upon MTS-ET (20 µM) modification. **F)** Modification of TRESK F352C mutant by MTS-ET (20 µM) upon DiC8 (20 µM) inhibition. **G)** TRESK WT channels at basal K^+ conditions and upon inhibition by 1 mM TPA and 1 µM DCPIB. **H)** TRESK F352C mutant upon Decyl-MTS (50 µM) modification. **I)** Modification of TRESK F352C mutant by Decyl-MTS (50 µM) upon DCPIB (10 µM) inhibition.

As shown in Figure 41 A and B, WT TRESK channels are largely insensitive to MTS-ET and Decyl-MTS reagents. Notably, the WT channel showed very high basal currents, yielding i.e. 5 nA at +40 mV in the measurements shown in A and B. In addition, the central cavity blocker TPA has a seemingly free access to the pore cavity, leading to a full current inhibition at 1 mM, as shown in Figure 41 D and G. Furthermore, application of 20 µM of the membrane permeable derivative of Diacylglycerol, DiC8 (1,2 dioctanoyl-*sn*-glycerol) as well as 1 µM of the NCA DCPIB lead to channel closure in WT TRESK channels (Figure 41 D, G). However, modification of the mutant F352C led to a full and irreversible current decrease by MTS-ET as well as by using Decyl-MTS, yielding time constants of 1.66 ± 0.49 s and 14.5 ± 1.2 s, respectively (Figure 41 E, H). Strikingly, if applied subsequent to channel inhibition (~80 %) by DiC8 (Figure 41 F) or DCPIB (Figure 41 I) the time curse of modification slowed down drastically to 18.43 ± 6.19 s and 51.26 ± 0.29 s (Figure 41 C).

4. Discussion

In this work several physiological and pharmacological gating stimuli of K2P channels were investigated. This includes the regulation of K2P channels by pH, polyanionic lipids such as PIP_2 and Oleoyl-CoA, as well as registered drugs like the antidepressant Norfluoxetine (NFx), the antidote of pulmonary hypertension ONO-RS-082 or the spasmolysant 2-APB. Thereby, not only the general effect on the current amplitude was studied and recorded, but the overall regulation mechanism of these stimuli was examined. Therefore, potentially gating relevant residues that were known from literature, but also so far undescribed residues were examined by mutagenetic analysis. Furthermore, pharmacological compounds with known binding sites like negatively charged activators (NCAs) or open channel blockers such as quaternary ammonium ions (i.e. TPA) were deployed to study WT and mutant channels in regard to their structural and functional properties. Additionally, cysteine modifying MTS reagents came into use to study i.e. the involvement of the C-terminal domain in channel gating and were further deployed to test the state dependency of residue accessibility, for example of intracellular pore residues under conditions (stimuli) that shift the channel to a more open or more closed conformation.

The experimental results of this study have further extended our knowledge on the diversity of gating regulation in K2P channels and have provided new insights into the structural variety within this channel family. In the following section, the examined stimuli as well as their mechanistical impact on gating structures, such as the selectivity filter, intracellular gates or gating critical residues like phosphorylation sites or pH sensors are discussed.

4.1 K2P channels are versatilely gated by the polyanionic lipids PIP_2 and Oleoyl-CoA

In this study, it was shown that the direct application of polyanionic lipids such as PIP_2 or Oleoyl-CoA effects the channel activity of all tested K2P channels (12 in total). The response to those lipids, however, varied strongly within the K2P channel family. Interestingly, with few exceptions, similar effects were observed for members of the individual subgroups, with TREK, TALK and THIK channels being activated and TWIK, TASK and TRESK channels being inhibited by either one or both tested lipids.

4.1.1 TREK/TRAAK subfamily

Within this work channels of the TREK/TRAAK subfamily were potently activated by PIP_2 (section 3.1.2). Similar results have been reported in previous studies and is explained by the interaction of the negatively charged lipid with a cluster of 5 positively charged (R297, K301, K302, K304, R311) residues at the proximal C-terminal domain (CDT) of the channels. When the positive charges are deleted or mutated to alanine PIP_2 sensitivity is lost (Chemin et al. 2005, 2007). This interaction of PIP_2 with the CTD is believed to pin the CTD to the plasma membrane, stabilizing the active state of the channel (Chemin et al. 2005, 2007; Honoré et al. 2002). However, until now there are no experimental evidences that verify this hypothesis.
Since a restrictive incorporation of the lipid into the cytoplasmic leaflet of the cell membrane alters the curvature and tension of an excised membrane patch (Sheetz and Singer 1974) it is further proposed that the PIP_2 regulation might be coupled to the mechano-gating of the channels (Aryal et al. 2017; Brohawn, Campbell, et al. 2014; Chemin et al. 2005, 2007). Interestingly, it was shown that TRAAK channels (that were the strongest activated channels in this work) begin to activate at lower tension values compared to TREK-1 channels (Brohawn, Su, and MacKinnon 2014). However, how these gating stimuli are related has to be investigated in more detail.
The other tested polyanionic lipid Oleoyl-CoA also produced strong activation of all TREK subfamily members, with TRAAK yet again the most activated channel (section 3.1.3). Since all members of the TREK/TRAAK subfamily are highly sensitive to several lipids (Honoré et al. 2002; Lesage, Terrenoire, et al. 2000; Lesage, Maingret, et al. 2000), this observation was not a surprise. However, until now the Oleoyl-CoA regulation of these channels was unreported and thus, can now be added to the polymodal regulation portfolio of this channel subfamily.

4.1.2 TALK subfamily

TALK-1 and TALK-2 channels were only weakly activated (< 4 -fold) by PIP_2 (section 3.1.2). However, the application of Oleoyl-CoA led to a very strong (100-fold) activation of TALK-2 channels (section 3.1.3). This activation most likely occurs due to an opening of an intracellular gate in TALK-2 channels, that was identified within this work (see section 3.3.2.3). This concept was supported by a cysteine accessibility assay, were the modification of an introduced

pore cysteine was only possible after the channel was activated upon Oleoyl-CoA application. The exact binding site of the polyanionic lipid, however, is still unclear.

TALK-1 and TALK-2 are expressed within pancreatic β-cells (Rorsman and Ashcroft 2018) that regulate the synthesis and release of insulin. It was shown that high glucose levels inhibit the oxidation of fatty acids within cells, leading to an increase of cytosolic long chain-CoA (LC-CoA) levels (Larsson et al. 1996). In the past, accumulation of LC-CoA in response to hyperglycaemia was shown to activate K_{ATP} channels (Shumilina et al. 2006) resulting in a hyperpolarization of the β-cell membrane potential. This hyperpolarization results in a reduced activity of the voltage-dependent calcium channels, important for the Ca^{2+} mediated insulin secretion. Similarly, a TALK-1 gain-of-function mutation (L114P), found in patients suffering under maturity-onset diabetes of the young (MODY), leads to a critical increase in K^+ currents, causing a reduced Ca^{2+} influx in β-cells (Graff et al. 2020). Possibly, the very potent Oleoyl-CoA activation of TALK-2 channels is also linked to the β-cell glucose-stimulated insulin secretion. In addition, it was shown that levels of LC-CoA are elevated in hypoxic cardiac tissue. An activation of cardiac K2P channels (similar as proposed for K_{ATP} channels (Liu et al. 2001)) might has a cardioprotective function. TALK-2 channels are expressed in cardiac tissue (Decher et al. 2001; Girard et al. 2001) and an activation by accumulated LC-CoA during ischemia or myocardial hypoxia could potentially stabilize the membrane potential. Intriguingly, a reduced expression or loss-of-function mutations of TALK-2 channels were recently associated with heart failure and atrial fibrillation (Chai et al. 2017; Staudacher et al. 2018).

In contrast to TALK-1 and TALK-2, TASK-2 channels were inhibited by Oleoyl-CoA and PIP_2. However, the PIP_2 regulation of TASK-2 channels was more complex as in two-thirds of the experiments a concentration dependent biphasic response was observed. Thereby, current rundown under basal conditions was rescued by the application of low PIP_2 concentrations, but did not lead to a current inhibition. Higher concentrations, however, clearly led to channel inhibition. This observation apparently contradicts in part previous studies where TASK-2 was described as a PIP_2 activated channel (Niemeyer et al. 2017). In their study a direct application of the short chained, membrane permeable C8-PIP_2 on HEK293 cells leads to a slight current increase (about 2-fold). Similarly, this was also reported for TASK-2 channels truncated at the C-terminal domain, indicating that the C-terminus is not critical for PIP_2 activation (Li et al. 2020). However, even though rundown was reported in those studies, no data are presented showing both, rundown and the PIP_2 application. Therefore, it is unclear whether their observed

effect resembles an actual activation or (as shown in this study) the rescue of channel activity to the level before rundown.

4.1.3 TWIK subfamily

Within the TWIK subfamily, only TWIK-1 can be functionally expressed in *Xenopus laevis* oocytes. In this study, it is shown that TWIK-1 is insensitive to PIP_2, but is inhibited by Oleoyl-CoA, representing a so far unrecognised regulation mechanism of TWIK-1. TWIK-1 is (similar to TALK-2) expressed within cardiac tissue as well as in pancreatic β-cells, but their functional role is yet unclear (Gaborit et al. 2007; Rorsman and Ashcroft 2018).

4.1.4 TASK subfamily

Within the TASK subfamily, only TASK-1 and TASK-3 can be functionally expressed in *Xenopus laevis* oocytes, while TASK-5 currents are not measurable. TASK-1 channels were not affected by Oleoyl-CoA, but inhibited by PIP_2. Further, it was shown in section 3.3.2.4 that this inhibition was dependent on the functionality of its intracellular x-gate. Accordingly, mutants opening this gate (L244A, R245A) lacked inhibition by PIP_2. This suggest that PIP_2 stabilizes the closed conformation of the channel at the intracellular gate.
A similar mechanism might also exist in TASK-3 channels, that were inhibited by PIP_2 and Oleoyl-CoA. The existence of such a gate in TASK-3 channels has not been shown, however, the residues 243 - 248 (VLRFMT) lining the x-gate are highly conserved within the TASK subfamily. Strikingly, as shown in this work, mutations of the homologue residues L244 and R245 to alanine also abolished the PIP_2 inhibition in TASK-3 channels, suggesting a similar gating mechanism as in TASK-1 channels. Notably, basal currents of TASK-3 at pH 7.4 are a multitude higher than those of TASK-1 channels, suggesting that a lower gate, if present in TASK-3 channels, is mostly open under physiological pH conditions (section 3.1.2 and 3.1.3) and forced to closure upon Oleoyl-CoA and PIP_2 application.

4.1.5 THIK subfamily

Within the THIK subfamily, both THIK-1 and THIK-2 were activated by PIP_2 and Oleoyl-CoA. This is a remarkable finding of this work as it represents the first reported physiological

regulatory mechanism of these channels. THIK channels are highly expressed within brain tissue like hippocampal pyramidal neurons, but also in trigeminal ganglion (TG) neurons, dorsal root ganglion (DRG) neurons and microglia (Kang et al. 2014; Madry et al. 2018; Rajan et al. 2001). However, their specific role is currently unknown in most of the tissues, except for microglial cells, where THIK-1 activation was shown to play a role in immune surveillance and inflammatory cytokine release (Madry et al. 2018). Interestingly, PIP_2 production in microglia cells has been reported to play a key role in immune response signalling (Nguyen et al. 2017), and thus, is possibly linked to THIK-1 activation in microglia.

4.1.6 TRESK subfamily

Here, Oleoyl-CoA was shown to inhibit TRESK channels. Similarly, diacylglycerol (DAG) also reduced channel activity (section 3.3.2.5), while PIP_2 had no effect. The mechanism of the observed Oleoyl-CoA inhibition is unclear. However, DAG inhibition was shown to decrease the accessibility of an introduced pore cysteine (F352C) for MTS reagents (section 3.3.2.5). This suggests a major structural change of the intracellular pore cavity upon DAG inhibition, possibly stabilising the closed conformation of an intracellular gate (or constriction). Potentially, a similar mechanism might also be involved in TRESK inhibition by Oleoyl-CoA, however, this has not been tested yet and must be the subject of future studies.

4.2 Role of the putative pH sensor in TASK-2 channels

pH sensitivity is a common feature in ion channels as it is present in all three structural classes of potassium channels (K_v, K_{ir} and K2P channels) (Lesage and Barhanin 2011; Schulte et al. 1999; Steidl and Yool 1999). It is linked to several physiological functions within the human body ranging from renal reabsorption of bicarbonates (HCO_3^-) and cell-volume regulation, to cell proliferation, apoptosis, chemo sensation and neuroprotection during ischemia (Buckler, Williams, and Honore 2000; Hebert 2003; Heurteaux et al. 2004; Lauritzen et al. 2003; Meuth et al. 2009; Mu et al. 2003; Schulte and Fakler 2000; Warth et al. 2004).

Within this work, but also in previous studies (Decher et al. 2001; Morton et al. 2005) , TALK-2 and TASK-2 channels were shown to be activated by intracellular alkalisation and inhibited by intracellular acidification. Further it is shown here, that TASK-1 is similarly inhibited by intracellular alkalisation (section 3.1.1). The underlaying mechanism of this pH regulation is

not fully understood, however, for TASK-2, the TM4 residue K245 was proposed repeatedly as pH sensor (Bustos et al. 2020; Li et al. 2020; Niemeyer et al. 2010). Within the latest publication by Li et al. (2020), this residue was shown to change its orientation upon alkalisation (or acidification, respectively). Thereby, a cryo-EM structure (PDB Entry: GWLV) obtained at acidic pH_i 6.5 shows the residue K245 pointing into the vestibule entrance sealing the pore cavity (pore radius ~1.2 Å). By contrast, a cryo-EM structure (PDB Entry: 6WMO) obtained under alkalic conditions (pH_i 8.5) exhibits a relatively large pore radius (~3.5 Å) with K245 being rotated by 90°, pointing now upwards in direction of TM2. This conformation allows the passage of hydrated K^+ ions to the upper selectivity filter gate, and thus, resembles the active conformation of the channel. Supposedly, this upward facing orientation of K245 resembles the deprotonated state of the residue, indicating a reduced p*K*a in respect to the usual (free amino acid) p*K*a of 10.5 due to a hydrophobic environment created by the bottom face of TM2. In accordance, a replacement of the lysine by a non-titratable alanine, was shown to abolish activation upon a pH step from 7 to 9 (Li et al. 2020). However, within the present work, the K245A mutant was shown to be less sensitive to pH changes as well, but it was still fully inhibited at pH 5 and showed a 5-fold higher current at pH 10 compared to acidic pH values. Similarly, a substitution of the lysine by cysteine did not abolish pH sensitivity. Notably, both mutants K245A and K245C showed an increased basal current compared to WT channels, suggesting that mutations of this residue influence channel activity. Similarly, mutation of the homolog lysine in TALK-2 channels (K261E) also evoked an increase of basal currents, while pH sensitivity was unaffected. These observations suggest, that this lysine residue might resembles an important site for the functionality of the intracellular gating machinery in TASK-2 (and also TALK-2 channels), but it dismisses its function as proton sensor.

However, to further analyse the role of the K245 residue as pH sensing domain or gating relevant residue in TASK-2 channels it is indispensable to perform further experiments where this residue is replaced by another non-titratable residue (i.e. V, M, G, L or I). Furthermore, the role of the interacting residues of K245 at TM2 and TM4 should be examined.

4.3 Role of the proximal C-terminal domain for TREK and TRAAK channel activation

The importance of the C-terminal domain (CTD) for TREK and TRAAK channel activation by stimuli such as pH or PIP_2 was shown in previous studies (Chemin et al. 2007; Dong et al. 2015;

Honoré et al. 2002; Kim et al. 2001). Furthermore, the CTD exhibits protein kinase A (PKA) as well as PKC phosphorylation sites and is believed to play an important role for the thermo sensibility of the channels (García et al. 2020; Maingret et al. 2000; Murbartián et al. 2005; Noël, Sandoz, and Lesage 2011; Schneider et al. 2014)

In contrast to TASK-1 and TASK-2 channels, crystal structures of the TREK/TRAAK subfamily show no intracellular gate (Brohawn et al. 2012; Dong et al. 2015; Lolicato et al. 2017). Therefore, it is believed that all stimuli altering the channel activity converge directly to the selectivity filter gate (Schewe et al. 2016), but so far it is unclear how this conversion occurs exactly. However, it was repeatedly suggested that an engagement of the CTD with the plasma membrane induces channel activation (Chemin et al. 2005; Dong et al. 2015; Honoré et al. 2002), but until now experimental proof for this concept is missing. Within this work, first experimental evidences are provided that support this theory. Therefore, 10 residues located at the proximal CTD in TREK-1 (and 3 in TRAAK) were mutated to cysteine and consequently modified using an MTS-reagent with a lipophilic decyl moiety (Decyl-MTS), likely to seek membrane incorporation. As a result, the CTD of the Decyl-MTS modified mutants should be pinned irreversibly to the plasma membrane, and thus, channel currents should be increased. Consistently, TREK-1 (and TRAAK) mutants with introduced cysteines at the CTD facing the membrane surface showed a potent and irreversible activation upon Decyl-MTS modification. To further test if this activation indeed stabilizes the active conformation of the channel, the sensitivity of a Decyl-MTS activated mutant (F325C) to the state-dependent TREK inhibitor Norfluoxetine (NFx) was examined. As depicted in Figure 42, NFx binds within side fenestrations only accessible at the less-conductive ‘down state’ conformation of TREK-2 channels, were the pore lining-helices project more into the cytosol (Dong et al. 2015). By contrast, the more conductive ‘up state’ conformation, were the helices are in close proximity to the plasma membrane, lack side fenestrations, and thus, is insensitive to NFx (Dong et al. 2015). Accordingly, it is shown in this work, that Decyl-MTS activated channels were significantly less sensitive to NFx compared to non-modified channels, suggesting that Decyl-MTS modification of CTD residues stabilizes the ‘up state’ conformation of the channels.

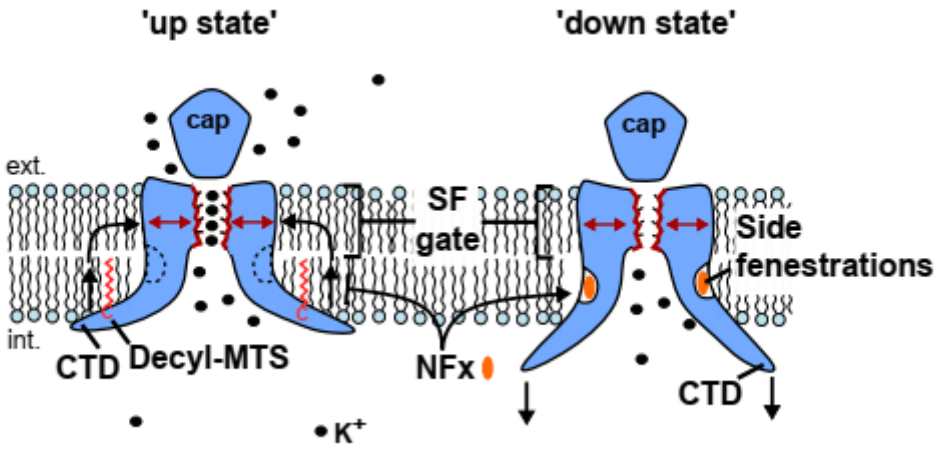

Figure 42 – Up- and down shift of the C-terminal domain. The cartoon depicts the up and down movement of the C-terminal domain (CTD). The up state resembles the active conformation of TREK/TRAAK channels and the selectivity filter (SF) is ion occupied. Cysteine modification by a Decyl-MTS reagent (red) that pin the CTD to the membrane is indicated. Side fenestrations are closed and NFx is unable to bind. The down state resembles the less active state of the channels, were the SF is ion depleted. The CTD projects more into the cytosol and side fenestrations are open. NFx binds within the fenestrations and stabilise the down conformation.

Interestingly, a similar shift in sensitivity to NFx was observed for WT channels activated by intracellular acidification (pH 5), suggesting that pH activation possibly also stabilises the 'up state'. This supports the idea, that protonation of the pH sensor (E321, E306 respectively, located at the proximal CTD in close proximity to the plasma membrane) increases the positively charged character of this protein section, and thus, increases the electrostatic interaction with the negatively charged headgroups of the membrane lipids (Chemin et al. 2005; Honoré et al. 2002).

Notably, mutated CTD residues facing the cytosol (K316C, E320C) showed no channel activation by Decyl-MTS at pH 7.4. However, activation by intracellular acidification and subsequent MTS-modification of those mutants, evoked full current inhibition. As a Decyl-MTS modification of cytosol facing residues potentially leads to a 180° torsion of the CTD helix, this suggest that not only the pure tethering of the CTD to the membrane is critical for channel activation, but also the orientation of the CTD residues.

To further study this hypothesis, the introduction of environmental sensitive unnatural amino acids that change their fluorescent emission in respect to their surroundings could be deployed. When placed at the C-terminal domain, the fluorescent signal should be altered when the residues shift from the cytosol to the lipophilic environment of the membrane upon channel activation. Additionally, further activating stimuli that are believed to act on the CTD, such as

PIP_2 or temperature should be tested in NFx competition experiments. However, this must be the subject of future studies.

4.4 Investigation of the gating mechanism in TALK-2 channels

TALK-2 channels are expressed in several tissues (i.e. heart, brain, liver, pancreas) within the human body (Decher et al. 2001; Girard et al. 2001), however, their gating regulation is poorly understood. Within this work, mechanisms of channel activation and inhibition by pharmacological and physiological stimuli were investigated. Strong activation was observed for reagents such as 2-APB, Drofenine and ONO-RS-082, as well as for negatively charged activators (Schewe et al. 2019) such as BL-1249, ML67-33, NS11021 and DCPIB (section 3.2.1 & unpublished data Björn Jürs, section 3.2.2, section 3.3.2.3). Furthermore, TALK-2 channels were shown to be potently activated by intracellular alkalisation (section 3.1.1, (Decher et al. 2001)) and by polyanionic lipids, such as Oleoyl-CoA (section 3.1.3 & unpublished data Björn Jürs). It is further reported here, that activation by 2-APB, BL-1249, ONO-RS-082 as well as Oleoyl-CoA leads to a major structural change of the cytoplasmatic mouth of the channel, removing an intracellular pore constriction (section 3.3.2.3, unpublished data Jan Langer). Evidence for this concept comes from a cysteine accessibility experiment. Thereby, an introduced pore cysteine was readily modified by MTS-reagents when TALK-2 channels were activated by 2-APB, BL-1249, ONO-RS-082 or Oleoyl-CoA. By contrast no or only very slow modification was observed under basal conditions at pH 7.4 or upon channel activation by extracellular alkalisation or Rb^+ ions. This is an important observation, as Rb^+ is believed to act directly on the selectivity filter (SF) gate (voltage gate), found in TALK-2 channels (Schewe et al. 2016). This suggest, that stimuli (i.e. 2-APB, BL-1249, ONO-RS-082, Oleoyl-CoA) potentially acting on intracellular domains (i.e. TM2, TM4, CTD) are able to open an intracellular pore constriction, while those affecting the SF gate (Rb^+) or extracellular residues (pH_e) do not.

Consistent with a potential structural change of the pore, we found that non-activated TALK-2 channels were not or only poorly blocked by pore blocker such as TPA (unpublished data Björn Jürs & section 3.3.2.1), AVE0118 and A1899 (section 3.3.2.3), but gained high sensitivity to these blockers upon activation. This observation presents a major difference of TALK-2 channel gating compared to other K2P channels, that were shown to be state independently blocked by open channel blockers (section 3.3.2.1, (Piechotta et al. 2011; Rapedius et al. 2012)).

Additionally, it was shown in this work, that a replacement of the TM4 residue L264 by alanine strongly increased TALK-2 channel activity (section 3.3.2.1). In previous studies it was shown, that the homolog TASK-1 mutation (L244A) disrupts the lower gate found in these channels (Rödström et al. 2020). Intriguingly, basal currents of the TALK-2 L264A mutant were potently blocked (unlike WT channels) by TPA, A1899 & AVE0118, and MTS reagents were able to modify an additionally introduced pore cysteine (L264A L145C). Furthermore, this mutant also showed a strongly decreased 2-APB sensitivity, while activation by Rb^+ ions was unaltered. This suggest that mutation of the residue L264 leads to a disruption of the intracellular gate in TALK-2 channels (similar as in TASK-1 channels) without affecting the functionality of the upper selectivity filter gate.

In conclusion, it is reported here, that TALK-2 channels possess an intracellular lower gate (in addition to the SF gate) that can be regulated by stimuli such as 2-APB, BL-1249, ONO-RS-082 as well as Oleoyl-CoA. An illustration of the here established gating model of TALK-2 channels is shown in Figure 43.

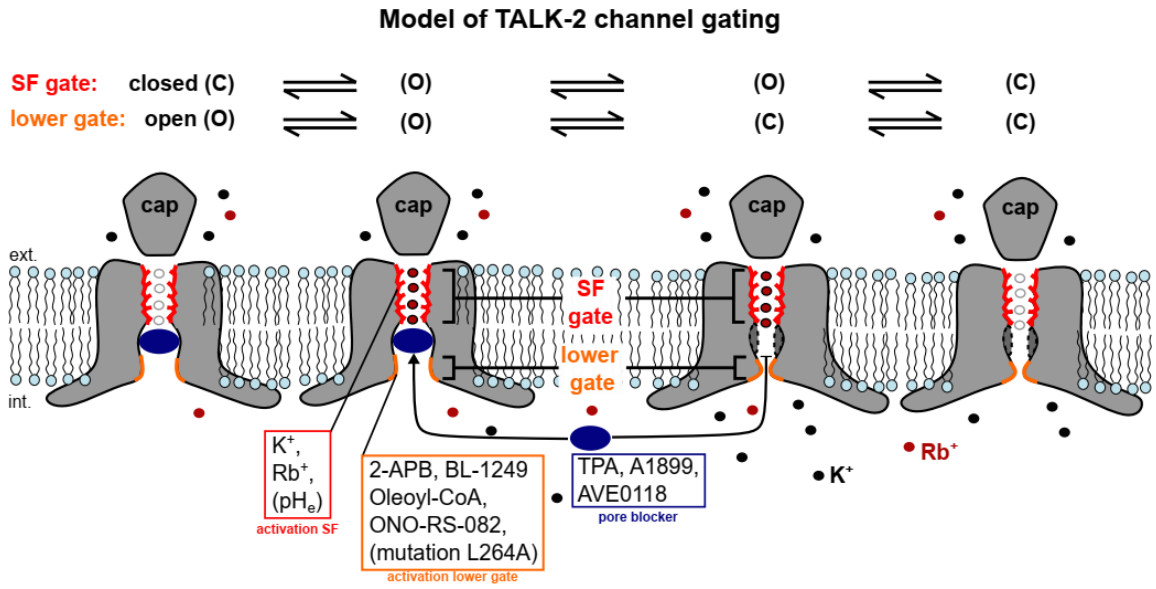

Figure 43 – Model of TALK-2 channel gating. Talk-2 channels possess an upper selectivity filter gate (red), that can be open (O) or closed (C) in response to permeant ions (i.e. K^+, Rb^+) or external pH alterations (pH_e). TALK-2 also possesses a lower gate (orange) that is regulated by 2-APB, BL-1249, Oleoyl-CoA, ONO-RS-082. Mutation of the residue L264 to alanine disrupts the lower gate and closure at the lower gate is not possible. Pore blocker are only able to block TALK-2 channels that are activated at the lower gate. SF activated channels are unable to bind pore blocker.

4.5 State-dependent modification of TRESK channels

TRESK channels expressed in TG neurons as well as in sensory neurones are thought to play an important role for sensory transduction and nociception (Andres-Bilbe et al. 2020; Lafrenière et al. 2010). However, the regulatory mechanisms and gating behaviour of these channels are widely unexplored. Within this work, TRESK channels were shown to conduct large currents (> 10 nA at +80 mV) at physiological pH 7.4 and the channels were blocked potently by TPA (section 3.3.2.1). Furthermore, a fast modification of an introduced pore cysteine by MTS-reagents was possible (section 3.3.2.5). However, as already discussed in section 4.1.6, this MTS-modification was state dependent, as channels inhibited by DAG were significantly slower modified compared to non-inhibited channels. This suggests that TRESK channels exhibit an intracellular gate that can be stabilised in its closed conformation by stimuli such as DAG. Intriguingly, a similar effect was observed for channels inhibited by the compound DCPIB (section 3.3.2.5). However, the binding site of this compound was suggested to be located within the pore cavity in TREK channels (Schewe et al. 2019) and a similar binding site in TRESK is possible (although, TREK channels are activated by DCPIB and not inhibited like TRESK). Therefore, it might be possible that DCPIB protects the introduced pore cysteine (when bound within the cavity), and thus, hinders its modification by MTS-reagents, resulting in an increase of the MTS-modification rate. To further test, whether TRESK channels exhibit a lower gate, it is necessary to study this mechanism in more detail. Therefore, other inhibitors, such as Oleoyl-CoA or intracellular acidification should be tested, as well as MTS modification of another pore cysteine should be examined. Additionally, it might be possible to study this potential conformational change of the pore cavity by FRET analysis, deploying unnatural amino acids. However, these experiments must be the subject of future studies.

4.6 A novel classification of K2P channels according to differences of their gating mechanisms

Voltage-gating was shown to be an intrinsic feature of the selectivity filter (SF) in K2P channels and was shown to be present (to some degree) within almost all subfamilies (section 3.3.1, (Ardestani 2017; Schewe et al. 2016). This SF gating was shown to be very prominent in TREK-1, TREK-2, TRAAK, TALK-1, TALK-2 and TASK-3 channels, while TASK-1, TASK-2 and TWIK-1 channels show a less pronounced SF gating (section 3.3.1, (Ardestani 2017; Schewe

et al. 2016). Only THIK-1 channels were shown to be poorly voltage gated (section 3.3.1) and, thus, the role of the SF-gating is currently unclear.

The presence of a lower gate was recently reported for TASK-1 and TASK-2 channels (Li et al. 2020; Rödström et al. 2020) and most likely, one also exist in TASK-3 channels, due to its strong sequential homology (to TASK-1) and very similar gating behaviour in response to PIP_2 (section 3.3.2.4), DAG (Wilke et al. 2014) or volatile anaesthetics (Ashmole et al. 2009). By contrast, structures of TREK-1, TREK-2, TRAAK and TWIK exhibit no lower gate and those channels are thought to be gated strictly at the SF-gate (Brohawn et al. 2012; Dong et al. 2015; Lolicato et al. 2014, 2017; Rapedius et al. 2012; Schewe et al. 2016). For TALK-1, TALK-2, TRESK and THIK-1 channels no structural information are currently available. Whether THIK-1 or TALK-1 channels possess a lower gate is currently unclear, however, for TALK-2, as well as TRESK channels evidences are provided within this work, indicating the presence of a lower gate (section 3.3.2.1, section 3.3.2.5). If there is a cross-talk between the lower and the upper SF-gate is unclear and must be studied in future experiments.

Concluding, these observations allow a novel categorisation of K2P channels in respect to their gating regulation, as shown in Figure 44. Thereby, K2P channels are classified as SF-gated (i.e. TREK-1, TREK-2, TRAAK and TWIK-1) or as gated at a lower cytoplasmatic gate and the SF (i.e. TASK-1, TASK-2, TASK-3, TALK-2 and TRESK). Gating mechanisms of THIK channels, however, are unclear and must be investigated in following studies. Furthermore, the relative contribution of the SF and/or a lower gate to the channel activity must be investigated in more detail for the respective K2P channels. For example, TREK-1 channels lack a lower gate and are gated strictly at the SF, while TASK-1 channels (that possess a lower gate) show a less pronounced SF gating and, thus, the regulation of the channel activity appears to occur primarily at their lower intracellular gate. However, the importance of the respective gates for channel activity as well as a potential communication between the two gates (if present) must be investigated in following studies.

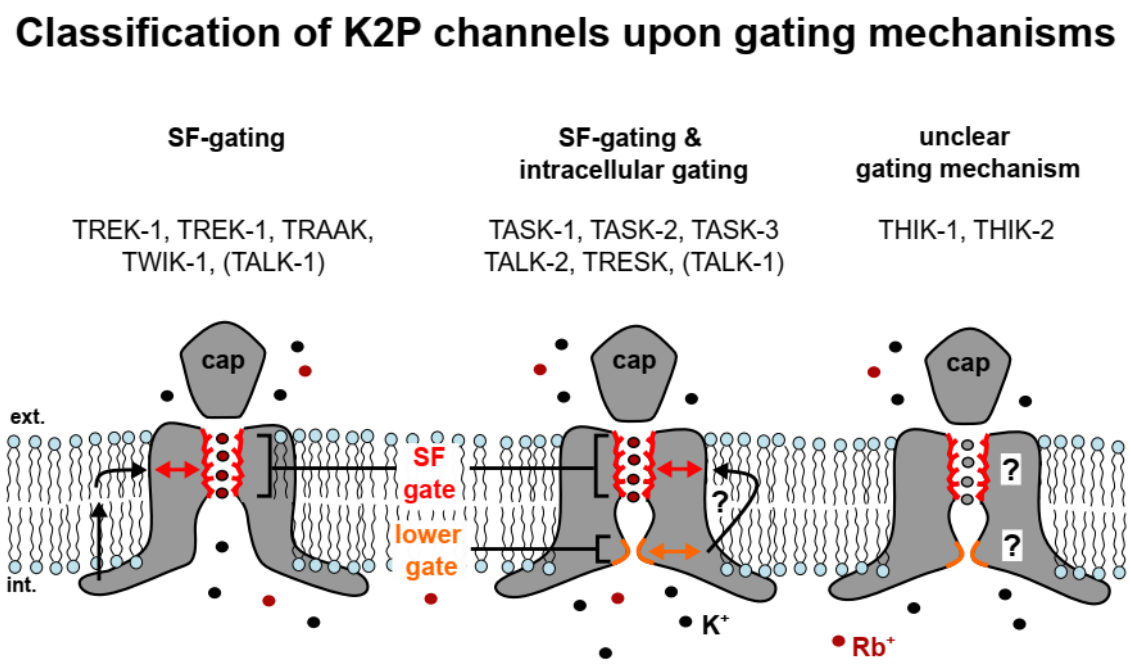

Figure 44 – Classification of K2P channels upon gating mechanism. The cartoon depicts left: K2P channels gated at the selectivity filter (SF) (i.e. TREK-1, TREK-2, TRAAK, TWIK-1, TALK-1). Stimuli altering channel activity are directly converged to the filter indicated with arrows. The cartoon in the middle shows K2P channels gated at the selectivity filter and at a lower gate (TASK-1, TASK-2, TASK-3, TALK-2, TRESK), if these gates communicate is so far unclear indicated with a question mark next to the black arrow. The cartoon on the right indicates that gating of THIK-1 and THIK-2 channels is unclear. TALK-1 shows SF-gating, but an intracellular gate was not investigated yet and a clear categorisation is not possible, indicated in parenthesis in both gating categories.

5. Conclusion and outlook

Within this work, gating mechanisms as well as the corresponding regulatory stimuli of K2P channels were studied. It was shown, that K2P channels are versatile regulated by negatively charged lipids, such as PIP_2 and Oleoyl-CoA. By screening all functional expressing mammalian K2P channels (12 in total), a strong PIP_2 activation for TREK-1, TREK-2, TRAAK (consistent with previous findings (Chemin et al. 2005, 2007; Honoré et al. 2002)) were observed. For the first time, it is reported here that THIK channels are potently activated by PIP_2 and Oleoyl-CoA, raising a number of physiological implications (i.e. microglia activation). In contrast TASK-1 and TASK-3 showed a marked inhibition by PIP_2. Furthermore, it was shown that TASK-2, most likely inherits two regulatory PIP_2 binding sites. The first, sensitive to low concentrations, stabilizes the channel activity under physiological conditions. The second, in contrast, gates the channel closed upon high PIP_2 concentrations. Oleoyl-CoA, has led to straight channel inhibition of TASK-2, but also of TASK-3 and TRESK. TASK-1, however, was unaffected. Interestingly, in contrast to TALK-1, that showed only week activating effects in response to PIP_2 and Oleoyl-CoA, TALK-2 channels surprised with a very potent channel activation upon Oleoyl-CoA application. As TALK-2 is expressed in pancreatic β-cells (Rorsman and Ashcroft 2018), this observation might represent an interesting link to the β-cell glucose-stimulated insulin secretion. Furthermore, this study provides evidence that the PIP_2 inhibition observed in TASK-1 and TASK-3 channels induces the closure of the recently identified intracellular X-gate (Rödström et al. 2020). Contra wise, it is shown here, that an intracellular gate in TALK-2 channels, identified within this study, is locked open by Oleoyl-CoA.

Apart of the lipid regulation, alterations in pH_i were also studied for TREK-1, TASK-1, TASK-2 and TALK-2. In accordance to the literature, TREK-1 is activated by intracellular acidification (Honoré et al. 2002), while the other three channels are inhibited (Li et al. 2020; Morton et al. 2005). Interestingly, it is shown here, that substitution of the putative proton sensor (Bustos et al. 2020; Li et al. 2020; Niemeyer et al. 2016) in TASK-2 by residues unlikely to response to pH changes (alanine, cysteine) does not abolish the pH sensitivity of the TASK-2 channels. This suggests, that the previously proposed residue most likely is not the proton sensor of these channels. However, as mutations at this specific site in TASK-2 were shown to alter channel activity, it is likely that this residue plays a critical role for channel gating. Therefore, the role of this residue for channel gating should be followed up in studies concerning intracellular gating in TASK-2, but also related channels.

In many cases the binding sites of pharmacological compounds or their role within the gating process of ion channels are known. Therefore, compounds such as open channel blocker (TPA, A1899, AVE0118) as well as NCAs or registered drugs i.e. ONO-RS-082, 2-APB or NFx were used to study K2P channel function within this work. Furthermore, cysteine modifying MTS-reagents were deployed to study (i) the involvement of the C-terminal domain in TREK-1, TRAAK and TALK-2 channel gating and (ii) to investigate the intracellular pore accessibility in TREK-1, TALK-2 and TRESK channels. Even though hypothesised earlier (Brohawn, Campbell, et al. 2014; Dong et al. 2015; Honoré et al. 2002), the results presented here show for the first time that TREK-1 and TRAAK channels are activated by the engagement of the C-terminal domain with the lipid bilayer. Also, consistent with previous studies (Rapedius et al. 2012), they lack an intracellular gate, and thus, the central pore cavity is accessible state-independently. By contrast, TALK-2 and TRESK channels comprise a state dependent accessibility, suggesting that these channels possess a lower cytoplasmatic gate, similar to TASK-1 and TASK-2 channels. These observations, led to the reassessment of the dogma, that all K2P channels are gated strictly at the SF. Therefore, a novel classification of K2P channels upon their gating regulation is presented, were K2P channels (i) are gated at the SF or (ii) use an intracellular gate and the SF gate to regulate channel activity.

In conclusion, this work identified several physiological and pharmacological regulation mechanisms within the K2P channel family and broadened our knowledge of their structural and functional gating mechanisms. These results allow a futher assessment of the physiological and pathophysiological role of K2P channels within the human body and might contribute to channel specific drug design in future studies.

6. References

Aikawa, Yoshikatsu, and Thomas F. J. Martin. 2003. 'ARF6 Regulates a Plasma Membrane Pool of Phosphatidylinositol(4,5)Bisphosphate Required for Regulated Exocytosis'. *The Journal of Cell Biology* 162(4):647–59. doi: 10.1083/jcb.200212142.

Andres-Bilbe, Alba, Aida Castellanos, Anna Pujol-Coma, Gerard Callejo, Nuria Comes, and Xavier Gasull. 2020. 'The Background K+ Channel TRESK in Sensory Physiology and Pain'. *International Journal of Molecular Sciences* 21(15):5206. doi: 10.3390/ijms21155206.

Ardestani, Ehsanollah. 2017. 'Identification and Characterization of a Novel Voltage Gating Mechanism in Extracellular PH-Sensitive K2P Channels'. *Dissertation, Christian-Albrechts University* 166.

Armstrong, C. M. 1971. 'Interaction of Tetraethylammonium Ion Derivatives with the Potassium Channels of Giant Axons'. *The Journal of General Physiology* 58(4):413–37. doi: 10.1085/jgp.58.4.413.

Aryal, Prafulla, Viwan Jarerattanachat, Michael V. Clausen, Marcus Schewe, Conor McClenaghan, Liam Argent, Linus J. Conrad, Yin Y. Dong, Ashley C. W. Pike, Elisabeth P. Carpenter, Thomas Baukrowitz, Mark S. P. Sansom, and Stephen J. Tucker. 2017. 'Bilayer-Mediated Structural Transitions Control Mechanosensitivity of the TREK-2 K2P Channel'. *Structure (London, England: 1993)* 25(5):708-718.e2. doi: 10.1016/j.str.2017.03.006.

Ashmole, I., P. A. Goodwin, and P. R. Stanfield. 2001. 'TASK-5, a Novel Member of the Tandem Pore K+ Channel Family'. *Pflugers Archiv: European Journal of Physiology* 442(6):828–33. doi: 10.1007/s004240100620.

Ashmole, I., D. V. Vavoulis, P. J. Stansfeld, Puja R. Mehta, J. F. Feng, M. J. Sutcliffe, and P. R. Stanfield. 2009. 'The Response of the Tandem Pore Potassium Channel TASK-3 (K(2P)9.1) to Voltage: Gating at the Cytoplasmic Mouth'. *The Journal of Physiology* 587(Pt 20):4769–83. doi: 10.1113/jphysiol.2009.175430.

Bayliss, Douglas A., and Paula Q. Barrett. 2008. 'Emerging Roles for Two-Pore-Domain Potassium Channels and Their Potential Therapeutic Impact'. *Trends in Pharmacological Sciences* 29(11):566–75. doi: 10.1016/j.tips.2008.07.013.

Beltrán, Leopoldo, Madeline Beltrán, Ainhara Aguado, Günter Gisselmann, and Hanns Hatt. 2013. '2-Aminoethoxydiphenyl Borate Activates the Mechanically Gated Human KCNK Channels KCNK 2 (TREK-1), KCNK 4 (TRAAK), and KCNK 10 (TREK-2)'. *Frontiers in Pharmacology* 4:63. doi: 10.3389/fphar.2013.00063.

Bentzen, Bo Hjorth, Antonio Nardi, Kirstine Calloe, Lars Siim Madsen, Søren-Peter Olesen, and Morten Grunnet. 2007. 'The Small Molecule NS11021 Is a Potent and Specific Activator of Ca2+-Activated Big-Conductance K+ Channels'. *Molecular Pharmacology* 72(4):1033–44. doi: 10.1124/mol.107.038331.

Berg, Allison P., Edmund M. Talley, Jules P. Manger, and Douglas A. Bayliss. 2004. 'Motoneurons Express Heteromeric TWIK-Related Acid-Sensitive K+ (TASK) Channels Containing TASK-1 (KCNK3) and TASK-3 (KCNK9) Subunits'. *The Journal of Neuroscience: The Official Journal of the Society for Neuroscience* 24(30):6693–6702. doi: 10.1523/JNEUROSCI.1408-04.2004.

Blin, Sandy, Ismail Ben Soussia, Eun-Jin Kim, Frédéric Brau, Dawon Kang, Florian Lesage, and Delphine Bichet. 2016. 'Mixing and Matching TREK/TRAAK Subunits Generate Heterodimeric K2P Channels with Unique Properties'. *Proceedings of the National Academy of Sciences of the United States of America* 113(15):4200–4205. doi: 10.1073/pnas.1522748113.

Blin, Sandy, Franck C. Chatelain, Sylvain Feliciangeli, Dawon Kang, Florian Lesage, and Delphine Bichet. 2014. 'Tandem Pore Domain Halothane-Inhibited K+ Channel Subunits THIK1 and THIK2 Assemble and Form Active Channels'. *The Journal of Biological Chemistry* 289(41):28202–12. doi: 10.1074/jbc.M114.600437.

Brohawn, Stephen G., Ernest B. Campbell, and Roderick MacKinnon. 2014. 'Physical Mechanism for Gating and Mechanosensitivity of the Human TRAAK K+ Channel'. *Nature* 516(7529):126–30. doi: 10.1038/nature14013.

Brohawn, Stephen G., Josefina del Mármol, and Roderick MacKinnon. 2012. 'Crystal Structure of the Human K2P TRAAK, a Lipid- and Mechano-Sensitive K+ Ion Channel'. *Science (New York, N.Y.)* 335(6067):436–41. doi: 10.1126/science.1213808.

Brohawn, Stephen G., Zhenwei Su, and Roderick MacKinnon. 2014. 'Mechanosensitivity Is Mediated Directly by the Lipid Membrane in TRAAK and TREK1 K $^+$ Channels'. *Proceedings of the National Academy of Sciences* 111(9):3614–19. doi: 10.1073/pnas.1320768111.

Buckler, K. J., B. A. Williams, and E. Honore. 2000. 'An Oxygen-, Acid- and Anaesthetic-Sensitive TASK-like Background Potassium Channel in Rat Arterial Chemoreceptor Cells'. *The Journal of Physiology* 525 Pt 1:135–42. doi: 10.1111/j.1469-7793.2000.00135.x.

Buckler, Keith J. 2015. 'TASK Channels in Arterial Chemoreceptors and Their Role in Oxygen and Acid Sensing'. *Pflügers Archiv - European Journal of Physiology* 467(5):1013–25. doi: 10.1007/s00424-015-1689-1.

Bustos, Daniel, Mauricio Bedoya, David Ramírez, Guierdy Concha, Leandro Zúñiga, Niels Decher, Erix W. Hernández-Rodríguez, Francisco V. Sepúlveda, Leandro Martínez, and Wendy González. 2020. 'Elucidating the Structural Basis of the Intracellular PH Sensing Mechanism of TASK-2 K2P Channels'. *International Journal of Molecular Sciences* 21(2). doi: 10.3390/ijms21020532.

Camino, Donato del, Miguel Holmgren, Yi Liu, and Gary Yellen. 2000. 'Blocker Protection in the Pore of a Voltage-Gated K + Channel and Its Structural Implications'. *Nature* 403(6767):321–25. doi: 10.1038/35002099.

Chai, Sam, Xiaoping Wan, Drew M. Nassal, Haiyan Liu, Christine S. Moravec, Angelina Ramirez-Navarro, and Isabelle Deschênes. 2017. 'Contribution of Two-Pore K+ Channels to Cardiac Ventricular Action Potential Revealed Using Human IPSC-Derived Cardiomyocytes'. *American Journal of Physiology. Heart and Circulatory Physiology* 312(6):H1144–53. doi: 10.1152/ajpheart.00107.2017.

Chapman, M. L., H. S. Krovetz, and A. M. VanDongen. 2001. 'GYGD Pore Motifs in Neighbouring Potassium Channel Subunits Interact to Determine Ion Selectivity'. *The Journal of Physiology* 530(Pt 1):21–33. doi: 10.1111/j.1469-7793.2001.0021m.x.

Chavez, R. A., A. T. Gray, B. B. Zhao, C. H. Kindler, M. J. Mazurek, Y. Mehta, J. R. Forsayeth, and C. S. Yost. 1999. 'TWIK-2, a New Weak Inward Rectifying Member of the Tandem Pore Domain Potassium Channel Family'. *The Journal of Biological Chemistry* 274(12):7887–92. doi: 10.1074/jbc.274.12.7887.

Chemin, Jean, Amanda Jane Patel, Fabrice Duprat, Inger Lauritzen, Michel Lazdunski, and Eric Honoré. 2005. 'A Phospholipid Sensor Controls Mechanogating of the K+ Channel TREK-1'. *The EMBO Journal* 24(1):44–53. doi: 10.1038/sj.emboj.7600494.

Chemin, Jean, Amanda Jane Patel, Fabrice Duprat, Frederick Sachs, Michel Lazdunski, and Eric Honore. 2007. 'Up- and down-Regulation of the Mechano-Gated K2P Channel TREK-1 by PIP2 and Other Membrane Phospholipids'. *Pflügers Archiv - European Journal of Physiology* 455(1):97–103. doi: 10.1007/s00424-007-0250-2.

Clausen, Michael V., Viwan Jarerattanachat, Elisabeth P. Carpenter, Mark S. P. Sansom, and Stephen J. Tucker. 2017. 'Asymmetric Mechanosensitivity in a Eukaryotic Ion Channel'. *Proceedings of the National Academy of Sciences of the United States of America* 114(40):E8343–51. doi: 10.1073/pnas.1708990114.

Czirják, Gábor, and Péter Enyedi. 2002. 'Formation of Functional Heterodimers between the TASK-1 and TASK-3 Two-Pore Domain Potassium Channel Subunits'. *The Journal of Biological Chemistry* 277(7):5426–32. doi: 10.1074/jbc.M107138200.

Decher, N., M. Maier, W. Dittrich, J. Gassenhuber, A. Brüggemann, A. E. Busch, and K. Steinmeyer. 2001. 'Characterization of TASK-4, a Novel Member of the PH-Sensitive, Two-Pore Domain Potassium Channel Family'. *FEBS Letters* 492(1–2):84–89. doi: 10.1016/s0014-5793(01)02222-0.

Decher, Niels, Anne K. Streit, Markus Rapedius, Michael F. Netter, Stefanie Marzian, Petra Ehling, Günter Schlichthörl, Tobias Craan, Vijay Renigunta, Annemarie Köhler, Richard C. Dodel, Ricardo A. Navarro-Polanco, Regina Preisig-Müller, Gerhard Klebe, Thomas Budde, Thomas

Baukrowitz, and Jürgen Daut. 2010. 'RNA Editing Modulates the Binding of Drugs and Highly Unsaturated Fatty Acids to the Open Pore of Kv Potassium Channels'. *The EMBO Journal* 29(13):2101–13. doi: 10.1038/emboj.2010.88.

Dickson, Eamonn J., and Bertil Hille. 2019. 'Understanding Phosphoinositides: Rare, Dynamic, and Essential Membrane Phospholipids'. *The Biochemical Journal* 476(1):1–23. doi: 10.1042/BCJ20180022.

Dong, Yin Yao, Ashley C. W. Pike, Alexandra Mackenzie, Conor McClenaghan, Prafulla Aryal, Liang Dong, Andrew Quigley, Mariana Grieben, Solenne Goubin, Shubhashish Mukhopadhyay, Gian Filippo Ruda, Michael V. Clausen, Lishuang Cao, Paul E. Brennan, Nicola A. Burgess-Brown, Mark S. P. Sansom, Stephen J. Tucker, and Elisabeth P. Carpenter. 2015. 'K2P Channel Gating Mechanisms Revealed by Structures of TREK-2 and a Complex with Prozac'. *Science* 347(6227):1256–59. doi: 10.1126/science.1261512.

Doyle, D. A., J. Morais Cabral, R. A. Pfuetzner, A. Kuo, J. M. Gulbis, S. L. Cohen, B. T. Chait, and R. MacKinnon. 1998. 'The Structure of the Potassium Channel: Molecular Basis of K+ Conduction and Selectivity'. *Science (New York, N.Y.)* 280(5360):69–77. doi: 10.1126/science.280.5360.69.

Dumont, J. N. 1972. 'Oogenesis in Xenopus Laevis (Daudin). I. Stages of Oocyte Development in Laboratory Maintained Animals'. *Journal of Morphology* 136(2):153–79. doi: 10.1002/jmor.1051360203.

Duprat, F., F. Lesage, M. Fink, R. Reyes, C. Heurteaux, and M. Lazdunski. 1997. 'TASK, a Human Background K+ Channel to Sense External PH Variations near Physiological PH'. *The EMBO Journal* 16(17):5464–71. doi: 10.1093/emboj/16.17.5464.

Enyedi, Péter, and Gábor Czirják. 2010. 'Molecular Background of Leak K+ Currents: Two-Pore Domain Potassium Channels'. *Physiological Reviews* 90(2):559–605. doi: 10.1152/physrev.00029.2009.

Fink, M., F. Duprat, F. Lesage, R. Reyes, G. Romey, C. Heurteaux, and M. Lazdunski. 1996. 'Cloning, Functional Expression and Brain Localization of a Novel Unconventional Outward Rectifier K+ Channel'. *The EMBO Journal* 15(24):6854–62.

Gaborit, Nathalie, Sabrina Le Bouter, Viktoria Szuts, Andras Varro, Denis Escande, Stanley Nattel, and Sophie Demolombe. 2007. 'Regional and Tissue Specific Transcript Signatures of Ion Channel Genes in the Non-Diseased Human Heart'. *The Journal of Physiology* 582(Pt 2):675–93. doi: 10.1113/jphysiol.2006.126714.

Gada, Kirin, and Leigh D. Plant. 2019. 'Two-Pore Domain Potassium Channels: Emerging Targets for Novel Analgesic Drugs: IUPHAR Review 26'. *British Journal of Pharmacology* 176(2):256–66. doi: https://doi.org/10.1111/bph.14518.

García, Guadalupe, Karina A. Méndez-Reséndiz, Norma Oviedo, and Janet Murbartián. 2020. 'PKC- and PKA-Dependent Phosphorylation Modulates TREK-1 Function in Naïve and Neuropathic Rats'. *Journal of Neurochemistry*. doi: 10.1111/jnc.15204.

Girard, C., F. Duprat, C. Terrenoire, N. Tinel, M. Fosset, G. Romey, M. Lazdunski, and F. Lesage. 2001. 'Genomic and Functional Characteristics of Novel Human Pancreatic 2P Domain K(+) Channels'. *Biochemical and Biophysical Research Communications* 282(1):249–56. doi: 10.1006/bbrc.2001.4562.

Goldstein, Matthias, Susanne Rinné, Aytug K. Kiper, David Ramírez, Michael F. Netter, Daniel Bustos, Beatriz Ortiz-Bonnin, Wendy González, and Niels Decher. 2016. 'Functional Mutagenesis Screens Reveal the "cap Structure" Formation in Disulfide-Bridge Free TASK Channels'. *Scientific Reports* 6:19492. doi: 10.1038/srep19492.

González, Carlos, David Baez-Nieto, Ignacio Valencia, Ingrid Oyarzún, Patricio Rojas, David Naranjo, and Ramón Latorre. 2012. 'K+ Channels: Function-Structural Overview'. Pp. 2087–2149 in *Comprehensive Physiology*. American Cancer Society.

González, Wendy, Braulio Valdebenito, Julio Caballero, Gonzalo Riadi, Janin Riedelsberger, Gonzalo Martínez, David Ramírez, Leandro Zúñiga, Francisco V. Sepúlveda, Ingo Dreyer, Michael Janta, and Dirk Becker. 2015. 'K_2p Channels in Plants and Animals'. *Pflugers Archiv: European Journal of Physiology* 467(5):1091–1104. doi: 10.1007/s00424-014-1638-4.

Graff, Sarah M., Stephanie R. Johnson, Paul J. Leo, Prasanna K. Dadi, Arya Y. Nakhe, Aideen M. McInerney-Leo, Mhairi Marshall, Matthew A. Brown, David A. Jacobson, and Emma L. Duncan. 2020. *A Novel Mutation in* KCNK16 *Causing a Gain-of-Function in the TALK-1 Potassium Channel: A New Cause of Maturity Onset Diabetes of the Young*. *preprint*. Genetics.

Hebert, Steven C. 2003. 'Bartter Syndrome'. *Current Opinion in Nephrology and Hypertension* 12(5):527–32. doi: 10.1097/00041552-200309000-00008.

Hedrich, Rainer. 2012. 'Ion Channels in Plants'. *Physiological Reviews* 92(4):1777–1811. doi: 10.1152/physrev.00038.2011.

Heurteaux, C., N. Guy, C. Laigle, N. Blondeau, F. Duprat, M. Mazzuca, L. Lang-Lazdunski, C. Widmann, M. Zanzouri, G. Romey, and M. Lazdunski. 2004. 'TREK-1, a K+ Channel Involved in Neuroprotection and General Anesthesia'. *The EMBO Journal* 23(13):2684–95. doi: 10.1038/sj.emboj.7600234.

Hille, Bertil. 2001. *Ion Channels of Excitable Membranes*. Vol. 18.

Honoré, Eric. 2007. 'The Neuronal Background K 2P Channels: Focus on TREK1'. *Nature Reviews Neuroscience* 8(4):251–61. doi: 10.1038/nrn2117.

Honoré, Eric, François Maingret, Michel Lazdunski, and Amanda Jane Patel. 2002. 'An Intracellular Proton Sensor Commands Lipid- and Mechano-Gating of the K(+) Channel TREK-1'. *The EMBO Journal* 21(12):2968–76. doi: 10.1093/emboj/cdf288.

Hoshi, T., W. N. Zagotta, and R. W. Aldrich. 1990. 'Biophysical and Molecular Mechanisms of Shaker Potassium Channel Inactivation'. *Science* 250(4980):533–38. doi: 10.1126/science.2122519.

Huang, Chou-Long. 2007. 'Complex Roles of PIP2 in the Regulation of Ion Channels and Transporters'. *American Journal of Physiology-Renal Physiology* 293(6):F1761–65. doi: 10.1152/ajprenal.00400.2007.

Huang, Dong-Yue, Bu-Wei Yu, and Qiu-Wei Fan. 2008. 'Roles of TRESK, a Novel Two-Pore Domain K+ Channel, in Pain Pathway and General Anesthesia'. *Neuroscience Bulletin* 24(3):166–72. doi: 10.1007/s12264-008-0225-0.

Hwang, Eun Mi, Eunju Kim, Oleg Yarishkin, Dong Ho Woo, Kyung-Seok Han, Nammi Park, Yeonju Bae, Junsung Woo, Donggyu Kim, Myeongki Park, C. Justin Lee, and Jae-Yong Park. 2014. 'A Disulphide-Linked Heterodimer of TWIK-1 and TREK-1 Mediates Passive Conductance in Astrocytes'. *Nature Communications* 5:3227. doi: 10.1038/ncomms4227.

Ingólfsson, Helgi I., Manuel N. Melo, Floris J. van Eerden, Clément Arnarez, Cesar A. Lopez, Tsjerk A. Wassenaar, Xavier Periole, Alex H. de Vries, D. Peter Tieleman, and Siewert J. Marrink. 2014. 'Lipid Organization of the Plasma Membrane'. *Journal of the American Chemical Society* 136(41):14554–59. doi: 10.1021/ja507832e.

Kang, Dawon, James O. Hogan, and Donghee Kim. 2014. 'THIK-1 (K2P13.1) Is a Small-Conductance Background K(+) Channel in Rat Trigeminal Ganglion Neurons'. *Pflugers Archiv: European Journal of Physiology* 466(7):1289–1300. doi: 10.1007/s00424-013-1358-1.

Kennard, Louise E., Justin R. Chumbley, Kishani M. Ranatunga, Stephanie J. Armstrong, Emma L. Veale, and Alistair Mathie. 2005. 'Inhibition of the Human Two-Pore Domain Potassium Channel, TREK-1, by Fluoxetine and Its Metabolite Norfluoxetine'. *British Journal of Pharmacology* 144(6):821–29. doi: https://doi.org/10.1038/sj.bjp.0706068.

Kim, D., and C. Gnatenco. 2001. 'TASK-5, a New Member of the Tandem-Pore K(+) Channel Family'. *Biochemical and Biophysical Research Communications* 284(4):923–30. doi: 10.1006/bbrc.2001.5064.

Kim, Eun-Jin, Dong Kun Lee, Seong-Geun Hong, Jaehee Han, and Dawon Kang. 2017. 'Activation of TREK-1, but Not TREK-2, Channel by Mood Stabilizers'. *International Journal of Molecular Sciences* 18(11). doi: 10.3390/ijms18112460.

Kim, Y., H. Bang, C. Gnatenco, and D. Kim. 2001. 'Synergistic Interaction and the Role of C-Terminus in the Activation of TRAAK K+ Channels by Pressure, Free Fatty Acids and Alkali'. *Pflugers Archiv: European Journal of Physiology* 442(1):64–72. doi: 10.1007/s004240000496.

Kim, Y., H. Bang, and D. Kim. 2000. 'TASK-3, a New Member of the Tandem Pore K(+) Channel Family'. *The Journal of Biological Chemistry* 275(13):9340–47. doi: 10.1074/jbc.275.13.9340.

Kindler, Christoph H., Matthias Paul, Hilary Zou, Canhui Liu, Bruce D. Winegar, Andrew T. Gray, and C. Spencer Yost. 2003. 'Amide Local Anesthetics Potently Inhibit the Human Tandem Pore Domain Background K+ Channel TASK-2 (KCNK5)'. *Journal of Pharmacology and Experimental Therapeutics* 306(1):84–92. doi: 10.1124/jpet.103.049809.

Kiper, Aytug K., Susanne Rinné, Caroline Rolfes, David Ramírez, Guiscard Seebohm, Michael F. Netter, Wendy González, and Niels Decher. 2015. 'Kv1.5 Blockers Preferentially Inhibit TASK-1 Channels: TASK-1 as a Target against Atrial Fibrillation and Obstructive Sleep Apnea?' *Pflügers Archiv - European Journal of Physiology* 467(5):1081–90. doi: 10.1007/s00424-014-1665-1.

Lafrenière, Ronald G., M. Zameel Cader, Jean-François Poulin, Isabelle Andres-Enguix, Maryse Simoneau, Namrata Gupta, Karine Boisvert, François Lafrenière, Shannon McLaughlan, Marie-Pierre Dubé, Martin M. Marcinkiewicz, Sreeram Ramagopalan, Olaf Ansorge, Bernard Brais, Jorge Sequeiros, Jose Maria Pereira-Monteiro, Lyn R. Griffiths, Stephen J. Tucker, George Ebers, and Guy A. Rouleau. 2010. 'A Dominant-Negative Mutation in the TRESK Potassium Channel Is Linked to Familial Migraine with Aura'. *Nature Medicine* 16(10):1157–60. doi: 10.1038/nm.2216.

Larsson, O., J. T. Deeney, R. Bränström, P. O. Berggren, and B. E. Corkey. 1996. 'Activation of the ATP-Sensitive K+ Channel by Long Chain Acyl-CoA. A Role in Modulation of Pancreatic Beta-Cell Glucose Sensitivity'. *The Journal of Biological Chemistry* 271(18):10623–26. doi: 10.1074/jbc.271.18.10623.

Lauritzen, Inger, Marc Zanzouri, Eric Honoré, Fabrice Duprat, Markus U. Ehrengruber, Michel Lazdunski, and Amanda J. Patel. 2003. 'K+-Dependent Cerebellar Granule Neuron Apoptosis. Role of Task Leak K+ Channels'. *The Journal of Biological Chemistry* 278(34):32068–76. doi: 10.1074/jbc.M302631200.

Lengyel, Miklós, Gábor Czirják, David A. Jacobson, and Péter Enyedi. 2020. 'TRESK and TREK-2 Two-Pore-Domain Potassium Channel Subunits Form Functional Heterodimers in Primary Somatosensory Neurons'. *The Journal of Biological Chemistry* 295(35):12408–25. doi: 10.1074/jbc.RA120.014125.

Lesage, F., E. Guillemare, M. Fink, F. Duprat, M. Lazdunski, G. Romey, and J. Barhanin. 1996. 'TWIK-1, a Ubiquitous Human Weakly Inward Rectifying K+ Channel with a Novel Structure.' *The EMBO Journal* 15(5):1004–11. doi: 10.1002/j.1460-2075.1996.tb00437.x.

Lesage, F., F. Maingret, and M. Lazdunski. 2000. 'Cloning and Expression of Human TRAAK, a Polyunsaturated Fatty Acids-Activated and Mechano-Sensitive K(+) Channel'. *FEBS Letters* 471(2–3):137–40. doi: 10.1016/s0014-5793(00)01388-0.

Lesage, F., R. Reyes, M. Fink, F. Duprat, E. Guillemare, and M. Lazdunski. 1996. 'Dimerization of TWIK-1 K+ Channel Subunits via a Disulfide Bridge'. *The EMBO Journal* 15(23):6400–6407.

Lesage, F., C. Terrenoire, G. Romey, and M. Lazdunski. 2000. 'Human TREK2, a 2P Domain Mechano-Sensitive K+ Channel with Multiple Regulations by Polyunsaturated Fatty Acids, Lysophospholipids, and Gs, Gi, and Gq Protein-Coupled Receptors'. *The Journal of Biological Chemistry* 275(37):28398–405. doi: 10.1074/jbc.M002822200.

Lesage, Florian, and Jacques Barhanin. 2011. 'Molecular Physiology of PH-Sensitive Background K_{2P} Channels'. *Physiology* 26(6):424–37. doi: 10.1152/physiol.00029.2011.

Levitz, Joshua, Perrine Royal, Yannick Comoglio, Brigitte Wdziekonski, Sébastien Schaub, Daniel M. Clemens, Ehud Y. Isacoff, and Guillaume Sandoz. 2016. 'Heterodimerization within the TREK Channel Subfamily Produces a Diverse Family of Highly Regulated Potassium Channels'. *Proceedings of the National Academy of Sciences of the United States of America* 113(15):4194–99. doi: 10.1073/pnas.1522459113.

Li, Baobin, Robert A. Rietmeijer, and Stephen G. Brohawn. 2020. 'Structural Basis for PH Gating of the Two-Pore Domain K + Channel TASK2'. *Nature* 1–6. doi: 10.1038/s41586-020-2770-2.

Liu, G. X., P. J. Hanley, J. Ray, and J. Daut. 2001. 'Long-Chain Acyl-Coenzyme A Esters and Fatty Acids Directly Link Metabolism to K(ATP) Channels in the Heart'. *Circulation Research* 88(9):918–24. doi: 10.1161/hh0901.089881.

Liu, Yang, and Vytas A. Bankaitis. 2010. 'Phosphoinositide Phosphatases in Cell Biology and Disease'. *Progress in Lipid Research* 49(3):201–17. doi: 10.1016/j.plipres.2009.12.001.

Logan, Michael R., and Craig A. Mandato. 2006. 'Regulation of the Actin Cytoskeleton by PIP2 in Cytokinesis'. *Biology of the Cell* 98(6):377–88. doi: 10.1042/BC20050081.

Lolicato, Marco, Cristina Arrigoni, Takahiro Mori, Yoko Sekioka, Clifford Bryant, Kimberly A. Clark, and Daniel L. Minor. 2017. 'K2P2.1(TREK-1):Activator Complexes Reveal a Cryptic Selectivity Filter Binding Site'. *Nature* 547(7663):364–68. doi: 10.1038/nature22988.

Lolicato, Marco, Paul M. Riegelhaupt, Cristina Arrigoni, Kimberly A. Clark, and Daniel L. Minor. 2014. 'Transmembrane Helix Straightening and Buckling Underlies Activation of Mechanosensitive and Thermosensitive K(2P) Channels'. *Neuron* 84(6):1198–1212. doi: 10.1016/j.neuron.2014.11.017.

Lopes, C. M., N. Zilberberg, and S. A. Goldstein. 2001. 'Block of Kcnk3 by Protons. Evidence That 2-P-Domain Potassium Channel Subunits Function as Homodimers'. *The Journal of Biological Chemistry* 276(27):24449–52. doi: 10.1074/jbc.C100184200.

Lopes, Coeli M. B., Tibor Rohács, Gábor Czirják, Tamás Balla, Péter Enyedi, and Diomedes E. Logothetis. 2005. 'PIP2 Hydrolysis Underlies Agonist-Induced Inhibition and Regulates Voltage Gating of Two-Pore Domain K+ Channels'. *The Journal of Physiology* 564(Pt 1):117–29. doi: 10.1113/jphysiol.2004.081935.

Ma, Lijiang, Mélanie Eyries, Marine Germain, David-Alexandre Trégouët, Erika Berman Rosenzweig, Marc Humbert, and Wendy K. Chung. 2013. 'A Novel Channelopathy in Pulmonary Arterial Hypertension'. *The New England Journal of Medicine* 11.

Ma, Liqun, Xuexin Zhang, and Haijun Chen. 2011. 'TWIK-1 Two-Pore Domain Potassium Channels Change Ion Selectivity and Conduct Inward Leak Sodium Currents in Hypokalemia'. *Science Signaling* 4(176):ra37. doi: 10.1126/scisignal.2001726.

Madry, Christian, Vasiliki Kyrargyri, I. Lorena Arancibia-Cárcamo, Renaud Jolivet, Shinichi Kohsaka, Robert M. Bryan, and David Attwell. 2018. 'Microglial Ramification, Surveillance, and Interleukin-1β Release Are Regulated by the Two-Pore Domain K+ Channel THIK-1'. *Neuron* 97(2):299-312.e6. doi: 10.1016/j.neuron.2017.12.002.

Maingret, F., I. Lauritzen, A. J. Patel, C. Heurteaux, R. Reyes, F. Lesage, M. Lazdunski, and E. Honoré. 2000. 'TREK-1 Is a Heat-Activated Background K(+) Channel'. *The EMBO Journal* 19(11):2483–91. doi: 10.1093/emboj/19.11.2483.

McLaughlin, Stuart, and Diana Murray. 2005. 'Plasma Membrane Phosphoinositide Organization by Protein Electrostatics'. *Nature* 438(7068):605–11. doi: 10.1038/nature04398.

Meuth, Sven G., Christoph Kleinschnitz, Tilman Broicher, Madeleine Austinat, Stefan Braeuninger, Stefan Bittner, Stephan Fischer, Douglas A. Bayliss, Thomas Budde, Guido Stoll, and Heinz Wiendl. 2009. 'The Neuroprotective Impact of the Leak Potassium Channel TASK1 on Stroke Development in Mice'. *Neurobiology of Disease* 33(1):1–11. doi: 10.1016/j.nbd.2008.09.006.

Meves, H. 2008. 'Arachidonic Acid and Ion Channels: An Update'. *British Journal of Pharmacology* 155(1):4–16. doi: https://doi.org/10.1038/bjp.2008.216.

Miller, Alexandria N., and Stephen B. Long. 2012. 'Crystal Structure of the Human Two-Pore Domain Potassium Channel K2P1'. *Science (New York, N.Y.)* 335(6067):432–36. doi: 10.1126/science.1213274.

Miller, Christopher. 2000. 'An Overview of the Potassium Channel Family'. *Genome Biology* 1(4):reviews0004.1-reviews0004.5.

Miyamoto, S., G. E. Duncan, C. E. Marx, and J. A. Lieberman. 2005. 'Treatments for Schizophrenia: A Critical Review of Pharmacology and Mechanisms of Action of Antipsychotic Drugs'. *Molecular Psychiatry* 10(1):79–104. doi: 10.1038/sj.mp.4001556.

Morais-Cabral, João H., Yufeng Zhou, and Roderick MacKinnon. 2001. 'Energetic Optimization of Ion Conduction Rate by the K + Selectivity Filter'. *Nature* 414(6859):37–42. doi: 10.1038/35102000.

Morton, Michael J., Abdulrahman Abohamed, Asipu Sivaprasadarao, and Malcolm Hunter. 2005. 'PH Sensing in the Two-Pore Domain K+ Channel, TASK2'. *Proceedings of the National Academy of Sciences* 102(44):16102–6. doi: 10.1073/pnas.0506870102.

Morton, Michael J., Anthony D. O'Connell, Asipu Sivaprasadarao, and Malcolm Hunter. 2003. 'Determinants of PH Sensing in the Two-Pore Domain K(+) Channels TASK-1 and -2'. *Pflugers Archiv: European Journal of Physiology* 445(5):577–83. doi: 10.1007/s00424-002-0901-2.

Mu, David, Liyun Chen, Xiping Zhang, Lei-Hoon See, Christina M. Koch, Clifford Yen, James Jiayuan Tong, Lori Spiegel, Ken C. Q. Nguyen, Allyson Servoss, Yue Peng, Lin Pei, Jeffrey R. Marks, Scott Lowe, Timothy Hoey, Lily Yeh Jan, W. Richard McCombie, Michael H. Wigler, and Scott Powers. 2003. 'Genomic Amplification and Oncogenic Properties of the KCNK9 Potassium Channel Gene'. *Cancer Cell* 3(3):297–302. doi: 10.1016/s1535-6108(03)00054-0.

Murbartián, Janet, Qiubo Lei, Julianne J. Sando, and Douglas A. Bayliss. 2005. 'Sequential Phosphorylation Mediates Receptor- and Kinase-Induced Inhibition of TREK-1 Background Potassium Channels *'. *Journal of Biological Chemistry* 280(34):30175–84. doi: 10.1074/jbc.M503862200.

Nayak, Tapan K., S. Harinath, S. Nama, K. Somasundaram, and S. K. Sikdar. 2009. 'Inhibition of Human Two-Pore Domain K+ Channel TREK1 by Local Anesthetic Lidocaine: Negative Cooperativity and Half-of-Sites Saturation Kinetics'. *Molecular Pharmacology* 76(4):903–17. doi: 10.1124/mol.109.056838.

Nguyen, Tu Thi Ngoc, Eunjeong Seo, Juyong Choi, Oanh Thi Tu Le, Ji Yun Kim, Ilo Jou, and Sang Yoon Lee. 2017. 'Phosphatidylinositol 4-Phosphate 5-Kinase α Contributes to Toll-like Receptor 2-Mediated Immune Responses in Microglial Cells Stimulated with Lipoteichoic Acid'. *Cellular Signalling* 38:159–70. doi: 10.1016/j.cellsig.2017.07.009.

Niemeyer, María Isabel, L. Pablo Cid, Wendy González, and Francisco V. Sepúlveda. 2016. 'Gating, Regulation, and Structure in K2P K+ Channels: In Varietate Concordia?' *Molecular Pharmacology* 90(3):309–17. doi: 10.1124/mol.116.103895.

Niemeyer, María Isabel, L. Pablo Cid, Marc Paulais, Jacques Teulon, and Francisco V. Sepúlveda. 2017. 'Phosphatidylinositol (4,5)-Bisphosphate Dynamically Regulates the K 2P Background K + Channel TASK-2'. *Scientific Reports* 7(1):45407. doi: 10.1038/srep45407.

Niemeyer, María Isabel, L. Pablo Cid, Gaspar Peña-Münzenmayer, and Francisco V. Sepúlveda. 2010. 'Separate Gating Mechanisms Mediate the Regulation of K2P Potassium Channel TASK-2 by Intra- and Extracellular PH'. *The Journal of Biological Chemistry* 285(22):16467–75. doi: 10.1074/jbc.M110.107060.

Noël, Jacques, Guillaume Sandoz, and Florian Lesage. 2011. 'Molecular Regulations Governing TREK and TRAAK Channel Functions'. *Channels* 5(5):402–9. doi: 10.4161/chan.5.5.16469.

Noël, Jacques, Katharina Zimmermann, Jérome Busserolles, Emanuel Deval, Abdelkrim Alloui, Sylvie Diochot, Nicolas Guy, Marc Borsotto, Peter Reeh, Alain Eschalier, and Michel Lazdunski. 2009. 'The Mechano-Activated K+ Channels TRAAK and TREK-1 Control Both Warm and Cold Perception'. *The EMBO Journal* 28(9):1308–18. doi: 10.1038/emboj.2009.57.

van Paridon, Peter A., Ben de Kruijff, Ronald Ouwerkerk, and Karel W. A. Wirtz. 1986. 'Polyphosphoinositides Undergo Charge Neutralization in the Physiological PH Range: A 31P-NMR Study'. *Biochimica et Biophysica Acta (BBA) - Lipids and Lipid Metabolism* 877(1):216–19. doi: 10.1016/0005-2760(86)90137-2.

Patel, A. J., E. Honoré, F. Lesage, M. Fink, G. Romey, and M. Lazdunski. 1999. 'Inhalational Anesthetics Activate Two-Pore-Domain Background K+ Channels'. *Nature Neuroscience* 2(5):422–26. doi: 10.1038/8084.

Pereira, Vanessa, Jérôme Busserolles, Marine Christin, Maïly Devilliers, Laura Poupon, Wassim Legha, Abdelkrim Alloui, Youssef Aissouni, Emmanuel Bourinet, Florian Lesage, Alain Eschalier, Michel Lazdunski, and Jacques Noël. 2014. 'Role of the TREK2 Potassium Channel in Cold and Warm Thermosensation and in Pain Perception'. *Pain* 155(12):2534–44. doi: 10.1016/j.pain.2014.09.013.

Piechotta, Paula L., Markus Rapedius, Phillip J. Stansfeld, Murali K. Bollepalli, Gunter Erhlich, Isabelle Andres-Enguix, Hariolf Fritzenschaft, Niels Decher, Mark S. P. Sansom, Stephen J. Tucker, and Thomas Baukrowitz. 2011. 'The Pore Structure and Gating Mechanism of K2P Channels: K2P Channel Gating'. *The EMBO Journal* 30(17):3607–19. doi: 10.1038/emboj.2011.268.

Plant, Leigh D., Leandro Zuniga, Dan Araki, Jeremy D. Marks, and Steve A. N. Goldstein. 2012. 'SUMOylation Silences Heterodimeric TASK Potassium Channels Containing K2P1 Subunits in Cerebellar Granule Neurons'. *Science Signaling* 5(251):ra84. doi: 10.1126/scisignal.2003431.

Pope, Lianne, Cristina Arrigoni, Hubing Lou, Clifford Bryant, Alejandra Gallardo-Godoy, Adam R. Renslo, and Daniel L. Minor. 2018. 'Protein and Chemical Determinants of BL-1249 Action and Selectivity for K2P Channels'. *ACS Chemical Neuroscience* 9(12):3153–65. doi: 10.1021/acschemneuro.8b00337.

Punke, Mark A., Thomas Licher, Olaf Pongs, and Patrick Friederich. 2003. 'Inhibition of Human TREK-1 Channels by Bupivacaine'. *Anesthesia and Analgesia* 96(6):1665–73, table of contents. doi: 10.1213/01.ane.0000062524.90936.1f.

Rajan, S., E. Wischmeyer, G. Xin Liu, R. Preisig-Müller, J. Daut, A. Karschin, and C. Derst. 2000. 'TASK-3, a Novel Tandem Pore Domain Acid-Sensitive K+ Channel. An Extracellular Histiding as PH Sensor'. *The Journal of Biological Chemistry* 275(22):16650–57. doi: 10.1074/jbc.M000030200.

Rajan, Sindhu, Leigh D. Plant, Michael L. Rabin, Margaret H. Butler, and Steve A. N. Goldstein. 2005. 'Sumoylation Silences the Plasma Membrane Leak K+ Channel K2P1'. *Cell* 121(1):37–47. doi: 10.1016/j.cell.2005.01.019.

Rajan, Sindhu, Erhard Wischmeyer, Christine Karschin, Regina Preisig-Müller, Karl-Heinz Grzeschik, Jürgen Daut, Andreas Karschin, and Christian Derst. 2001. 'THIK-1 and THIK-2, a Novel Subfamily of Tandem Pore Domain K+ Channels * 210'. *Journal of Biological Chemistry* 276(10):7302–11. doi: 10.1074/jbc.M008985200.

Rapedius, Markus, Matthias R. Schmidt, Chetan Sharma, Phillip J. Stansfeld, Mark S. P. Sansom, Thomas Baukrowitz, and Stephen J. Tucker. 2012. 'State-Independent Intracellular Access of Quaternary Ammonium Blockers to the Pore of TREK-1'. *Channels (Austin, Tex.)* 6(6):473–78. doi: 10.4161/chan.22153.

Rapedius, Markus, Malle Soom, Ekaterina Shumilina, Dirk Schulze, Roland Schönherr, Cornelia Kirsch, Florian Lang, Stephen J. Tucker, and Thomas Baukrowitz. 2005. 'Long Chain CoA Esters as Competitive Antagonists of Phosphatidylinositol 4,5-Bisphosphate Activation in Kir Channels'. *Journal of Biological Chemistry* 280(35):30760–67. doi: 10.1074/jbc.M503503200.

Raucher, D., T. Stauffer, W. Chen, K. Shen, S. Guo, J. D. York, M. P. Sheetz, and T. Meyer. 2000. 'Phosphatidylinositol 4,5-Bisphosphate Functions as a Second Messenger That Regulates Cytoskeleton-Plasma Membrane Adhesion'. *Cell* 100(2):221–28. doi: 10.1016/s0092-8674(00)81560-3.

Renigunta, Vijay, Günter Schlichthörl, and Jürgen Daut. 2015. 'Much More than a Leak: Structure and Function of K2P-Channels'. *Pflügers Archiv - European Journal of Physiology* 467(5):867–94. doi: 10.1007/s00424-015-1703-7.

Reyes, R., F. Duprat, F. Lesage, M. Fink, M. Salinas, N. Farman, and M. Lazdunski. 1998. 'Cloning and Expression of a Novel PH-Sensitive Two Pore Domain K+ Channel from Human Kidney'. *The Journal of Biological Chemistry* 273(47):30863–69. doi: 10.1074/jbc.273.47.30863.

Rödström, Karin E. J., Aytuğ K. Kiper, Wei Zhang, Susanne Rinné, Ashley C. W. Pike, Matthias Goldstein, Linus J. Conrad, Martina Delbeck, Michael G. Hahn, Heinrich Meier, Magdalena Platzk, Andrew Quigley, David Speedman, Leela Shrestha, Shubhashish M. M. Mukhopadhyay, Nicola A. Burgess-Brown, Stephen J. Tucker, Thomas Müller, Niels Decher, and Elisabeth P. Carpenter. 2020. 'A Lower X-Gate in TASK Channels Traps Inhibitors within the Vestibule'. *Nature* 582(7812):443–47. doi: 10.1038/s41586-020-2250-8.

Rorsman, Patrik, and Frances M. Ashcroft. 2018. 'Pancreatic β-Cell Electrical Activity and Insulin Secretion: Of Mice and Men'. *Physiological Reviews* 98(1):117–214. doi: 10.1152/physrev.00008.2017.

Roux, Benoît, and Roderick MacKinnon. 1999. 'The Cavity and Pore Helices in the KcsA K+ Channel: Electrostatic Stabilization of Monovalent Cations'. *Science* 285(5424):100–102. doi: 10.1126/science.285.5424.100.

Royal, Perrine, Alba Andres-Bilbe, Pablo Ávalos Prado, Clément Verkest, Brigitte Wdziekonski, Sébastien Schaub, Anne Baron, Florian Lesage, Xavier Gasull, Joshua Levitz, and Guillaume Sandoz. 2019. 'Migraine-Associated TRESK Mutations Increase Neuronal Excitability through Alternative Translation Initiation and Inhibition of TREK'. *Neuron* 101(2):232-245.e6. doi: 10.1016/j.neuron.2018.11.039.

Salinas, M., R. Reyes, F. Lesage, M. Fosset, C. Heurteaux, G. Romey, and M. Lazdunski. 1999. 'Cloning of a New Mouse Two-P Domain Channel Subunit and a Human Homologue with a Unique Pore Structure'. *The Journal of Biological Chemistry* 274(17):11751–60. doi: 10.1074/jbc.274.17.11751.

Sandoz, Guillaume, Dominique Douguet, Franck Chatelain, Michel Lazdunski, and Florian Lesage. 2009. 'Extracellular Acidification Exerts Opposite Actions on TREK1 and TREK2 Potassium Channels via a Single Conserved Histidine Residue'. *Proceedings of the National Academy of Sciences of the United States of America* 106(34):14628–33. doi: 10.1073/pnas.0906267106.

Sano, Yorikata, Kohei Inamura, Akira Miyake, Shinobu Mochizuki, Chika Kitada, Hiromichi Yokoi, Katsura Nozawa, Hidetsugu Okada, Hitoshi Matsushime, and Kiyoshi Furuichi. 2003. 'A Novel Two-Pore Domain K+ Channel, TRESK, Is Localized in the Spinal Cord'. *The Journal of Biological Chemistry* 278(30):27406–12. doi: 10.1074/jbc.M206810200.

Schewe, Marcus, Ehsan Nematian-Ardestani, Han Sun, Marianne Musinszki, Sönke Cordeiro, Giovanna Bucci, Bert L. de Groot, Stephen J. Tucker, Markus Rapedius, and Thomas Baukrowitz. 2016. 'A Non-Canonical Voltage-Sensing Mechanism Controls Gating in K2P K+ Channels'. *Cell* 164(5):937–49. doi: 10.1016/j.cell.2016.02.002.

Schewe, Marcus, Han Sun, Ümit Mert, Alexandra Mackenzie, Ashley C. W. Pike, Friederike Schulz, Cristina Constantin, Kirsty S. Vowinkel, Linus J. Conrad, Aytug K. Kiper, Wendy Gonzalez, Marianne Musinszki, Marie Tegtmeier, David C. Pryde, Hassane Belabed, Marc Nazare, Bert L. de Groot, Niels Decher, Bernd Fakler, Elisabeth P. Carpenter, Stephen J. Tucker, and Thomas Baukrowitz. 2019. 'A Pharmacological Master Key Mechanism That Unlocks the Selectivity Filter Gate in K^+ Channels'. *Science* 363(6429):875–80. doi: 10.1126/science.aav0569.

Schneider, Eve R., Evan O. Anderson, Elena O. Gracheva, and Sviatoslav N. Bagriantsev. 2014. 'Temperature Sensitivity of Two-Pore (K2P) Potassium Channels'. *Current Topics in Membranes* 74:113–33. doi: 10.1016/B978-0-12-800181-3.00005-1.

Schulte, U., and B. Fakler. 2000. 'Gating of Inward-Rectifier K+ Channels by Intracellular PH'. *European Journal of Biochemistry* 267(19):5837–41. doi: 10.1046/j.1432-1327.2000.01671.x.

Schulte, U., H. Hahn, M. Konrad, N. Jeck, C. Derst, K. Wild, S. Weidemann, J. P. Ruppersberg, B. Fakler, and J. Ludwig. 1999. 'PH Gating of ROMK (Kir1.1) Channels: Control by an Arg-Lys-Arg Triad Disrupted in Antenatal Bartter Syndrome'. *Proceedings of the National Academy of Sciences* 96(26):15298–303. doi: 10.1073/pnas.96.26.15298.

Šedivá, Marie, Petra Laššuthová, Josef Zámečník, Lucie Sedláčková, Pavel Seeman, and Jana Haberlová. 2020. 'Novel Variant in the KCNK9 Gene in a Girl with Birk Barel Syndrome'. *European Journal of Medical Genetics* 63(1):103619. doi: 10.1016/j.ejmg.2019.01.009.

Sheetz, M. P., and S. J. Singer. 1974. 'Biological Membranes as Bilayer Couples. A Molecular Mechanism of Drug-Erythrocyte Interactions'. *Proceedings of the National Academy of Sciences of the United States of America* 71(11):4457–61. doi: 10.1073/pnas.71.11.4457.

Shukla, Sankalp, Rui Jin, Jaclyn Robustelli, Zachary E. Zimmerman, and Tobias Baumgart. 2019. 'PIP2 Reshapes Membranes through Asymmetric Desorption'. *Biophysical Journal* 117(5):962–74. doi: 10.1016/j.bpj.2019.07.047.

Shumilina, Ekaterina, Nikolaj Klöcker, Ganna Korniychuk, Markus Rapedius, Florian Lang, and Thomas Baukrowitz. 2006. 'Cytoplasmic Accumulation of Long-Chain Coenzyme A Esters Activates KATP and Inhibits Kir2.1 Channels'. *The Journal of Physiology* 575(Pt 2):433–42. doi: 10.1113/jphysiol.2006.111161.

Staudacher, Ingo, Claudius Illg, Sam Chai, Isabelle Deschenes, Sebastian Seehausen, Dominik Gramlich, Mara Elena Müller, Teresa Wieder, Ann-Kathrin Rahm, Christina Mayer, Patrick A. Schweizer, Hugo A. Katus, and Dierk Thomas. 2018. 'Cardiovascular Pharmacology of K2P17.1 (TASK-4, TALK-2) Two-Pore-Domain K+ Channels'. *Naunyn-Schmiedeberg's Archives of Pharmacology* 391(10):1119–31. doi: 10.1007/s00210-018-1535-z.

Steidl, J. V., and A. J. Yool. 1999. 'Differential Sensitivity of Voltage-Gated Potassium Channels Kv1.5 and Kv1.2 to Acidic PH and Molecular Identification of PH Sensor'. *Molecular Pharmacology* 55(5):812–20.

Suzuki, Yoshiaki, Kanako Tsutsumi, Tatsuya Miyamoto, Hisao Yamamura, and Yuji Imaizumi. 2017. 'Heterodimerization of Two Pore Domain K+ Channel TASK1 and TALK2 in Living Heterologous Expression Systems'. *PLoS ONE* 12(10). doi: 10.1371/journal.pone.0186252.

Talley, Edmund M., and Douglas A. Bayliss. 2002. 'Modulation of TASK-1 (Kcnk3) and TASK-3 (Kcnk9) Potassium Channels: Volatile Anesthetics and Neurotransmitters Share a Molecular Site of Action'. *The Journal of Biological Chemistry* 277(20):17733–42. doi: 10.1074/jbc.M200502200.

Thümmler, Susanne, Fabrice Duprat, and Michel Lazdunski. 2007. 'Antipsychotics Inhibit TREK but Not TRAAK Channels'. *Biochemical and Biophysical Research Communications* 354(1):284–89. doi: 10.1016/j.bbrc.2006.12.199.

Toner, Maureen, Gerard Vaio, Alan McLaughlin, and Stuart McLaughlin. 1988. 'Adsorption of Cations to Phosphatidylinositol 4,5-Bisphosphate'. *Biochemistry* 27(19):7435–43. doi: 10.1021/bi00419a039.

Warth, Richard, Hervé Barrière, Pierre Meneton, May Bloch, Jörg Thomas, Michel Tauc, Dirk Heitzmann, Elisa Romeo, François Verrey, Raymond Mengual, Nicolas Guy, Saïd Bendahhou, Florian Lesage, Philippe Poujeol, and Jacques Barhanin. 2004. 'Proximal Renal Tubular Acidosis in TASK2 K+ Channel-Deficient Mice Reveals a Mechanism for Stabilizing Bicarbonate Transport'. *Proceedings of the National Academy of Sciences of the United States of America* 101(21):8215–20. doi: 10.1073/pnas.0400081101.

Wilke, Bettina U., Moritz Lindner, Lea Greifenberg, Alexandra Albus, Yannick Kronimus, Moritz Bünemann, Michael G. Leitner, and Dominik Oliver. 2014. 'Diacylglycerol Mediates Regulation of TASK Potassium Channels by Gq-Coupled Receptors'. *Nature Communications* 5(1):5540. doi: 10.1038/ncomms6540.

Yellen, Gary. 2002. 'The Voltage-Gated Potassium Channels and Their Relatives'. *Nature* 419(6902):35–42. doi: 10.1038/nature00978.

Zhou, Jun, Corinne E. Augelli-Szafran, Jenifer A. Bradley, Xian Chen, Bryan J. Koci, Walter A. Volberg, Zhuoqian Sun, and Jason S. Cordes. 2005. 'Novel Potent Human Ether-a-Go-Go-Related Gene (HERG) Potassium Channel Enhancers and Their in Vitro Antiarrhythmic Activity'. *Molecular Pharmacology* 68(3):876–84. doi: 10.1124/mol.105.014035.

Zhou, Yufeng, João H. Morais-Cabral, Amelia Kaufman, and Roderick MacKinnon. 2001. 'Chemistry of Ion Coordination and Hydration Revealed by a K + Channel–Fab Complex at 2.0 Å Resolution'. *Nature* 414(6859):43–48. doi: 10.1038/35102009.

Acknowledgments

Here, I would like to thank all members of my lab that have supported me in the past 3 years and have made this thesis possible even during the still present Covid-19 pandemic.

First of all, I would like to thank all MTAs that have helped me tremendously with my work, Sandra Grüssel, Michaela Unmack and Dr. Hariolf Fritzenschaft for their hard work creating new mutants and providing me with oocytes and fresh solutions, as well as Kerstin Viertmann and Petra Breiden that supported me during my final steps.

My special gratitude also goes to my 3 headed Post-Doc supervisor team, resembled by Dr. Marcus Schewe, Dr. Marianne Musinszki and Dr. Sönke Cordeiro, that have helped me a lot with my work. Thereby, I would like to thank Marcus especially for his patient and thoughtful supervision, his planning and constructive criticism. Also, I would like to thank Marianne for the insights she gave me into new methods, as well as, I am very grateful not only for Sönke sharing his scientific expertise, but also for his emotional support and humorous character, that has strengthened me even in difficult situations. It was a pleasure working with you.

Especially, I would like to thank Prof. Dr. Thomas Baukrowitz for giving me the chance to do my PhD in his working group. I am very grateful for the numerous talks about my work and for him sharing his knowledge and scientific expertise with me. I always enjoyed those visionary moments, where new ideas and hypothesis were created. Thank you for that.

Finally, I would like to thank my dear friends and family that have supported me during the last years. Particularly, I would like to thank Julian Vehrke for his emotional support, for providing me with coffee and his efforts to create a nice and peaceful homeoffice environment, that has helped me a lot during the writing process of this work.

Eidesstattliche Erklärung

Hiermit bestätige ich an Eides statt, dass die vorliegende Arbeit abgesehen von der Beratung durch meinen Betreuer, nach Inhalt und Form eigenständig und nur mit den angegebenen Hilfsmitteln verfasst wurde. Ich versichere, dass die Arbeit unter Einhaltung der Regeln guter wissenschaftlicher Praxis der Deutschen Forschungsgemeinschaft entstanden ist und alle Ausführungen, die anderen Schriften wörtlich oder sinngemäß entnommen wurden, kenntlich gemacht sind. Die Dissertation wurde von mir vorher weder in einem anderen Prüfungsverfahren eingereicht noch veröffentlicht und mir wurde kein akademischer Grad entzogen. Die eingereichte schriftliche Fassung entspricht der auf dem elektronischen Speichermedium. Ich bin damit einverstanden, dass die Dissertation veröffentlicht wird.

Ort/ Datum **Elena Riel**